

NASA CR-130162

AED R-3553F  
April 30, 1970

## ITOS D and E System Design Report

Prepared for  
Goddard Space Flight Center  
National Aeronautics and Space Administration  
Washington, D.C.  
Contract No. NAS5-10306

Volume III

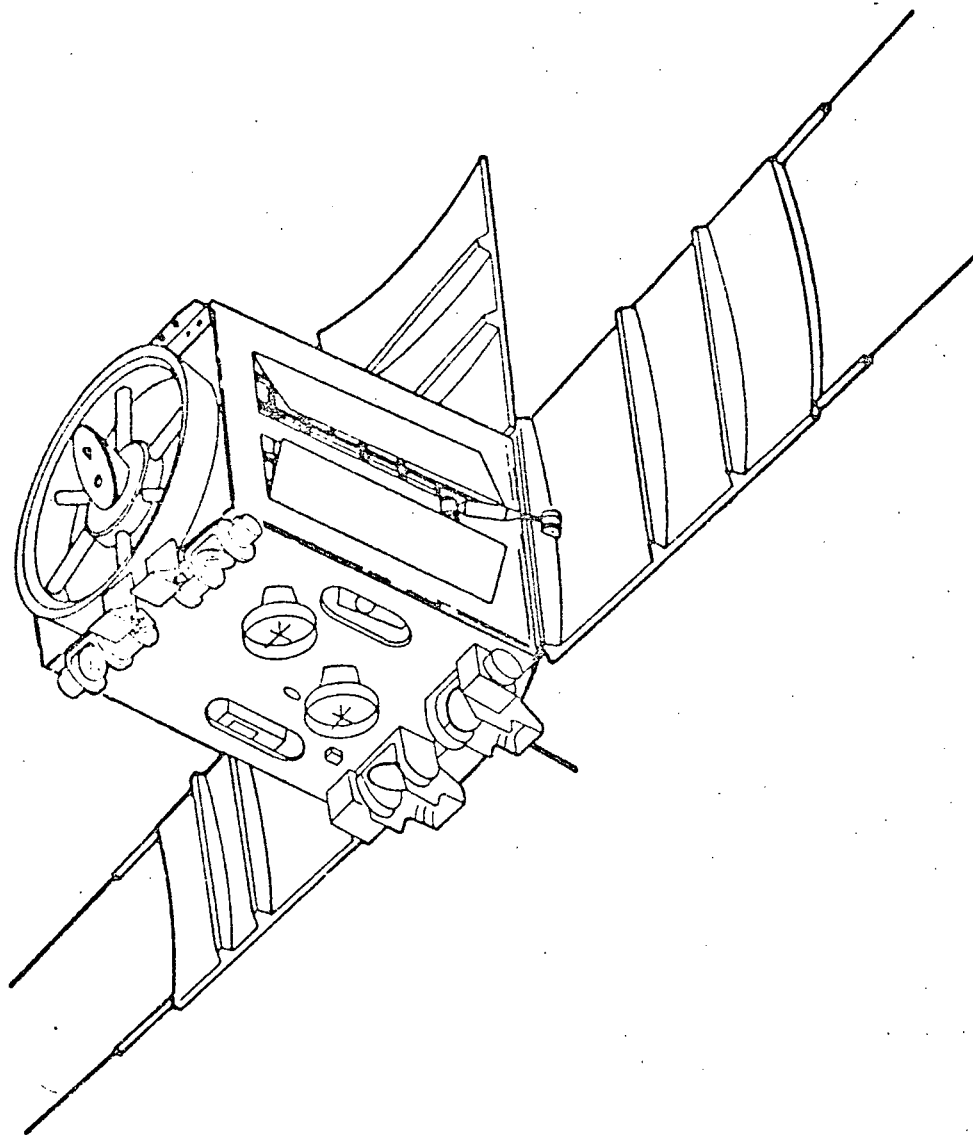
(NASA-CR-130162) ITOS D AND E SYSTEM  
DESIGN REPORT, VOLUME 3 (Radio Corp. of  
America) - 144 p HC \$9.25  
CSSL 22B

N73-18865

G3/31

Unclas  
54427

RCA | Defense Electronic Products  
Astro Electronics Division | Princeton, New Jersey



PRECEDING PAGE BLANK NOT FILMED

The ITOS D and E Spacecraft

## PREFACE

This report describes the system, spacecraft, and ground installation design, as well as related studies, for the ITOS D and E meteorological satellite system. The ITOS D and E design study program has been conducted by the Astro-Electronics Division of RCA Corporation for the Goddard Space Flight Center of the National Aeronautics and Space Administration, under contract NAS5-10306.

## TABLE OF CONTENTS

Section	Page
I	SYSTEM DESIGN ..... I-1
A.	Introduction ..... I-1
1.	Mission Requirements ..... I-1
2.	System Summary ..... I-2
a.	General ..... I-2
b.	Spacecraft ..... I-2
c.	Orbit ..... I-5
d.	Ground Complex ..... I-6
B.	System Functional Description ..... I-7
1.	Spacecraft ..... I-7
a.	Physical Description ..... I-7
(1)	Configuration ..... I-7
(2)	Central Equipment Module ..... I-7
(3)	Solar Array ..... I-10
(4)	Thermal Control ..... I-10
(5)	Pitch-Control Loop ..... I-13
(6)	Separation Ring ..... I-13
b.	Launch Vehicle Compatibility ..... I-16
c.	Functional Description ..... I-17
(1)	General ..... I-17
(2)	Command Subsystem ..... I-17
(3)	Primary Sensors ..... I-18
(a)	Real-Time Data ..... I-18
(b)	Stored Data ..... I-18
(4)	Solar Proton Monitor ..... I-21
(5)	Communications Subsystem ..... I-21
(a)	S-Band Link ..... I-21
(b)	Real-Time Link ..... I-22
(c)	Command and Beacon Link ..... I-22
(6)	Power Subsystem ..... I-22
d.	Subsystem Redundancy ..... I-23
(1)	Operating Goals ..... I-23
2.	Spacecraft/CDA Station Interface ..... I-25
a.	Command Link ..... I-25
b.	Beacon Link ..... I-26
c.	Real-Time VHF Link ..... I-27
d.	S-Band Playback Link ..... I-28
e.	S-Band Real-Time Link ..... I-29
3.	Local Ground Stations ..... I-30
a.	General ..... I-30
b.	Spacecraft/APT Ground-Station Interface .. I-30
c.	Spacecraft/VHRR Ground-Station Interface ..... I-31

TABLE OF CONTENTS (Continued)

Section	Page
4. Orbit Characteristics .....	I-31
a. The ITOS Orbit .....	I-31
b. Operational Effects of Orbit Characteristics .....	I-33
(1) Spacecraft Sun Angle and Eclipse Time .....	I-34
(2) Effect of Date and Time of Launch .....	I-35
(3) Effects of Injection Errors .....	I-35
5. Sensor Coverage .....	I-40
a. SR Radiometry .....	I-40
(1) General .....	I-40
(2) Spectral Response .....	I-40
(3) Resolution .....	I-41
(4) SR Image Characteristic .....	I-41
b. VHRR Radiometry .....	I-43
(1) General .....	I-43
(2) Resolution .....	I-43
(3) Spectral Response .....	I-43
(4) VHRR Image Characteristic .....	I-44
c. VTPR Radiometry .....	I-44
(1) General .....	I-44
(2) Spectral Considerations .....	I-46
(3) Angular Resolution .....	I-46
(4) VTPR Image Characteristics .....	I-46
d. SPM Radiometry .....	I-47
(1) General .....	I-47
(2) Sensors .....	I-47
6. ITOS Ground Complex .....	I-47
a. General .....	I-47
b. Command, Programming, and Analysis Centers .....	I-47
c. Command and Data Acquisition (CDA) Stations .....	I-48
d. Spacecraft Checkout Facilities .....	I-49
e. Scope of Ground Equipment Coverage .....	I-49
C. System Operation .....	I-50
1. ITOS Mission Profile .....	I-50
2. VHRR, SR and VTPR Radiometers, and QOMAC Programming .....	I-53
a. General .....	I-53
b. Radiometer Programming .....	I-53

## TABLE OF CONTENTS (Continued)

Section	Page
c. QOMAC Programming .....	I-53
d. SR Recorder Programming .....	I-54
3. CDA Station Contact Time .....	I-54
4. Effect of Date and Time of Launch .....	I-57
5. Use of Redundancy .....	I-57
a. Philosophy of Redundancy .....	I-57
b. Subsystem Component Selectivity .....	I-57
(1) SR Subsystem .....	I-57
(2) VHRR Subsystem .....	I-58
(3) VTPR Subsystem .....	I-58
(4) Pitch Control Loop .....	I-58
(5) Command Subsystem .....	I-58
II MECHANICAL AND STRUCTURAL DESIGN .....	II-1
A. General .....	II-1
B. Design Approach .....	II-4
1. Requirements and Constraints .....	II-4
2. Modifications to the TIROS M Design .....	II-4
3. Spacecraft Structure .....	II-7
4. Mechanisms .....	II-8
5. Stress Analysis .....	II-9
C. Design Philosophy .....	II-9
1. General .....	II-9
2. Mechanical Alignment .....	II-9
3. Component Assembly .....	II-11
4. Weight .....	II-12
5. Fabrication and Assembly .....	II-12
6. Integration of Electronic Equipment .....	II-14
7. Interchangeability .....	II-14
D. Structural Components .....	II-15
1. Separation Ring .....	II-15
2. Baseplate .....	II-17
3. Equipment Mounting Panels .....	II-18
4. Earth-Facing Access Panel .....	II-19
5. Anti-Earth Access Panel .....	II-19
6. Crossbrace Assembly .....	II-22
7. Thermal Fence .....	II-22
8. Solar Array Structure and Deployment Mechanism .....	II-22
9. Momentum and Attitude Control Coils .....	II-29

## TABLE OF CONTENTS (Continued)

Section	Page
10. Nutation Dampers .....	II-29
11. Active Thermal Controller (ATC) .....	II-29
a. Actuator Sensor Unit .....	II-30
b. Louver and Hinge Assembly .....	II-35
E. Interior Electronics Arrangement .....	II-38
1. General .....	II-38
2. Accessibility of Components .....	II-38
III THERMAL DESIGN .....	III-1
A. General .....	III-1
B. Functional Description .....	III-3
1. Thermal Fence .....	III-3
2. Active Thermal Controller .....	III-6
3. Thermal Insulation .....	III-6
4. Thermal Painting .....	III-8
5. Temperature Sensors .....	III-8
C. Design History .....	III-9
1. Flight Correlation for TIROS M .....	III-9
2. Modification of the TIROS M Thermal Design for ITOS D and E .....	III-9
3. Prediction of Flight Temperatures .....	III-10
IV VEHICLE DYNAMICS .....	IV-1
A. Subsystem Description .....	IV-1
B. Initial Orientation Maneuver .....	IV-4
1. Sequence .....	IV-4
2. Biased Flywheel Operation .....	IV-6
C. Nutation Damping .....	IV-7
1. General .....	IV-7
2. Basic Design .....	IV-8
a. Mathematical Analysis .....	IV-8
b. Mechanical Configuration .....	IV-9
c. Pressurization .....	IV-9
3. Damping Time Constant .....	IV-11
D. Attitude Sensing .....	IV-11
1. General .....	IV-11
2. Digital Solar Aspect Sensor .....	IV-12
3. Infrared Sensors .....	IV-14
a. General .....	IV-14
b. Electronics .....	IV-15

TABLE OF CONTENTS (Continued)

Section	Page
E. Magnetic Attitude Control and Momentum Control .....	IV-24
1. General .....	IV-24
2. Coordinate System .....	IV-24
3. Geomagnetic Field Equations .....	IV-26
4. Quarter-Orbit Magnetic Attitude Control .....	IV-27
5. Unipolar Torque .....	IV-28
6. Magnetic Bias Switch .....	IV-31
7. Momentum Control After Pitch Lock .....	IV-31
8. Magnetic Bias Control (MBC) .....	IV-32
a. Spin Momentum Change ( $T_{SPIN}$ ) .....	IV-34
b. Precession Due To Momentum Correction ( $T_{PREC}$ ) .....	IV-35
9. Momentum Control Prior To Pitch Lock .....	IV-36
F. Pitch Control .....	IV-43
1. General .....	IV-43
2. Pitch Sensing .....	IV-45
3. Servo Design .....	IV-47
4. Three-Axis Considerations .....	IV-49
5. Component Description .....	IV-63
a. General .....	IV-63
b. Pulse Width Modulator (PWM) Error Detector .....	IV-66
c. Compensation Amplifier .....	IV-67
d. Gain Switching Circuit .....	IV-67
e. Summing Amplifier .....	IV-68
f. Power Amplifier .....	IV-68
g. Torque Motor .....	IV-68
h. Encoder .....	IV-70
i. Encoder Electronics .....	IV-70
j. DC-to-DC Converter .....	IV-70
k. Pitch Sensor Threshold Amplifiers .....	IV-71
l. Earth Blanking .....	IV-71
m. Electronics Box .....	IV-71
6. MWA Mechanical Design .....	IV-76
G. Systems Interfaces .....	IV-76
1. Power .....	IV-76
2. Command and Control .....	IV-76
3. Telemetry .....	IV-76

## TABLE OF CONTENTS (Continued)

Section	Page
H. Disturbance Analysis .....	IV-77
1. Residual Magnetic Dipoles .....	IV-77
2. Solar Torques .....	IV-82
3. Magnetic Losses .....	IV-86
a. Hysteresis .....	IV-86
b. Eddy Current .....	IV-86
4. Gravity Gradient .....	IV-86
5. Internal Rotating Components .....	IV-87
 V POWER SUPPLY .....	 V-1
A. Introduction .....	V-1
B. Functional Description .....	V-2
1. General .....	V-2
2. Solar-Cell Array .....	V-6
a. General .....	V-6
b. Components .....	V-6
(1) Solar Cells .....	V-6
(2) Solar Cell Cover Glass .....	V-7
(3) Solar Cell Cover Glass Adhesive .....	V-7
(4) Solar Cell Bonding Adhesive .....	V-7
(5) Solar Cell Interconnection .....	V-7
(6) Substrate .....	V-8
c. Characteristics .....	V-8
(1) Dimensions .....	V-8
(2) Weight .....	V-8
d. Functional Description .....	V-8
(1) Design Parameters .....	V-8
(2) Solar Cell I-V Characteristics .....	V-9
e. Secondary Design Parameters .....	V-9
f. Shunt Dissipator .....	V-9
3. Batteries .....	V-12
a. General .....	V-12
b. Mechanical Design .....	V-12
c. Electrical Design .....	V-12
d. System Considerations .....	V-14
4. Power Supply Electronics .....	V-14
a. General .....	V-14
b. Functional Operation .....	V-15
(1) Voltage Regulator .....	V-15
(2) Shunt Limiter .....	V-16
(3) Charge Controllers .....	V-17

## TABLE OF CONTENTS (Continued)

Section	Page
c. System Outputs .....	VI-56
(1) Sensitivity and Radiometric Accuracy .....	VI-56
(2) Dynamic Range .....	VI-57
(3) Thermal Video Channel Outputs .....	VI-57
(4) Synchronizing Signals .....	VI-57
(5) Telemetry .....	VI-57
3. Optical System .....	VI-58
a. Filter Wheel and Chopper .....	VI-58
b. Field-of-View .....	VI-60
4. Operation of Electrical Circuits .....	VI-60
a. Data Channel .....	VI-63
b. Calibration Sequence Logic .....	VI-64
c. Staircase Generator .....	VI-65
d. Digital Data Interface .....	VI-65
e. Thermal Control .....	VI-66
f. Phase Reference Pickup Circuits (PRP)...	VI-66
g. Power Supply .....	VI-66
h. Torquer Drive .....	VI-67
i. Scan Drive .....	VI-67
E. Solar Proton Monitor .....	VI-69
1. Introduction .....	VI-69
2. Sensor Assembly .....	VI-69
a. General .....	VI-69
b. Sensors .....	VI-72
(1) Proton Sensors 1 and 2 ( $E_p > 60$ MeV and $E_p > 30$ MeV) .....	VI-72
(2) Proton Sensor 3 ( $E_p > 10$ MeV) .....	VI-72
(3) Electron Sensor ( $100 < E_e < 750$ keV) ..	VI-72
(4) Dual Channel Proton Sensors (5 and 6) .....	VI-74
3. Data Processing Electronics .....	VI-74
a. General .....	VI-74
b. Amplifier-Discriminator Chains .....	VI-75
c. Pulse-Handling Logic .....	VI-75
d. Data Commutator and Accumulator Control .....	VI-75
e. Data Accumulator .....	VI-76
f. Floating Point Compressor .....	VI-76
g. Processor Control .....	VI-76
h. Data Sync (Box) Modification .....	VI-76
i. Real Time Output .....	VI-77
j. Remote Output .....	VI-77
k. Power and Telemetry .....	VI-77

## TABLE OF CONTENTS (Continued)

Section	Page
VII	
DATA HANDLING .....	VII-1
A. Introduction .....	VII-1
B. Scanning Radiometer Processor .....	VII-2
1. General .....	VII-2
a. Functional Description .....	VII-2
(1) Multiplex Mode .....	VII-2
(2) IR/Visible Backup Mode .....	VII-4
b. Dual Processor .....	VII-4
2. Requirements .....	VII-4
a. Functional Operation .....	VII-4
(1) Input/Output Functions .....	VII-4
(2) Internal Functions .....	VII-5
(3) Commutator .....	VII-8
(4) Seven-Pulse Sync Generator .....	VII-8
(5) Time-Code Buffer .....	VII-8
(6) Eight-Stage Divide Chain .....	VII-11
(7) Sample-and-Hold Network .....	VII-11
(8) Signal-Select Network .....	VII-12
(9) Balanced Modulator System .....	VII-12
b. Input/Output Interface Signals .....	VII-12
(1) Input Signals .....	VII-14
(2) Output Signals .....	VII-15
c. Telemetry .....	VII-16
3. Electrical Characteristics .....	VII-16
a. Circuit Elements .....	VII-16
b. Power Requirements .....	VII-16
4. Physical Characteristics .....	VII-16
C. Very High Resolution Radiometer Processor .....	VII-16
1. Real-Time Processing of VHRR Video .....	VII-17
2. VHRR Video Recording .....	VII-20
3. Playback .....	VII-24
D. Digital Data Processor .....	VII-24
1. General Description .....	VII-24
a. System Function .....	VII-24
b. Frame Description .....	VII-25
(1) Recorded Digital Frame .....	VII-25
(2) Real-Time Telemetry Frame .....	VII-29
c. Telemetry Modes of Operation .....	VII-38
2. Interface Description	

TABLE OF CONTENTS (Continued)

Section	Page
3. Functional Operation .....	VII-45
a. Frame Counter .....	VII-45
b. Counter Decoder .....	VII-47
c. Counter Reset Control .....	VII-47
d. Commutator Shift Register .....	VII-47
e. Mode Control .....	VII-47
f. Clock Generator .....	VII-47
g. Commutator Input Gating and Buffers .....	VII-48
h. Commutator and Output Buffer .....	VII-48
i. Signal Conditioner .....	VII-49
j. Seven-Bit A/D Converter .....	VII-49
k. Parallel In/Serial Out Register .....	VII-49
l. Sync Generator .....	VII-49
m. Time Code Update Control and Shift Register .....	VII-50
n. SPM and VTPR Input Buffer .....	VII-50
o. Bit Synchronizer .....	VII-50
p. VTPR and SPM Register Control .....	VII-50
q. Master Reset Generator .....	VII-50
r. DC-DC Converter .....	VII-50
4. Electrical Characteristics .....	VII-51
a. Power .....	VII-51
b. Logic .....	VII-51
(1) Low Power .....	VII-51
(2) Design Flexibility .....	VII-51
(3) Medium Scale Integration (MSI) .....	VII-51
(4) Reliability .....	VII-52
5. Packaging .....	VII-52
E. Scanning Radiometer Recorder .....	VII-52
1. General .....	VII-52
a. Electrical Design .....	VII-53
b. Mechanical Design .....	VII-61
2. New Design .....	VII-66
3. Functional Description .....	VII-68
a. General .....	VII-68
b. Record Mode .....	VII-68
c. Playback Mode .....	VII-69
d. Mechanical Design .....	VII-69
e. Telemetry .....	VII-71
F. Very High Resolution Radiometer Recorder .....	VII-71
1. General .....	VII-71
2. Interface Signals .....	VII-74
3. Tape Transport Assembly .....	VII-74
4. Electronics Unit .....	VII-77

TABLE OF CONTENTS (Continued)

Section		Page
VIII	COMMAND SUBSYSTEM .....	VIII-1
	A. Function .....	VIII-1
	B. Design .....	VIII-7
	1. General .....	VIII-7
	C. Dual Command Decoder .....	VIII-8
	1. General Description .....	VIII-8
	a. Power and Signal Interfaces .....	VIII-8
	b. Decoder Data Format .....	VIII-9
	2. Functional Operation .....	VIII-9
	a. General Decoding Processes .....	VIII-9
	b. Detailed Circuit Description .....	VIII-17
	(1) Analog Circuits .....	VIII-20
	(2) Digital (Integrated) Circuits .....	VIII-21
	(3) Buffer Circuits .....	VIII-23
	D. Dual Time Base Unit .....	VIII-24
	1. General .....	VIII-24
	2. Response to Commands .....	VIII-24
	3. Time Base Generator Description .....	VIII-26
	4. Time Code Generator Description .....	VIII-26
	5. Packaging .....	VIII-29
	E. Dual Command Programmer .....	VIII-31
	1. General .....	VIII-31
	2. Program Data Loading .....	VIII-32
	3. SR Subsystem Control .....	VIII-41
	a. SR Recorder Sequencing .....	VIII-41
	b. SR Control .....	VIII-42
	4. Programmer Interfaces .....	VIII-43
	5. Packaging .....	VIII-43
	F. Command Distribution Unit (CDU) .....	VIII-43
	1. General Characteristics .....	VIII-43
	2. Functional Description .....	VIII-47
	a. General .....	VIII-47
	b. Command Decoding .....	VIII-48
	c. Commands and Their Functional Operation .....	VIII-49
	(1) General .....	VIII-49
	(2) Power Subsystem .....	VIII-51
	(3) Time Base Unit (TBU) .....	VIII-51
	(4) Programmer (DCP) .....	VIII-52
	(5) Scanning Radiometer (SR) Subsystem .....	VIII-52
	(6) SRR Processor Control Logic .....	VIII-54

## TABLE OF CONTENTS (Continued)

Section	Page
(7) Scanning Radiometer Recorders (SRR) .....	VIII-54
(8) VHF Real-Time Transmitter .....	VIII-61
(9) Vertical Temperature Profile Radiometer .....	VIII-61
(10) Very High Resolution Radiometer (VHRR) Subsystem .....	VIII-62
(11) VHRR Recorder Subsystem .....	VIII-66
(12) S-Band Transmitter Subsystem .....	VIII-70
(13) Pitch Control Subsystem .....	VIII-72
(14) Attitude Control Coils .....	VIII-72
(15) Squib Firing .....	VIII-76
(16) Solar Proton Monitor .....	VIII-78
(17) Beacon Transmitter .....	VIII-78
(18) Digital Data Processor .....	VIII-79
(19) Beacon Telemetry Subsystem .....	VIII-81
d. Special Operational Control Features .....	VIII-87
(1) PTT Operation .....	VIII-87
(2) Enable Tone Telemetry Request .....	VIII-87
<b>IX COMMUNICATIONS .....</b>	<b>IX-1</b>
A. Introduction .....	IX-1
B. Command Link .....	IX-1
1. General Description .....	IX-1
2. Signal Characteristics .....	IX-4
3. Antenna Subsystem .....	IX-5
4. Dual Command Receiver .....	IX-5
5. Subsystem Analysis .....	IX-7
C. Beacon and Telemetry Link .....	IX-8
1. General Description .....	IX-8
a. 3.9-kHz Channel .....	IX-10
b. 2.3-kHz Channel .....	IX-11
2. Signal Characteristics .....	IX-12
a. Housekeeping Telemetry .....	IX-12
b. Command Data Verification .....	IX-13
c. Solar Proton Monitor .....	IX-15
d. Digital Solar Aspect Sensor (DSAS) .....	IX-15
e. Pitch and Roll Sensors .....	IX-15
f. Time Code Data .....	IX-17
g. Vertical Temperature Profile Radiometer .....	IX-17
h. Accelerometer Data .....	IX-17

## TABLE OF CONTENTS (Continued)

Section	Page
3. Dual Subcarrier Oscillator Assembly .....	IX-19
4. Beacon Transmitter .....	IX-21
5. Antenna Subsystem .....	IX-24
6. Subsystem Analysis Summary .....	IX-26
D. VHF Real-Time Video Link .....	IX-27
1. General Description .....	IX-27
2. SR Signal Characteristics .....	IX-27
3. SR Processor .....	IX-30
4. Time Multiplexing of SR Signals .....	IX-33
5. VHF Real-Time Transmitter .....	IX-33
6. Real-Time Antenna Group .....	IX-35
7. Subsystem Analysis Summary .....	IX-37
E. S-Band Real-Time Video Link .....	IX-38
1. General Description .....	IX-38
2. VHRR Signal Characteristics .....	IX-39
3. VHRR Processor .....	IX-39
4. S-Band Transmitter .....	IX-44
a. Introduction .....	IX-44
b. Design Approach .....	IX-44
c. Description .....	IX-45
d. Telemetry .....	IX-48
5. S-Band Antenna .....	IX-48
6. Subsystem Analysis Summary .....	IX-49
F. S-Band Playback Link .....	IX-50
1. General .....	IX-50
2. Signal Characteristics .....	IX-53
a. VHRR Signals .....	IX-53
b. SR Signals .....	IX-54
c. Digital Data Signals .....	IX-56
3. Dual Multiplexer .....	IX-58
4. S-Band Transmitter .....	IX-64
5. S-Band Antenna .....	IX-65
6. Subsystem Analysis Summary .....	IX-65
<b>X</b> SPACECRAFT TESTING .....	X-1
A. ITOS D and E Test Philosophy .....	X-1
B. Spacecraft Qualification Testing .....	X-1
1. Test Flow .....	X-1
2. Vibration .....	X-2
3. Thermal-Vacuum Tests .....	X-2

Preceding page blank

TABLE OF CONTENTS (Continued)

Section	Page
4. Test Implementation .....	X-4
a. Spacecraft Integration .....	X-5
b. Prequalification Alignment and Calibration .....	X-6
c. Environmental Qualification .....	X-6
d. Final Spacecraft Calibration .....	X-6
5. Test Equipment .....	X-7
a. Spacecraft Test Console .....	X-7
b. Target Control Rack .....	X-8
c. Data Reduction Computer .....	X-9
d. Spacecraft Test Configuration in Thermal-Vacuum .....	X-10
XI GROUND STATION EQUIPMENT .....	XI-1
A. Introduction .....	XI-1
B. Command, Programming, and Analysis Centers ...	XI-2
1. TOS Evaluation Center/TIROS-TOS Check- out Center (TEC/TTCC) .....	XI-2
a. Function .....	XI-2
b. New Facilities .....	XI-2
2. TOS Operations Center (TOC) .....	XI-3
a. Functions .....	XI-3
b. New Facilities .....	XI-3
3. Data Processing and Analysis Facility (DAPAF) .....	XI-4
a. Functions .....	XI-4
b. Data Inputs .....	XI-4
(1) SR Data .....	XI-4
(a) Video Signal .....	XI-4
(b) Flutter-and-Wow Signal .....	XI-4
(2) VHRR Data .....	XI-6
(a) Video Signal .....	XI-6
(b) Flutter-and-Wow Signal .....	XI-6
(3) Digital Data .....	XI-6
(4) Beacon Data .....	XI-9
(5) CDA Station-Events Signals .....	XI-9
c. New Facilities .....	XI-9
(1) SR Demodulator .....	XI-9
(2) VHRR Demodulator .....	XI-10
(3) Digital Translator .....	XI-10
(4) Digital Signal Conditioner .....	XI-10

## TABLE OF CONTENTS (Continued)

Section	Page
C. Command and Data Acquisition Stations .....	XI-10
1. General .....	XI-10
2. Data Acquisition Facilities .....	XI-11
3. Ground Station Redundancy .....	XI-11
4. Radio Frequency Equipment .....	XI-11
a. Introduction .....	XI-12
b. Command Link .....	XI-12
c. Beacon Data Link .....	XI-13
d. Real-Time VHF Link .....	XI-13
e. S-Band Playback Link .....	XI-14
5. Video Equipment .....	XI-14
a. Introduction .....	XI-15
b. Demultiplexing .....	XI-15
c. Tape Recorders .....	XI-21
d. Long Lines Interface .....	XI-21
e. A-Scan Display of Data .....	XI-21
(1) S-Band Data .....	XI-21
(a) SR Data .....	XI-21
(b) VHRR Data .....	XI-25
(c) AVCS Data .....	XI-26
(d) Digital Data .....	XI-26
(e) Real-Time VHRR Data .....	XI-26
(2) Beacon Data .....	XI-26
(3) Real-Time SR Data .....	XI-26
f. Chart Recorder Display of Data .....	XI-27
D. Programming Commands and Equipment .....	XI-27
1. Satellite Commands .....	XI-27
a. General .....	XI-27
b. Direct Commands .....	XI-27
c. Remote Commands .....	XI-28
d. Additional Command Requirements .....	XI-28
2. Equipment Modifications .....	XI-28
a. Command Rack 35, Drawer D .....	XI-28
(1) Key-Enabled Command Circuits .....	XI-28
(2) Inhibit Automatic Update Circuits .....	XI-29
b. Beacon Equipment .....	XI-29
c. Station Control Equipment .....	XI-29
(1) Station Control Panel .....	XI-29
(2) Recorder Playback Controls .....	XI-30
(3) Oscilloscope Displays .....	XI-34
3. Additional Equipment .....	XI-34

TABLE OF CONTENTS (Continued)

Section	Page
E. Long Lines .....	XI-34
1. General .....	XI-34
2. Channel Allocation .....	XI-34
3. Long Line Utilization .....	XI-37
F. RCA Astro-Electronics Division Checkout Facility and Ground Station .....	XI-38
1. General .....	XI-38
2. Radio Frequency Signal Handling .....	XI-38
3. Data Processing .....	XI-38
a. S-Band Data .....	XI-39
b. Beacon Data .....	XI-39
c. Real-Time SR Data .....	XI-39
4. Commands .....	XI-39
G. Launch Support Station .....	XI-39

APPENDICES

A	ITOS D AND E STRESS ANALYSIS .....	A-1
B	MECHANICAL DESIGN PARAMETERS .....	B-1
C	COMMUNICATION LINK ANALYSES .....	C-1
D	PERFORMANCE TESTS OF ITOS D AND E S-BAND ANTENNAS .....	D-1

## LIST OF ILLUSTRATIONS

Figure		Page
I-1	ITOS D and E Satellite, Identification of External Features .....	I-3
I-2	The ITOS D and E System .....	I-4
I-3	ITOS D and E Spacecraft Orientation .....	I-8
I-4	ITOS D and E Spacecraft in Operational Mode, Showing Sensor Field of View .....	I-9
I-5	ITOS D and E Spacecraft Component Layout .....	I-11
I-6	ITOS D and E Thermal Radiators .....	I-14
I-7	Thermal Control Fence .....	I-15
I-8	ITOS D and E System Block Diagram .....	I-19
I-9	Geometry of the Sun-Synchronous Orbit .....	I-33
I-10	Seasonal Variation of Spacecraft Sun Angle for Afternoon AN Orbits .....	I-34
I-11	ITOS Spacecraft Time in Sunlight .....	I-36
I-12	Nodal Drift Rate Error vs Inclination Error .....	I-37
I-13	Nodal Drift Rate Error vs Mean Altitude Error .....	I-37
I-14	Spacecraft Pitch Attitude Offset vs Altitude .....	I-38
I-15	Effect of Launch Window and Injection Error on Mission Mode Sun Angle (Worst Case) .....	I-39
I-16	Typical SR Transfer Function .....	I-40
I-17	SR Image Characteristics .....	I-42
I-18	VHRR Image Characteristics .....	I-45
I-19	Launch to Mission Mode Events .....	I-51
I-20	Typical Ground-Contact Boundaries for Wallops Island and Alaska CDA Stations .....	I-55
I-21	Typical CDA Station Contact Time .....	I-56
II-1	ITOS D and E Spacecraft Orientation .....	II-2
II-2	Basic Structure, Showing Panel Access Ports (Cutouts) and Hinged Equipment Panel Opened .....	II-3
II-3	ITOS D and E Spacecraft Launch Compatibility .....	II-5
II-4	Stud Mounting for Spacecraft Handling .....	II-8
II-5	Front Access Panel .....	II-10
II-6	Baseplate (Panel No. 2) Layout .....	II-16
II-7	Equipment Panel No. 1 .....	II-20
II-8	Equipment Panel No. 3 .....	II-21
II-9	Cross Brace Assembly and Thermal Fence .....	II-23
II-10	ITOS D and E Thermal Fence Assembly Configuration .....	II-24
II-11	Solar Panel, Mechanical Configuration .....	II-25
II-12	Solar Panel Hydraulic Actuator .....	II-28
II-13	Solar Panel Retention and Release Mechanism .....	II-31
II-14	Deployment of Solar Panel .....	II-33
II-15	ATC Actuator Sensor Unit .....	II-34

## LIST OF ILLUSTRATIONS (Continued)

Figure		Page
II-16	ATC Louver and Hinge Assembly .....	II-36
II-17	Spacecraft Alignment Reference Axes .....	II-39
III-1	Thermal Radiators .....	III-1
III-2	Thermal Control Fence .....	III-3
III-3	Net Heat Exchange Between Thermal Fenceplate and 20°C Spacecraft .....	III-5
III-4	Active Thermal Control, Functional Characteristics .....	III-7
III-5	Nodal Definitions for Analytical Thermal Model .....	III-11
IV-1	Vehicle Dynamics Subsystem, Block Diagram .....	IV-2
IV-2	Typical Signals Telemetered on 2.3-kHz Subcarrier .....	IV-5
IV-3	Equipment Module Momentum Versus Spin Rate .....	IV-8
IV-4	Liquid-Filled Nutation Damper .....	IV-10
IV-5	Digital Solar Aspect Sensor Alignment Angles Relative to Spacecraft Reference Axis .....	IV-13
IV-6	Scan Lines of Attitude Sensors .....	IV-15
IV-7	Pitch and Roll Sensor Electronics, Block Diagram .....	IV-16
IV-8	Attitude Sensor Configuration .....	IV-17
IV-9	Pitch Sensor Scan Geometry .....	IV-19
IV-10	Horizon Sensor Pre-Amplifier Output .....	IV-21
IV-11	Pitch Horizon Pulse Offset as a Function of Horizon Temperature Variation .....	IV-22
IV-12	Pitch Offset Versus Orbit .....	IV-23
IV-13	Orbital Coordinates .....	IV-25
IV-14	Spacecraft Coordinates and Attitude Angles .....	IV-25
IV-15	Unipolar Pulse Mode .....	IV-29
IV-16	Unipolar Torque Correction for Solar Pressure Disturbance .....	IV-30
IV-17	Magnetic Momentum Vector Control, Simplified Block Diagram .....	IV-32
IV-18	Momentum Change Versus Torquing Period (Single Coil) .....	IV-35
IV-19	Attitude Change Versus Torquing Period (Single Coil) .....	IV-37
IV-20	Geometry for Momentum Control Prior to Pitch Lock .....	IV-38
IV-21	Dipole Definition and Phasing for Momentum Control Prior to Pitch Lock .....	IV-39
IV-22	Commutation Time Versus Anomaly Angle .....	IV-41
IV-23	Time Between Required Momentum Coil Dipole Reversals Prior to Pitch Lock .....	IV-42
IV-24	Commutation Error Effect on Torquing Efficiency .....	IV-42
IV-25	Pitch Axis Control Loop, Operational Block Diagram .....	IV-44
IV-26	Geometry of Horizon Pulse and Reference Index Pulse .....	IV-46

## LIST OF ILLUSTRATIONS (Continued)

Figure		Page
IV-27	Open Loop Fine Gain Frequency Response of Single Axis Pitch Servo .....	IV-50
IV-28	Open Loop Coarse Gain Frequency Response of Single Axis Pitch Servo .....	IV-51
IV-29	Open Loop Frequency Response of Tachometer Loop ..	IV-52
IV-30	Digital Computer Simulation of Pitch Loop System ....	IV-54
IV-31	Typical Gain-Phase Presentation for G(s), F(s), and M(s) .....	IV-59
IV-32	Stability Study Worst-Case Results (Preliminary) .....	IV-62
IV-33	Error Detection .....	IV-66
IV-34	Operational Amplifier, Simplified Schematic Diagram .	IV-67
IV-35	Gain Switching Circuit, Block Diagram .....	IV-67
IV-36	Summing Amplifier, Simplified Schematic Diagram ....	IV-68
IV-37	Torque and Speed Characteristics for Inland Torque Motor Model T-4437A .....	IV-69
IV-38	Molecular Flow Loss of MWA Lubricant P-10 (Diethyl-Hexyl Sebacate) .....	IV-75
IV-39	Nutation Cone Angles Due to Transverse Momentum...	IV-88
V-1	ITOS D and E Power Supply Subsystem, Block Diagram .....	V-3
V-2	Solar Cell I-V Characteristics .....	V-10
V-3	Power Dissipation versus Shunt Current (per Shunt Dissipator) .....	V-11
V-4	Battery Pack, Schematic Diagram .....	V-13
V-5	Voltage (-24.5V) Regulator, Block Diagram .....	V-17
V-6	Shunt Limiter, Functional Block Diagram .....	V-18
V-7	Battery Charge Controller, Functional Block Diagram .	V-20
V-8	Specified Voltage Limit versus Temperature .....	V-21
V-9	ITOS D and E Acquisition and Pre-operational Load Current Profile .....	V-25
V-10	ITOS D and E Operational Load Current Profile .....	V-26
VI-1	Scanning Radiometer Subsystem, Block Diagram .....	VI-5
VI-2	SR Scan Projection .....	VI-6
VI-3	Scanning Radiometer, Block Diagram .....	VI-7
VI-4	SR Subsystem Timing .....	VI-11
VI-5	Scanning Radiometer, Optical Schematic .....	VI-13
VI-6	Scanning Radiometer, Detailed Optical Schematic .....	VI-13
VI-7	Aft Optics Assembly .....	VI-15
VI-8	IR Response versus Displacement Angle .....	VI-17
VI-9	Visible Channel, Relative Spectral Response .....	VI-18
VI-10	IR Channel, Relative Spectral Response .....	VI-18
VI-11	Scanner Housing Module, Outline Dimensions .....	VI-21

## LIST OF ILLUSTRATIONS (Continued)

Figure		Page
VI-12	Settling Time of Channel Amplifiers .....	VI-25
VI-13	Lenticular Lens Dispersing Characteristics .....	VI-27
VI-14	Sample Lens, Transmission Curve .....	VI-27
VI-15	Scanning Radiometer Mounted on ITOS D and E Showing Locations of Transmitting and Reflecting Targets .....	VI-28
VI-16	Typical Scan Line Showing Timing of Electrically Generated Functions .....	VI-32
VI-17	Composite Signal of Both IR and Visible Channel .....	VI-34
VI-18	Very High Resolution Radiometer, Optics Schematic ..	VI-35
VI-19	Relative Spectral Response of Visible Channel VHRR ..	VI-36
VI-20	Relative Spectral Response of IR Channel of VHRR....	VI-37
VI-21	VHRR Electronics, Block Diagram .....	VI-39
VI-22	Calibration Step Voltage Timing Chart .....	VI-43
VI-23	Timing Diagram-Dual Polarity Pulse Circuits .....	VI-44
VI-24	Typical IR Scan Line Timing Chart .....	VI-45
VI-25	Motor Drive, Block Diagram .....	VI-46
VI-26	Scan Motor Drive System, Block Diagram .....	VI-47
VI-27	Brushless DC Torque Motor Drive .....	VI-48
VI-28	VTPR Outputs .....	VI-53
VI-29	Full Calibration Sequence .....	VI-54
VI-30	VTPR Optics .....	VI-59
VI-31	VTPR Block Diagram of Electrical Circuits .....	VI-61
VI-32	Cam Scanning Electronics, Timing Diagram .....	VI-68
VI-33	Detector Response to Protons, Electrons, and Alpha Particles .....	VI-71
VI-34	SPM Sensor Units .....	VI-73
VI-35	Data Sync Modification (SPM) .....	VI-78
VII-1	SRPR Input-Output Data Format .....	VII-3
VII-2	SRPR Functional Block Diagram .....	VII-6
VII-3	IR Channel Commutator, Simplified Diagram .....	VII-9
VII-4	Time-Code Buffer, Block Diagram .....	VII-10
VII-5	Eight-Stage Divide Chain, Simplified Block Diagram...	VII-11
VII-6	Sample-and-Hold Network, Simplified Block Diagram ..	VII-12
VII-7	Signal-Select Mode Network .....	VII-13
VII-8	Balanced Modulator System, Block Diagram .....	VII-13
VII-9	VHRR Processor Configuration .....	VII-18
VII-10	Control Translator (CT), Schematic Representation....	VII-21
VII-11	Signal Routing Unit (SRU), Schematic Representation ..	VII-21

## LIST OF ILLUSTRATIONS (Continued)

Figure		Page
VII-12	Power Routing Unit (PRU), Schematic Representation ...	VII-22
VII-13	Signal Conditioning Functions (Channel No. 1 Only), Block Diagram .....	VII-23
VII-14	Recorded Data Word Sequence .....	VII-25
VII-15	Recorded Digital Frame .....	VII-26
VII-16	Recorded Time Code Words .....	VII-26
VII-17	Digitized Telemetry Word .....	VII-27
VII-18	Digital Sensor and DDP Interface .....	VII-28
VII-19	Real-Time Telemetry Frame, Normal Mode .....	VII-30
VII-20	DDP Interface Diagram .....	VII-40
VII-21	Standard Interface .....	VII-43
VII-22	Relay Closure Output .....	VII-43
VII-23	Grounded Base Transistor Output .....	VII-44
VII-24	LP/DTL Output .....	VII-44
VII-25	Analog Telemetry Output .....	VII-44
VII-26	CDU Command Output .....	VII-45
VII-27	Digital Data Processor, Block Diagram .....	VII-46
VII-28	Signal Electronics, Block Diagram .....	VII-54
VII-29	Flutter-to-Torque Ratio versus Frequency .....	VII-62
VII-30	Simplified Servo Drive, Block Diagram .....	VII-63
VIII-1	Command Subsystem Block Diagram .....	VIII-3
VIII-2	Decoder Input and Output Interfaces .....	VIII-10
VIII-3	Decoder Logic Flow Diagram .....	VIII-15
VIII-4	ITOS D and E Decoder Block Diagram .....	VIII-18
VIII-5	Decoder Timing Diagram .....	VIII-19
VIII-6	Time Base Unit Interface Diagram .....	VIII-25
VIII-7	Time Base Generator Logic Diagram .....	VIII-27
VIII-8	Time Code Generator Block Diagram .....	VIII-28
VIII-9	Time Code Outputs - Timing Diagram .....	VIII-30
VIII-10	Programmer Block Diagram .....	VIII-33
VIII-11	VHRR Record Timing Diagram .....	VIII-38
VIII-12	Proportional QOMAC Cycle .....	VIII-41
VIII-13	Dual Command Programmer Interface Diagram .....	VIII-45
VIII-14	Typical CDU Decoding Gate, Schematic Diagram .....	VIII-50
VIII-15	Decoder and CDU Interconnections .....	VIII-50
VIII-16	Dual Time Base Unit Selection .....	VIII-52
VIII-17	Programmer Selection .....	VIII-53
VIII-18	SR Control Logic .....	VIII-55
VIII-19	SR Processor Control .....	VIII-56
VIII-20	SRR Selection Logic .....	VIII-59
VIII-21	SRR Command Decoding Logic .....	VIII-60
VIII-22	VHF Real-Time Transmitter Control Logic .....	VIII-63

LIST OF ILLUSTRATIONS (Continued)

Figure		Page
VIII-23	VTPR Control Logic .....	VIII-64
VIII-24	VHRR Subsystem Control Logic .....	VIII-67
VIII-25	VHRR Recorder Control Logic .....	VIII-71
VIII-26	S-Band Transmitter Subsystem Control .....	VIII-73
VIII-27	QOMAC and Magnetic Bias Coil Control Logic .....	VIII-75
VIII-28	Momentum Coil Control Logic .....	VIII-77
VIII-29	Squib Firing Control Logic .....	VIII-78
VIII-30	Digital Data Processor Control Logic .....	VIII-80
VIII-31	3900 Hz SCO Beacon Telemetry Control .....	VIII-83
VIII-32	Beacon 3900 Hz SCO Telemetry Operation .....	VIII-85
VIII-33	Beacon 2300 Hz SCO Telemetry Operations .....	VIII-86
IX-1	Command Link .....	IX-3
IX-2	Command Receiver Block Diagram .....	IX-7
IX-3	Beacon and Telemetry Link Block Diagram .....	IX-9
IX-4	Data Verification of a Valid Command .....	IX-14
IX-5	Data Verification Response to an Invalid Command ...	IX-14
IX-6	Solar Proton Monitor Real-Time Data Characteristics .	IX-16
IX-7	Typical Roll Sensor and Pitch Index Telemetry .....	IX-18
IX-8	Dual Subcarrier Oscillator .....	IX-22
IX-9	Beacon Transmitter .....	IX-23
IX-10	Beacon and Command Antenna Group .....	IX-25
IX-11	VHF Real-Time Link, Spacecraft Equipment .....	IX-28
IX-12	VHF Real-Time Link, Typical APT Ground Station Equipment .....	IX-29
IX-13	SR Sensor Signal Characteristics Prior to Processing by SR Processor and Time Multiplexing of Channels by SR Tape Recorder .....	IX-31
IX-14	SR Signal Characteristics after Processing by the SR Processor .....	IX-32
IX-15	SRR Time Multiplexing Circuits, Simplified Block Diagram .....	IX-34
IX-16	SR Signal Characteristics After Time Multiplexing by SR Recorder .....	IX-35
IX-17	Real-Time Transmitter .....	IX-37
IX-18	S-Band Real-Time Video Link, Spacecraft Equipment .....	IX-40
IX-19	S-Band Real-Time Link, Typical Local User Ground Station Equipment .....	IX-41
IX-20	VHRR Signal Characteristics Prior to Time Multiplex- ing of IR and Visible Signals .....	IX-42
IX-21	Time Multiplexed IR and Visible Signals from the VHRR Sensors .....	IX-43

## LIST OF ILLUSTRATIONS (Continued)

Figure		Page
IX-22	VHRR Processor, Output Spectrum .....	IX-45
IX-23	ITOS D and E S-Band Transmitter .....	IX-47
IX-24	S-Band Playback Link, Spacecraft Equipment, Block Diagram .....	IX-51
IX-25	S-Band Playback Link, CDA Station Equipment, Block Diagram .....	IX-52
IX-26	Composite Playback Spectrum .....	IX-53
IX-27	SR Recorder — MUX Interface .....	IX-61
IX-28	Dual Multiplexer, Block Diagram .....	IX-63
X-1	General Unit Test Flow .....	X-2
X-2	ITOS D and E Spacecraft Test and Calibration Program .....	X-3
XI-1	Data Processing and Analysis Facility at NESC, Suitland, Md., Block Diagram .....	XI-5
XI-2	DAPAF Signal Processing Subsystem, Block Diagram .....	XI-7
XI-3	S-Band Data Handling of CDA Stations, Block Diagram .....	XI-17
XI-4	Demultiplexer, Block Diagram .....	XI-19
XI-5	New Rack Configuration to Accommodate ITOS D and E Demultiplexer Chassis .....	XI-20
XI-6	Ground Processing of VHRR Signal, Modified Block Diagram .....	XI-31
XI-7	Ground Processing of Digital Data Signals, Modified Block Diagram .....	XI-32
XI-8	Ground Processing of Scanning Radiometer Signal, Modified Block Diagram .....	XI-33
XI-9	Long Lines Communications System .....	XI-35
XI-10	Long Lines Channel Allocations .....	XI-36
XI-11	Long Line Transmission Time for One and Two Orbits .....	XI-37
	Prototype Thrust Sine Vibration Level .....	A-3
	Prototype Lateral Sine Vibration Levels .....	A-4
	Design Random Vibration Levels — Prototype .....	A-5
	Composite Subcarrier Spectrum of Demodulated Beacon and Telemetry Baseband .....	C-17
D-1	S-Band Antenna Test Model .....	D-2
D-2	Antenna Coordinates .....	D-3
D-3	Antenna No. 1 Pattern for $\beta = 0^\circ, 180^\circ$ Plane .....	D-4
D-4	Antenna No. 1 Envelope of Patterns for $\beta = 22-1/2^\circ$ to $167-1/2^\circ$ Planes .....	D-4
D-5	Antenna No. 2 Pattern for $\beta = 0^\circ, 180^\circ$ Plane .....	D-6

LIST OF ILLUSTRATIONS (Continued)

Figure		Page
D-6	Antenna No. 2 Envelope of Patterns for $\beta = 22-1/2^\circ$ to $167-1/2^\circ$ Planes .....	D-6
D-7	ITOS D and E, Antenna No. 1, Directivity Contours Relative to RHC Isotropic .....	D-7
D-8	ITOS D and E Antenna No. 2, Directivity Contours Relative to RHC Isotropic .....	D-7
D-9	TIROS M ETM Antenna, Directivity Contours Relative to RHC Isotropic. (For Gain, Subtract 3 dB for Hybrid and 1.3 dB Circuit Losses.) .....	D-8
D-10	TIROS M S-Band Antenna, Directivity Contours for Antenna without Spacecraft Relative to RHC Isotropic .....	D-8

## LIST OF TABLES

Table		Page
I-1	Spacecraft Subsystem Complement .....	I-24
I-2	Command Link Characteristics .....	I-26
I-3	Beacon Link Characteristics .....	I-26
I-4	Real-Time VHF Link Characteristics .....	I-28
I-5	S-Band Playback Link Characteristics .....	I-29
I-6	S-Band Real-Time Link Characteristics .....	I-30
I-7	Particulars of the ITOS Nominal Orbit .....	I-32
II-1	ITOS D and E Spacecraft, Estimated Weight Summary .....	II-13
II-2	Actuator Sensor Characteristics .....	II-35
II-3	Mechanical and Physical Parameters of ITOS D and E .....	II-40
III-1	Spacecraft Thermal Control System Performance Requirements .....	III-4
III-2	Thermal Paint Specifications .....	III-8
III-3	ITOS D and E Operational and Acquisition Flight Temperature Predictions .....	III-13
IV-1	Damping Time Constants .....	IV-12
IV-2	Cross-Coupling Parameters Worst-Case Combinations .....	IV-60
IV-3	Pitch Servo Parameters Matrix .....	IV-61
IV-4	PCS Electronic Specifications .....	IV-64
IV-5	Operational Power Requirements .....	IV-76
IV-6	Summary of Disturbance and Effects .....	IV-78
IV-7	Rotating Component Disturbances .....	IV-90
V-1	Summary of ITOS D and E Power Supply Subsystem Parameters .....	V-4
V-2	Summary of Telemetry Characteristics .....	V-22
VI-1	Scanning Radiometer Parameters .....	VI-4
VI-2	VHRR Characteristics .....	VI-30
VI-3	Decoder Functions .....	VI-41
VI-4	Voltage Calibration Levels .....	VI-55
VI-5	Radiometer Filter Characteristics at 35° C .....	VI-63
VI-6	Solar Proton Monitor Detector Characteristics .....	VI-70
VII-1	Video, Telemetry Timing States .....	VII-5
VII-2	SR Processor Input and Output Functions .....	VII-7
VII-3	VHRRP Real-Time Operating Modes .....	VII-9
VII-4	S-Band Transmitter Deviations for the VHRRP Operating Modes .....	VII-20
VII-5	Signals Sent to VHRRR as a Function of Mode Selected .....	VII-24

## LIST OF TABLES (Continued)

Table		Page
VII-6	Commutator Inputs for Real-Time Telemetry .....	VII-31
VII-7	DDP Interface Signal Inputs .....	VII-41
VII-8	DDP Interface Signal Outputs .....	VII-42
VII-9	SR Recorder Command and Control Signals .....	VII-55
VII-10	SR Recorder Characteristics .....	VII-56
VII-11	Record Mode Required Torque .....	VII-64
VII-12	Playback Mode Maximum Required Torque .....	VII-65
VII-13	VHRR Recorder Characteristics .....	VII-72
VII-14	VHRR Tape Recorder Signal Data .....	VII-74
VII-15	VHRR Recorder and Spacecraft Interface Signals .....	VII-75
VIII-1	ITOS D and E Commands .....	VIII-4
VIII-2	Decoder Output Interface Signals .....	VIII-11
VIII-3	Decoder Data Format .....	VIII-13
VIII-4	Counter States .....	VIII-22
VIII-5	T <sub>0</sub> Word Format .....	VIII-35
VIII-6	Rephasing Word Format .....	VIII-36
VIII-7	QOMAC Program Word Format .....	VIII-39
VIII-8	Dual Command Programmer Inputs .....	VIII-44
VIII-9	Programmer Outputs .....	VIII-46
VIII-10	VHRR Control Function Activation Corresponding to S/C Commands .....	VIII-66
VIII-11	VHRR Modes .....	VIII-69
VIII-12	Telemetry Priorities .....	VIII-82
IX-1	Summary of ITOS D and E Communications Links .....	IX-2
IX-2	Command Receiver Specifications .....	IX-6
IX-3	Types of Telemetry Allocated to 3.9-kHz SCO .....	IX-10
IX-4	Types of Telemetry Allocated to 2.3-kHz SCO .....	IX-11
IX-5	Dual SCO Assembly Characteristics .....	IX-20
IX-6	Beacon Transmitter Specifications .....	IX-24
IX-7	VHF Real-Time Transmitter Specifications .....	IX-36
IX-8	Abbreviated Specifications of ITOS D and E S-Band Transmitter .....	IX-46
IX-9	VHRR Recorder Channel Assignments .....	IX-54
IX-10	VHRR Channel Signal Parameters .....	IX-55
IX-11	SR Channel Signal Parameters .....	IX-57
IX-12	Digital Channel Signal Parameters .....	IX-58
IX-13	MUX Input Signals .....	IX-60
IX-14	SRR Playback Selection Modes .....	IX-62
IX-15	MUX Output Signals .....	IX-64

LIST OF TABLES (Continued)

Table		Page
IX-16	S-Band Carrier Deviations and Resultant RF Link Baseband S/N Ratios .....	IX-65
IX-17	Overall Baseband Signal-to-Noise Ratios of Playback Video Channels .....	IX-66
X-1	Temperatures and Durations for Thermal-Vacuum Testing .....	X-4
XI-1	Control and Indicator Interface .....	XI-12
XI-2	Demultiplexer Functional Parameters .....	XI-16
XI-3	Tape Recorder Channel Assignments .....	XI-22
XI-4	Long Line Channel Data .....	XI-23
XI-5	Demodulator Signal Characteristics .....	XI-24
XI-6	Characteristics of Long Lines Data Channels .....	XI-36
C-1	Slant Ranges for Circular Orbit .....	C-2
C-2	Path Loss for Command Link as a Function of Elevation Angle .....	C-4
C-3	Worst-Case RF Command Link Calculation .....	C-5
C-4	Improvement in Command RF Signal Margins with Various Alternate Command Transmitter/Antenna Combinations .....	C-7
C-5	Required Worst-Case Command Receiver IF Bandwidth ....	C-9
C-6	Interface Levels at the Command Receiver Port .....	C-10
C-7	Subcarrier-to-Noise Ratios at Receiver AGC Threshold ...	C-14
C-8	Principal Distortion Products and Relative Amplitude.....	C-18
C-9	CDA Ground Station Parameters (Beacon Reception).....	C-19
C-10	Subcarrier Noise Power Computations .....	C-20
C-11	Modulation Loss of Beacon Subcarriers .....	C-20
C-12	Worst-Case RF Beacon Link Calculation .....	C-22
C-13	Worst-Case Link Calculation for 3.9 kHz Channel .....	C-23
C-14	Worst-Case Link Calculation for 2.3 kHz Channel .....	C-24
C-15	S/N Contribution by the Long Lines .....	C-25
C-16	Real-Time Link Parameters (Field Stations) .....	C-26
C-17	Worst-Case Baseband S/N Ratios of VHF Real-Time System at the Field Stations .....	C-29
C-18	Variation of RF Margin with Elevation and Nadir Angles .....	C-32
C-19	Worst-Case S-Band Real-Time Link Calculation .....	C-34
C-20	VHRR Real-Time Subcarrier S/N Ratios .....	C-34

LIST OF TABLES (Continued)

Table		Page
C-21	VHRR Real-Time Link Baseband S/N Ratios .....	C-35
C-22	Summary of VHRR Real-Time Ground Station RF Parameters .....	C-35
C-23	Overall S/N Ratios VHRR Real-Time Data .....	C-36
C-24	CDA Station RF Parameters .....	C-37
C-25	Worst-Case S-Band Playback Link Calculation .....	C-39
C-26	Worst-Case Subcarrier Signal-to-Noise Ratios, S-Band Playback Link .....	C-40
C-27	Baseband S/N Ratios of S-Band Playback Link .....	C-43
C-28	Worst-Case Overall SR Baseband S/N Ratios at DAPAF End of Long Lines .....	C-45
C-29	Worst-Case Overall VHRR S/N Ratio at DAPAF End of Long Lines .....	C-46

# APPENDIX A

## ITOS D AND E STRESS ANALYSIS

### I. INTRODUCTION

The analysis presented in this appendix provides verification that the ITOS D and E structure can safely withstand the design load levels with a safety factor of 1.15 without permanent deformation and with a safety factor of 1.25 without failures. The design loads in the analysis are for full vibration levels although the actual input levels may be notched to protect the MDAC attachment fitting during qualification tests as was done for TIROS M (Ref. C, steps 33 and 55).

The ITOS D and E specified input levels are two-thirds of the TIROS M test levels at the structural natural resonances. (See pages A3 to A5 for a comparison of these loadings.) The margins of safety for structural parts that are common to both the ITOS D and E and TIROS M have been adjusted to reflect this decrease in load, and are summarized in Section III on pages A11 and A12. The redesigned front panel and other structural elements affected by the front panel redesign have their margins of safety listed on page A10.

The top section of the front panel has been stiffened by increasing the depth of the panel from .88 inch to 1.50 inches in this region. This has been done to keep the local lateral frequency of the top section, which now supports black boxes, above 28 Hz and thereby preventing any undesirable vibration coupling with the spacecraft lateral resonances which would tend to drive the ITOS spacecraft resonance below the desired minimum value of 20 Hz. The top section is stress analyzed for an anticipated amplification response factor of  $Q=10$  (Ref. page A13) and has large margins of safety.

The sides of the front panel have large longitudinal slots for Vertical Temperature Profile Radiometer (VTPR) fields of view. This region has been suitably reinforced by enclosing the periphery of the slot with a channel section and by adding an additional skin to the free channel flange side. This area is critical for sinusoidal vibration inputs in the lateral Y-Y direction at the spacecraft resonant frequency (Ref. page A20).

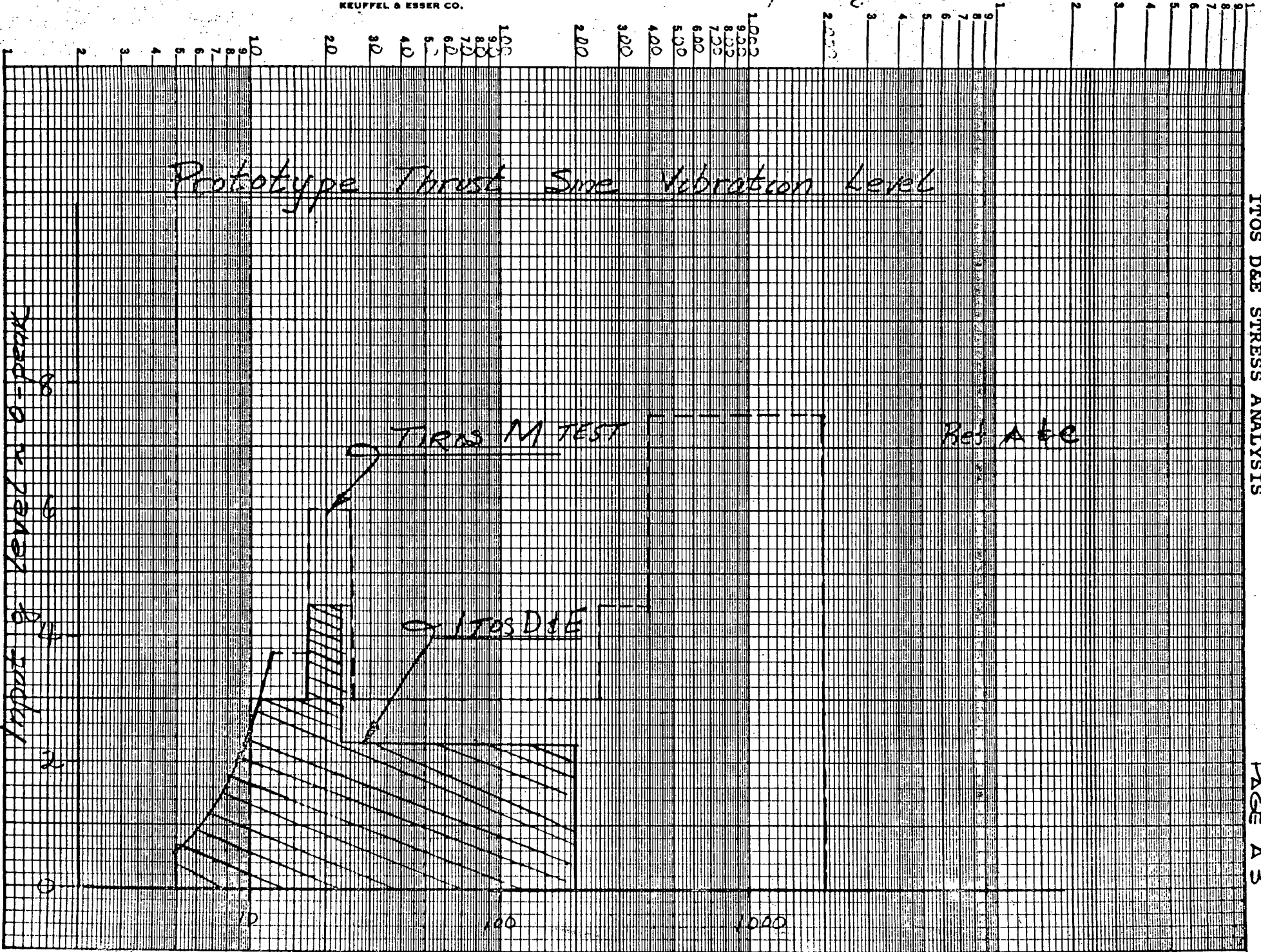
The bottom portion of the front panel supports two 35-pound Very High Resolution Radiometers (VHRR)\*. These units are mounted on channel-shaped beams which are attached to the front panel. A brace located at the centerline of the front panel and attached to the baseplate provides additional support for the VHRR's. The stress analysis for the loads from the VHRR's starts on page A28. In addition, the bottom portion of the front panel is also checked for the overall spacecraft loadings (Ref. page A25).

\*This analysis was made with these VHRR weights. The VHRR's are now lighter (i.e. 20 pounds instead of 35 pounds).

As in TIROS M, analysis sinusoidal vibrations are the critical environmental conditions. The ITOS D and E structure has also been analyzed for a constant-acceleration unidirectional load in thrust (Ref. pages A47 to A54). The structure can safely withstand a maximum constant load of 28.2g.

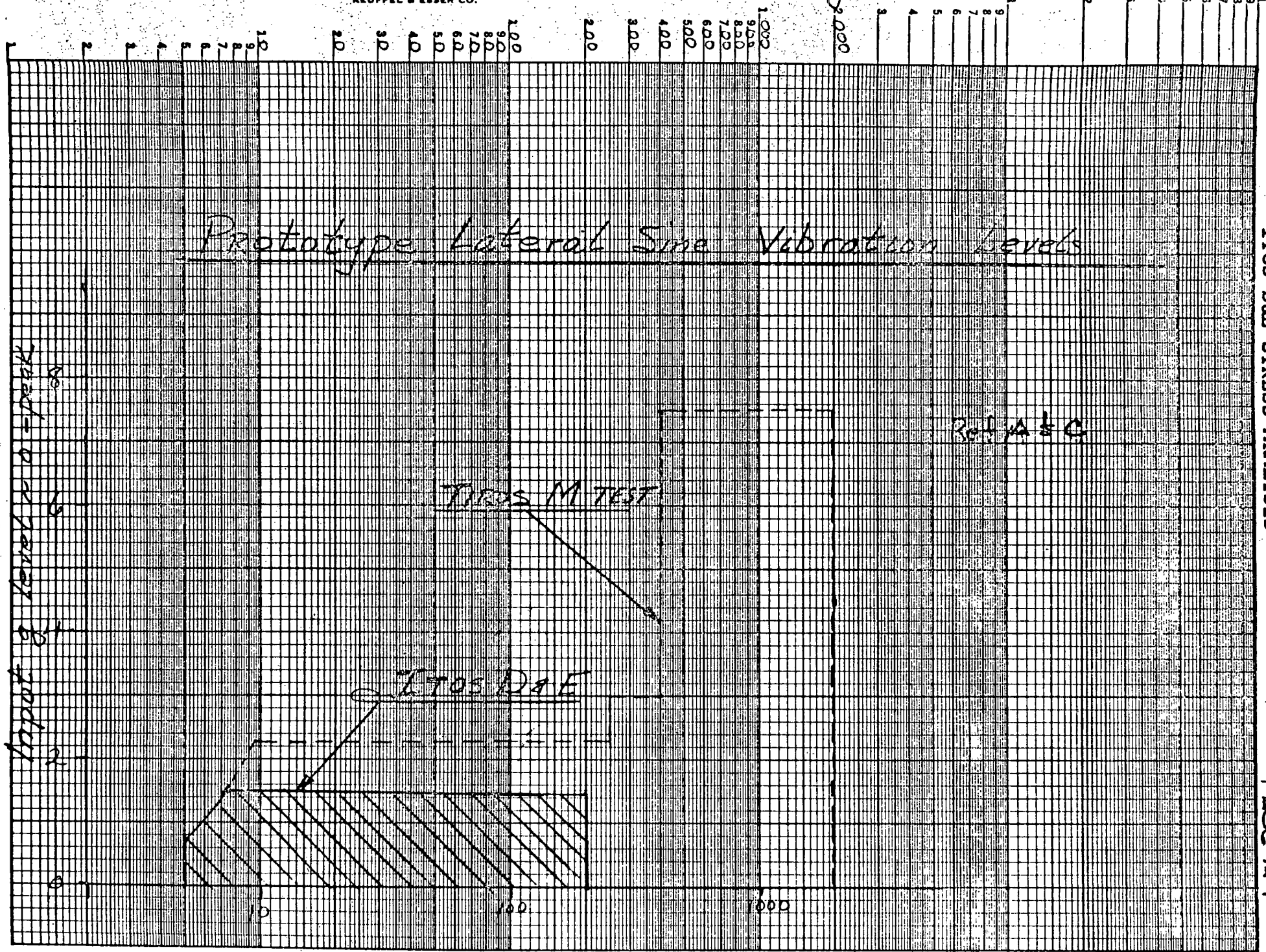
Weight reduction of the two VHRR's from a total of 70 pounds to 39.4 pounds, plus the relocation of the VHRR's on the earth viewing access panel, has eliminated the need for the channel-shaped brackets, (pages A-29 to A-46).

Frequency - Hz



# Prototype Lateral Sine Vibration Levels

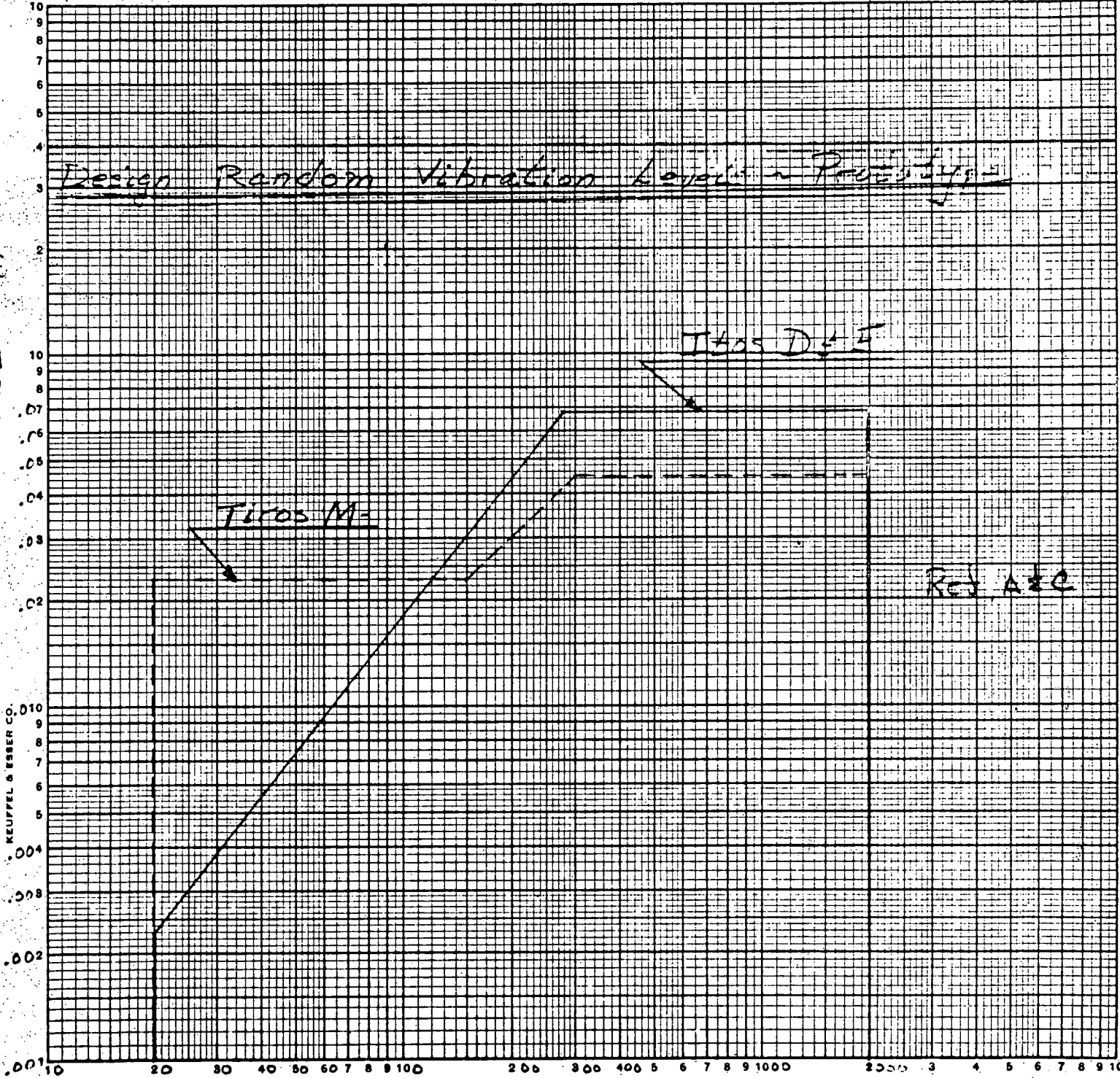
Input level is peak to peak



Frequency ~ Hz

PSD = 21/1E

KE LOGARITHMIC 46 7403  
3 X 3 CYCLES  
MADE IN U.S.A.  
KEUFFEL & ESSER CO.



Frequency ~ Hz



Astro Electronics  
Division

Princeton, New Jersey

Prepared for: \_\_\_\_\_ Report No. \_\_\_\_\_

Approved: \_\_\_\_\_ Project: \_\_\_\_\_

Date: \_\_\_\_\_ Contract No. \_\_\_\_\_

Subject: ITOS D&E STRESS ANALYSIS Page No. A6 of \_\_\_\_\_

## II. LIST OF SYMBOLS

M.S.	Margin of Safety
K	Load Factor
Res.	Resonance
I	Moment of Inertia (in. <sup>4</sup> )
f	Actual Stress (lbs/in. <sup>2</sup> )
F	Allowable Stress (lbs/in. <sup>2</sup> )
A	Area (in. <sup>2</sup> )
P	Load (lbs)
$\ell, L$	Length (in.)
y	Deflection (in.)
fn	Natural Frequency (Hz) (CPS)
W	Weight (lbs)
g, G	Gravitational Constant (32.2 ft/sec <sup>2</sup> )
V	Shear (lbs)
M	Bending Moment (in. lbs)
E	Young's Modulus (lbs/in. <sup>2</sup> )
Q	Amplification Factor
R	Reaction Load (lbs)
b	Width (in.)
t	Thickness (in.)
C	Distance to Outermost Fibers (in.)
T	Torque (lb in.)
N	Maximum Allowable Constant Acceleration Level in Thrust (Number of g's)



Astro Electronics  
Division  
Princeton, New Jersey

Prepared for: \_\_\_\_\_ Report No. \_\_\_\_\_  
Approved: \_\_\_\_\_ Project: \_\_\_\_\_  
Date: \_\_\_\_\_ Contract No. \_\_\_\_\_  
Subject: ITOS D&E STRESS ANALYSIS Page No. A7 of \_\_\_\_\_

---

w	Load per Unit Area (lbs/in. <sup>2</sup> )
m	Reciprocal of Poisson's Ratio
M'	Bending Moment per Unit Length (in lb./in.)

SUBSCRIPTS

Fat	Fatigue
cr	Crippling
x, y, z	Coordinate Directions
b	Bending
t	Axial, tension
f	Flange
s	Shear Direction
n	Normal Direction
su	Shear Ultimate
All	Allowable
TOT	Total
br	Bearing



Astro Electronics  
Division

Princeton, New Jersey

Prepared for: \_\_\_\_\_ Report No. \_\_\_\_\_

Approved: \_\_\_\_\_ Project: \_\_\_\_\_

Date: \_\_\_\_\_ Contract No. \_\_\_\_\_

Subject: ITOS D&E STRESS ANALYSIS Page No. A8 of \_\_\_\_\_

### III. TABLE OF MINIMUM MARGINS OF SAFETY

THE MARGINS OF SAFETY (M.S.) LISTED IN THIS REPORT ARE CALCULATED FROM THE FOLLOWING RELATIONSHIP:

$$M.S. = \frac{\text{ALLOWABLE STRESS}}{\text{ACTUAL STRESS} \times F.S.} - 1$$

WHERE: F.S. = FACTOR OF SAFETY

WHEN THE ALLOWABLE STRESS IS THE ULTIMATE OR FRACTURE STRENGTH OF THE MATERIAL, THE F.S. USED IS 1.25. WHEN THE ALLOWABLE IS THE YIELD STRENGTH OF THE MATERIAL, THE F.S. USED IS 1.15. OF THESE TWO MARGINS OF SAFETY ONLY THE LOWEST IS REPORTED.

MARGINS OF SAFETY FOR ITEMS NOT MODIFIED FROM TIROS M WERE OBTAINED IN THE FOLLOWING MANNER USING LOAD FACTOR  $K = \text{TIROS M LOAD} / \text{ITOS D\&E LOAD}$

$$(M.S.)_{\text{ITOS D\&E}} = \left[ 1 + (M.S.)_{\text{TIROS M}} \right] K - 1$$

THE TIROS SINUSOIDAL VIBRATION INPUTS ARE: 1.5 X ITOS D&E VIBRATION INPUTS. REF P6.A3 & A4

1) FOR TIROS M ITEMS CRITICAL AT SPACECRAFT RESONANCES

$$K = 1.5 \left( \frac{\text{TIROS M WEIGHT}}{\text{ITOS D\&E WEIGHT}} \right) = 1.5 \times \left( \frac{720}{770} \right) = 1.4$$



Astro Electronics  
Division  
Princeton, New Jersey

Prepared for: \_\_\_\_\_ Report No. \_\_\_\_\_  
Approved: \_\_\_\_\_ Project: \_\_\_\_\_  
Date: \_\_\_\_\_ Contract No. \_\_\_\_\_  
Subject: ITCS DCS STRESS ANALYSIS Page No. A9 of \_\_\_\_\_

2) FOR ITEMS CRITICAL AT LOCAL RESONANCE  
 $K = 1.5$

SINCE THE ITEMS NOT ANALYZED IN THIS  
REPORT REMAINED THE SAME AS IN TIRDS M,  
IT IS VALID TO RATIO THE MARGINS OF  
SAFETY AS EXPLAINED ABOVE.



Astro Electronics  
Division

Princeton, New Jersey

Prepared for: \_\_\_\_\_

Report No. \_\_\_\_\_

Approved: \_\_\_\_\_

Project: \_\_\_\_\_

Date: \_\_\_\_\_

Contract No. \_\_\_\_\_

Subject: **ITOS D&E STRESS ANALYSIS**

Page No. **A10**

## CRITICAL MARGINS OF SAFETY FOR CHANGED STRUCTURE

ITEM	CRITICAL CONDITION	TYPE OF STRESS	REF. P.	M.S.
<u>FRONT PANEL</u>				
TOP CHANNEL	Y EXCITATION 3/4 RES.	BENDING FATIGUE	A17	1.54
STRINGER	Y EXCITATION 5/8 RES	BENDING CRIPPLING	A17	1.37
WEB	LAT. EXCITATION 3/4 RES.	SHEAR BUCKLING	A23	.83
CHANNEL	Y EXCITATION 3/4 RES.	AXIAL FATIGUE	A27	.31
BKT ATTACHMENTS	X EXCITATION PANEL RES.	RIVET TENSION	A31	.16
VHRR BKTS.	Z EXCITATION PANEL RES.	BENDING FATIGUE	A40	.15
<u>BASEPLATE</u>				
RIB	Z EXCITATION PANEL RES.	BENDING CRIPPLING	A45	1.34

## CRITICAL MARGINS OF SAFETY FOR UNCHANGED STRUCTURE

ITEM	TIROS M DWB NO.	CRITICAL CONDITION	TYPE OF STRESS	TIROS M MS	TIROS D/E MS
<u>BASEPLATE</u>					
RIB	-6	Z EXCIT. PANEL RES.	BENDING - CRIPPLING	.87	.91
INTERCOSTAL	-7,8	Z EXCIT. PANEL RES.	RIVET BRG. AT SPLICE	.17	.76
EQUIP. CHANNEL	-4	X EXCIT. S/C RES.	BENDING YIELD	.09	.53
BASEPLATE & CHANNEL	-2,3	Y EXCIT S/C RES.	BENDING YIELD	.03	.44
SKIN	-22	Z EXCIT PANEL RES.	BENDING CRIPPLING	.27	.91
RIB	-6	Z EXCIT PANEL RES.	TORSION	.00	.50
<u>EQUIPMENT PANEL</u>					
INTERNAL CHANNEL	-9,10,16	X EXCIT. PANEL RES.	BENDING CRIPPLING	.86	.89
INTERNAL CHANNEL	-9,10,16	X EXCIT. PANEL RES.	RIVET BRG. AT SPLICE	.01	.52
VERTICAL CHANNEL	-5,6	X EXCIT S/C RES.	AXIAL BUCKLING	.32	.85
SKIN	-11	Y EXCIT. S/C RES.	SHEAR BUCKLING	.00	.40
TOP CHANNEL	-3	X EXCIT. PANEL RES.	BENDING FATIGUE	.53	1.30
<u>BACK PANEL</u>					
INTERCOSTAL	-5	X EXCIT. S/C RES.	BENDING CRIPPLING	.31	.83
RIB	-27	Y EXCIT S/C RES.	BENDING FATIGUE	.14	.60
BRACE	-40	Y EXCIT S/C RES.	ATTACHMENTS	.06	.48
SKIN	-17	Y EXCIT S/C RES.	SHEAR BUCKLING	.40	.96
<u>SEPARATION RING ADAPTOR</u>					
"	-2	LAT EXCIT S/C RES.	BUCKLING AT CENTER	.41	.97
"	-2	"	FAT. NEAR VEE CLAMP	.09	.53
"	-2	"	FAT UPPER WEB	.09	.53
"	-2	"	FAT UPPER FLANGE	.09	.53

Prepared for: \_\_\_\_\_

Report No. \_\_\_\_\_

Approved: \_\_\_\_\_

Project: \_\_\_\_\_

Date: \_\_\_\_\_

Contract No. \_\_\_\_\_

Subject: \_\_\_\_\_

TIROS D/E STRESS ANALYSIS

Page No. 51

ALL



Astro Electronics  
Division

Princeton, New Jersey

Prepared for: \_\_\_\_\_

Report No. \_\_\_\_\_

Approved: \_\_\_\_\_

Project: \_\_\_\_\_

Date: \_\_\_\_\_

Contract No. \_\_\_\_\_

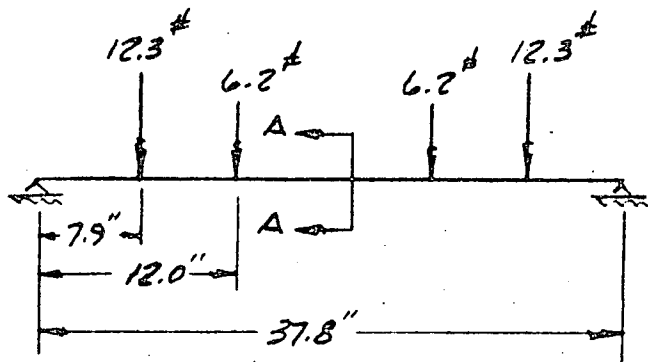
Subject: **TIROS DAE STRESS ANALYSIS**

Page No. **A12** of \_\_\_\_\_

ITEM	TIROS M Dwg. NO.	CRITICAL CONDITION	TYPE OF STRESS	TIROS M MS	TIROS DAE MS
<u>CROSS BRACE</u> CHANNELS	1769716 -	2 EXCIT PANEL RES.	BENDING FATIGUE	.20	.80
SPLICE AT CENTER	-5,6,7,25	2 EXCIT PANEL RES.	RIVET BRG. YIELD	.08	.62
END ATTACH.	"	2 EXCIT PANEL RES.	RIVET BRG. YIELD	.30	.95
KNEE BRACE	"	2 EXCIT PANEL RES.	ATTACH BRG.	.11	.67
<u>SOLAR PANEL</u> HONEYCOMB	1769625 -	LAT. EXCIT PANEL RES.	INTER CELL BUCKLING	.06	.59
DAMPEN ATTACH	-1,2,3	X EXCIT. SIG RES.	BRG YIELD	.26	.76
<u>BASEPLATE P&amp;T.</u>	1762711-1	2 EXCIT. PANEL RES.	BENDING FATIGUE	.31	.97

IV. FRONT PANEL

THE MOST CRITICAL LOADING IN THE TOP SECTION IS DUE TO THE RADIOMETERS AND TWO BLACK BOXES MOUNTED TO THE TOP CHANNEL AND FIRST STRINGER. THESE ITEMS WILL BE SUBJECTED TO A LATERAL LOADING OF 1.5 G AT A Q OF 10. DURING LATERAL SINE VIBRATION. (REF B)



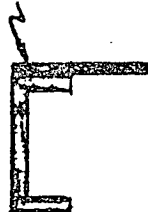
RADIOMETERS = 12.3<sup>±</sup> EA.  
BLACK BOXES = 6.2<sup>±</sup> EA.

THE MAXIMUM MOMENT WILL OCCUR AT MID SPAN AND IS EQUAL TO :

$$M = 1.5(10) [12.3(7.9) + 6.2(12.)] = 2578 \text{ IN LBS.}$$

THIS MOMENT ACTS ON THE SECTION A-A AND IS DISTRIBUTED TO EACH BEAM IN THE SECTION IN PROPORTION TO THE INERTIAS.

TOP CHANNEL



STRINGER



$$I_c = .105 \text{ IN}^4$$

$$I_s = .0734 \text{ IN}^4$$

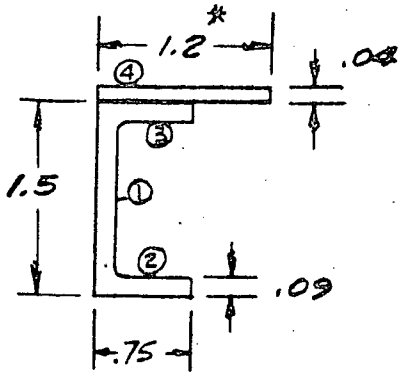
$$I_{tot} = .1784 \text{ IN}^4$$

SECTION A-A

REF. P. A14, A15

## TOP CHANNEL - SECTION PROPERTIES

\* EFFECTIVE SKIN WIDTH = 30%



ITEM	A	Y	AY	AY <sup>2</sup>	I <sub>0</sub>
① 1.5 x .09	.135	.75	.1012	.076	.0253
② .66 x .09	.0594	.045	.0027	.00012	.000004
③ .66 x .09	.0594	1.455	.0867	.126	.000004
④ 1.2 x .04	.048	1.52	.073	.111	.00001
$\Sigma$	.2978		.2636	.3131	.0254

$$\bar{Y} = \frac{\Sigma AY}{\Sigma A} = \frac{.2636}{.2978} = .886 \text{ IN.}$$

$$I_y = \Sigma AY^2 + \Sigma I_0 - (\Sigma AY) \bar{Y}$$

$$I_y = .3131 + .0254 - (.2636)(.886)$$

$$I_y = .105 \text{ IN}^4$$

ITEM	A	X	AX	AX <sup>2</sup>	I <sub>0</sub>
① 1.5 x .09	.135	.045	.006	.00027	.000009
② .66 x .09	.0594	.375	.0223	.00835	.00316
③ .66 x .09	.0594	.375	.0223	.00835	.00316
④ 1.2 x .04	.048	.60	.0288	.01728	.00576
$\Sigma$	.2978		.0794	.03425	.01217

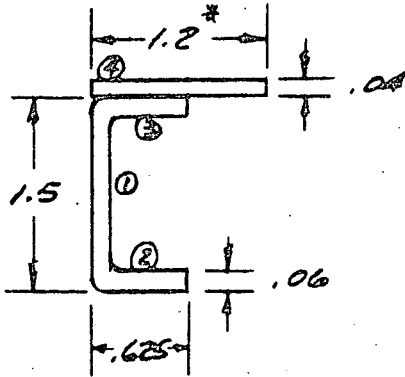
$$\bar{X} = \frac{\Sigma AX}{\Sigma A} = \frac{.0794}{.2978} = .267 \text{ IN.}$$

$$I_x = \Sigma AX^2 + \Sigma I_0 - (\Sigma AX) \bar{X} = .025 \text{ IN}^4$$

$$I_x = .025 \text{ IN}^4$$

## STEINER - SECTION PROPERTIES

\* EFFECTIVE SKIN WIDTH = 30t



ITEM	A	Y	AY	AY <sup>2</sup>	I <sub>o</sub>
① 1.5 x .06	.09	.75	.0675	.0506	.0168
② .565 x .06	.0339	.03	.00102	.00003	.00001
③ .565 x .06	.0339	1.47	.0498	.0733	.00001
④ 1.2 x .04	.048	1.52	.0731	.111	.00001
$\Sigma$	.2058		.1914	.2349	.0168

$$\bar{Y} = \frac{\Sigma AY}{\Sigma A} = \frac{.1914}{.2058} = .931 \text{ IN.}$$

$$I_y = \Sigma AY^2 + \Sigma I_o - (\Sigma AY) \bar{Y}$$

$$I_y = .2349 + .0168 - (.1914)(.931)$$

$I_y = .0734 \text{ IN}^4$

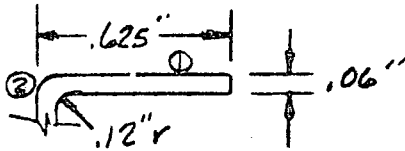
ITEM	A	X	AX	AX <sup>2</sup>	I <sub>o</sub>
① 1.5 x .06	.09	.03	.0027	.00008	.00027
② .565 x .06	.0339	.3125	.01059	.00331	.00009
③ .565 x .06	.0339	.3125	.01059	.00331	.00009
④ 1.2 x .04	.048	.60	.0288	.01728	.00576
$\Sigma$	.2058		.05268	.02398	.007587

$$\bar{X} = \frac{\Sigma AX}{\Sigma A} = \frac{.05268}{.2058} = .256 \text{ IN.}$$

$$I_x = \Sigma AX^2 + \Sigma I_o - (\Sigma AX) \bar{X}$$

$I_x = .0181 \text{ IN}^4$

FOR BENDING LOADS, THE CRIPPLING ALLOWABLE MAY BE FOUND AS FOLLOWS:



2024 - TA AL AL

ITEM	b/t	F <sub>cr</sub>	A	P
①	9.85	34500	.0276	950
②	.12r	50000	.0150	750
Σ			.0426	1700

THEREFORE:

$$F_{cr} = \frac{1700}{.0426} = 39800 \text{ PSI}$$

THE CHANNEL IS A MACHINING WITH .090 IN THICK FLANGES. THE CRIPPLING ALLOWABLE WILL EXCEED THE FATIGUE ALLOWABLE  $F_{FAT} = 40,800 \text{ PSI}$  BY COMPARISON WITH THE ABOVE CALCULATIONS.



Astro Electronics  
Division  
Princeton, New Jersey

Prepared for: \_\_\_\_\_ Report No. \_\_\_\_\_  
Approved: \_\_\_\_\_ Project: \_\_\_\_\_  
Date: \_\_\_\_\_ Contract No. \_\_\_\_\_  
Subject: IT03 D&E STRESS ANALYSIS Page No. A17

TOP SECTION (CONT.)

THE MOMENT TAKEN BY EACH BEAM IS:

$$\text{CHANNEL: } M_C = \frac{2578(.105)}{.1784} = 1520 \text{ IN. LBS.}$$

$$\text{STRINGER: } M_S = \frac{2578(.0734)}{.1784} = 1058 \text{ IN LBS.}$$

THE BENDING STRESS IN EACH BEAM IS FOUND FROM:

$$f_b = \frac{MY}{I}$$

HENCE:

$$f_{bc} = \frac{1520(.886)}{.105} = 12820 \text{ PSI}$$

$$f_{bs} = \frac{1058(.981)}{.0734} = 13400 \text{ PSI}$$

THE BEAMS ARE MADE OF 2024-T3 AL AL

THUS:  $E = 10^7 \text{ PSI}$        $F_{FAT} = 40800 \text{ PSI}$ ,       $F_{CP} = 39800 \text{ PSI}$

REF. P. A16

THE MARGINS OF SAFETY ARE:

$$\text{CHANNEL: } MS = \frac{40800}{12820(1.25)} - 1 = 1.54$$

$$\text{STRINGER: } MS = \frac{39800}{13400(1.25)} - 1 = 1.37$$

THE ABOVE MARGINS OF SAFETY ARE HIGH BECAUSE THIS AREA OF THE STRUCTURE WAS DESIGNED BY STIFFNESS REQUIREMENTS. REF. PG. A19

TOP SECTION (CONT.)FREQUENCY CHECK

FOR A BEAM WHICH IS SYMMETRICALLY LOADED AS IN THE SKETCH ON PG. A13, THE STATIC DEFLECTION UNDER THE LOAD IS GIVEN BY:

$$y_a = \frac{P_1 a^2}{6EI} [3L - 4a]$$

FROM SUPERPOSITION OF CASE 12 TABLE III IN REF. E

USING THIS EQUATION, THE DEFLECTIONS ARE:

UNDER  
RADIOMETERS

$$y_R = \frac{12.3(7.9)^2}{6(10^7)(.1784)} [3(37.8) - 4(7.9)]$$

$$y_R = 5850 \times 10^{-6} \text{ IN.}$$

UNDER  
BLACK BOXES

$$y_{BB} = \frac{6.2(12)^2}{6(10^7)(.1784)} [3(37.8) - 4(12)]$$

$$y_{BB} = 5500 \times 10^{-6} \text{ IN.}$$

NOW, THE NATURAL FREQUENCY FOR A SINGLE MASS SYSTEM IS GIVEN BY:

$$f_n = \frac{1}{2\pi} \sqrt{g/y}$$

WHERE:  $g$  = GRAVITATIONAL CONST. = 386 IN/SEC<sup>2</sup>

$y$  = DEFLECTION UNDER 1  $g$  IN INCHES.



Astro Electronics  
Division  
Princeton, New Jersey

Prepared for: \_\_\_\_\_ Report No. \_\_\_\_\_  
 Approved: \_\_\_\_\_ Project: \_\_\_\_\_  
 Date: \_\_\_\_\_ Contract No. \_\_\_\_\_  
 Subject: ITOS D&E STRESS ANALYSIS A19  
 Page 150

FREQUENCY CHECK (CONT.)

THE FREQUENCIES THEN, ARE:

FOR  
RADIOMETERS

$$f_R = \frac{1}{2\pi} \sqrt{356/5850 \times 10^{-6}} = 40.88 \text{ CPS}$$

FOR  
BLACK BOXES

$$f_{BB} = \frac{1}{2\pi} \sqrt{386/5500 \times 10^{-6}} = 42.16 \text{ CPS}$$

FROM DUNKERLEY'S RULE:

$$\frac{1}{f_n^2} = \frac{1}{f_R^2} + \frac{1}{f_{BB}^2} = \frac{1}{(40.88)^2} + \frac{1}{(42.16)^2}$$

$$f_n = 29.3 \text{ Hz}$$

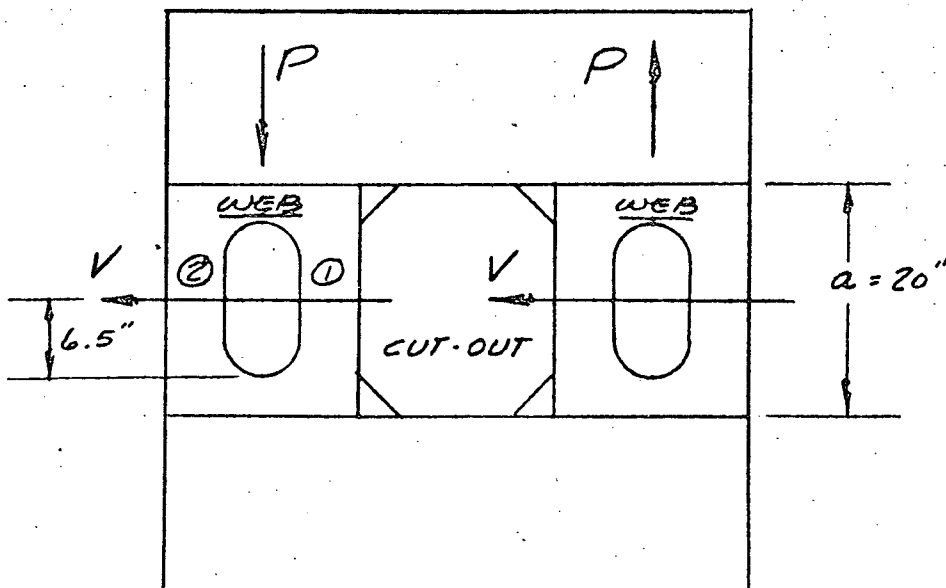
THE TOP SECTION WAS LOCALLY STIFFENED BY INCREASING THE CROSS-SECTIONAL AREA TO PREVENT THE EQUIPMENT IN THIS AREA FROM DYNAMICALLY COUPLING WITH THE SPACECRAFT NATURAL FREQUENCY MODES AND DRIVING THEM BELOW THE MINIMUM SPECIFIED VALUE OF 20 Hz. A MINIMUM TOP SECTION LOCAL FREQUENCY OF 40% ABOVE THE MINIMUM 20 Hz (OR 28 Hz) WAS THE DESIGN GOAL.

## FRONT PANEL

BECAUSE OF THE SIMILARITY IN STRUCTURE THE LOADS ON THE ITOS FRONT PANEL WILL BE FOUND BY RATIOING THE SAME LOADS ON THE TIROS FRONT PANEL ACCORDING TO WEIGHT AND INPUT g LOADS. THUS:

$$\begin{aligned} \text{LOAD}_{\text{ITOS}} &= \text{LOAD}_{\text{TIROS}} \left[ \frac{W_{\text{ITOS}}}{W_{\text{TIROS}}} \right] \left[ \frac{\text{INPUT } G_{\text{ITOS}}}{\text{INPUT } G_{\text{TIROS}}} \right] \\ &= \text{LOAD}_{\text{TIROS}} \left[ \frac{770}{720} \right] \left[ \frac{1.5}{2.3} \right] \end{aligned}$$

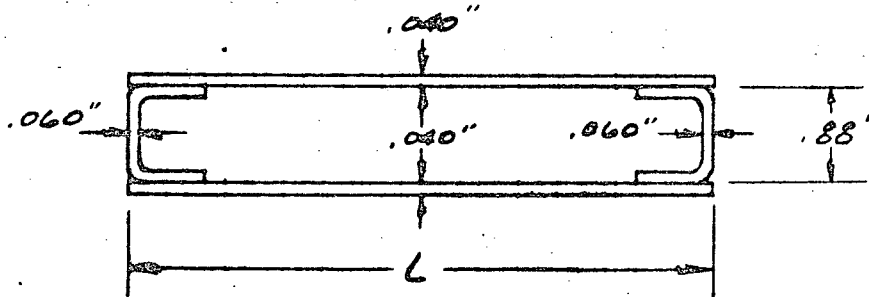
$$\text{LOAD}_{\text{ITOS}} = \text{LOAD}_{\text{TIROS}} (.6975)$$



LOAD	TIROS	ITOS
V	1359 #	948 #
P	412 #	287 #

TIROS LOADS p. 6.3.2 OF REF A

FRONT PANEL (CONT.)



SECTION 1 L = 3.4"  
SECTION 2 L = 1.65"

SECTION 1, 2

THE WEB WILL ACT AS A SLOTTED BEAM WITH THE SHEAR AND AXIAL LOADS BEING DISTRIBUTED ACCORDING TO THE RELATIVE SECTION INERTIAS. THE WORST STRESS WILL BE COMBINED BENDING AND COMPRESSION AND WILL OCCUR AT THE ENDS OF THE WEB CUT-OUTS.

SECTION 1

$$I_1 = \frac{2(.040)(3.4)^3}{12} + 2(.06)(.88)\left(\frac{3.4}{2}\right)^2 = .567 \text{ IN}^4$$

$$C_1 = \frac{3.4}{2} = 1.70 \text{ IN.}$$

$$A_1 = 2(.040)(3.4) + 2(.06)(.88) = .378 \text{ IN}^2$$

SECTION 2

$$I_2 = \frac{2(.040)(1.65)^3}{12} + 2(.06)(.88)\left(\frac{1.65}{2}\right)^2 = .102 \text{ IN}^4$$

$$C_2 = \frac{1.65}{2} = .825 \text{ IN.}$$

$$A_2 = 2(.040)(1.65) + 2(.06)(.88) = .238 \text{ IN}^2$$



Astro Electronics  
Division  
Princeton, New Jersey

Prepared for: \_\_\_\_\_ Report No. \_\_\_\_\_  
 Approved: \_\_\_\_\_, \_\_\_\_\_ Project: \_\_\_\_\_  
 Date: \_\_\_\_\_ Contract No. \_\_\_\_\_  
 Subject: ITOS D&E STRESS ANALYSIS Page No. A22 of \_\_\_\_\_

FRONT PANEL (CONT.)

$$A_{TOT} = A_1 + A_2 = .616 \text{ IN}^2$$

$$I_{TOT} = I_1 + I_2 = .669 \text{ IN}^4$$

THE SHEAR IS DISTRIBUTED AS :

$$V_1 = \frac{V(I_1)}{I_{TOT}} = \frac{(948)(.567)}{.669} = 803 \#$$

$$V_2 = \frac{V(I_2)}{I_{TOT}} = \frac{(948)(.102)}{.669} = 145 \#$$

AT THE END OF THE SLOT THE MOMENT IS EQUAL TO :

$$M_i = 6.5 V_i$$

AND THE COMBINED STRESS IS :

$$f_i = \left(\frac{M_i}{I}\right)_i + \frac{P}{A}$$

THE STRESSES IN THE SECTIONS THEN ARE :

$$f_1 = \frac{(6.5)(803)(1.70)}{.567} + \frac{287}{.616} = 15650 + 470$$

$$f_1 = 14,120 \text{ PSI}$$

$$f_2 = \frac{(6.5)(145)(.825)}{.102} + \frac{287}{.616} = 7620 + 470$$

$$f_2 = 8090 \text{ PSI}$$



Astro Electronics  
Division  
Princeton, New Jersey

Prepared for: \_\_\_\_\_ Report No. \_\_\_\_\_  
 Approved: \_\_\_\_\_ Project: \_\_\_\_\_  
 Date: \_\_\_\_\_ Contract No. \_\_\_\_\_  
 Subject: XPOS D&E STRESS ANALYSIS Page No. A23

FRONT PANEL (CONT.)

THE FATIGUE ALLOWABLE FOR 2024-T3 IS

$$F_{fat.} = 40,800 \text{ PSI} \quad \text{REF. A}$$

HENCE THE MARGIN OF SAFETY IS:

$$MS = \frac{40800}{16180 (1.25)} - 1 = 1.02$$

WEB SHEAR

THE MAXIMUM SHEAR STRESS WILL OCCUR ON SECTION 2 AND WILL BE EQUAL TO:

$$f_{s1} = \left( \frac{V}{2LE} \right)_1 = \frac{803}{3.4 (.08)} = 2950 \text{ PSI}$$

THE ALLOWABLE PANEL BUCKLING STRESS IS GIVEN BY:

$$F_{all.} = \frac{\pi^2 K_3 E}{12(1-\mu^2)} \left( \frac{t}{b} \right)^2 \quad \text{REF. D}$$

VALUES:  $\mu = .3$

$$K_3 = 5.4 \quad \text{FOR } a/b = 20/3.4 \approx 6$$

THEN:

$$F_{all} = \frac{\pi^2 (5.4) (10^7)}{12 (.91)} \left( \frac{.040}{3.4} \right)^2 = 6760 \text{ PSI}$$

THE SHEAR MARGIN OF SAFETY IS THEREFORE:

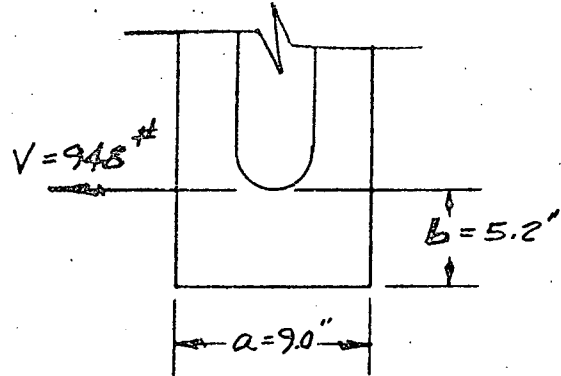
$$MS = \frac{6760}{2950 (1.25)} - 1 = .83$$

## WEB SHEAR (CONT.)

AT THE FULL SECTION :

$$f_s = V/A_s = \frac{948}{9(2)(.04)}$$

$$f_s = 1317 \text{ PSI}$$



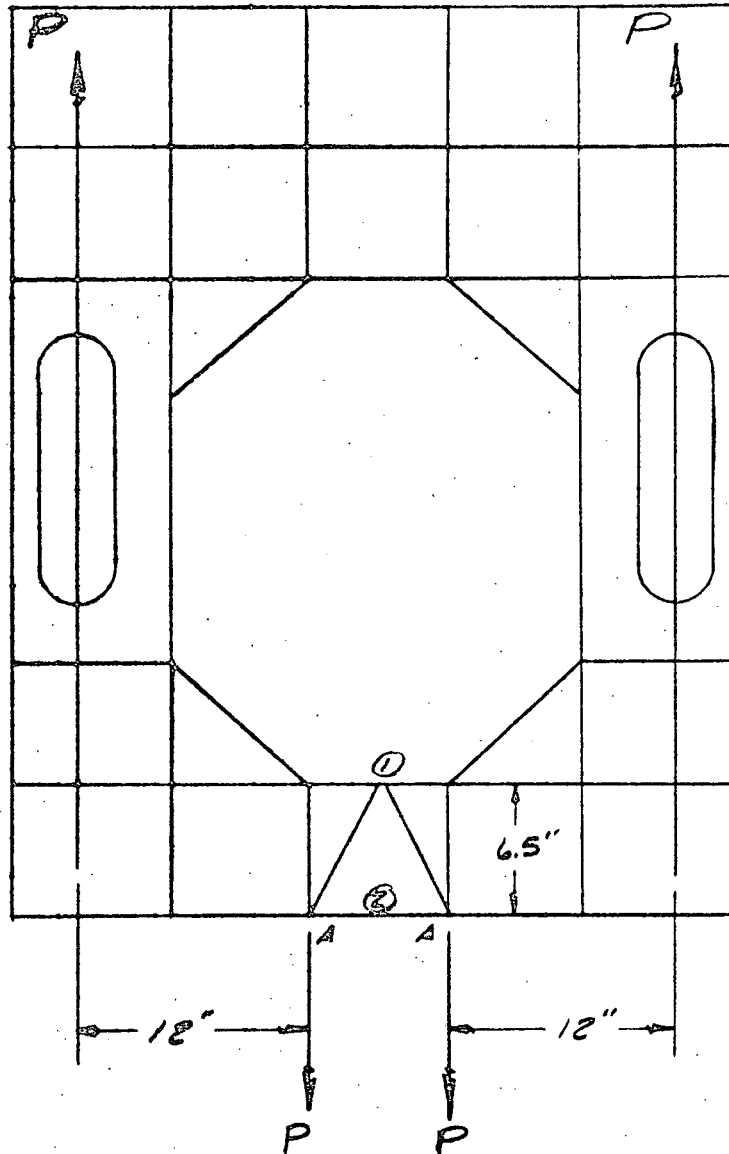
AGAIN, USING REF. D AND HAVING  
 $a/b = 9/5.2 = 1.73 \Rightarrow K_s = 6.5$  WE FIND THE  
 SHEAR BUCKLING ALLOWABLE TO BE :

$$F_{all} = \frac{\pi^2(6.5)(10^7)(.040/5.2)^2}{12(.91)}$$

$$F_{all} = 3480 \text{ PSI}$$

THE MARGIN IS THEN :

$$MS = \frac{3480}{1317(1.25)} - 1 = 1.11$$

ASTRO SECTION

DURING YY SINE EXCITATION THE STRUCTURE WILL EXPERIENCE "ROCKING" WHICH WILL GENERATE THE P LOADING, SHOWN ABOVE, IN THE FRONT PANEL AROUND THE CUTOUT. THIS LOADING IS REACTED AT TWO HARD POINTS (A) AND PRODUCES BENDING IN THE LOWER SECTION OF THE FRONT PANEL



Astro Electronics  
Division  
Princeton, New Jersey

Prepared for: \_\_\_\_\_ Report No. \_\_\_\_\_  
 Approved: \_\_\_\_\_, \_\_\_\_\_ Project: \_\_\_\_\_  
 Date: \_\_\_\_\_ Contract No. \_\_\_\_\_  
 Subject: ITOS D&E STRESS ANALYSIS Page A26 of \_\_\_\_\_

BOTTOM SECTION (CONT.)

WHICH CAUSES BEAMS ① & ② TO FEEL TENSION AND COMPRESSION ALTERNATELY.

THE LOAD P MAY BE FOUND BY RATIOING THE SAME TIROS LOAD ACCORDING TO WEIGHT AND INPUT  $\eta$  LOAD. THUS:

$$LOAD_{ITOS} = LOAD_{TIROS} \left[ \frac{W_{ITOS}}{W_{TIROS}} \right] \left[ \frac{INPUT \ \eta_{ITOS}}{INPUT \ \eta_{TIROS}} \right]$$

$$P = \frac{6130}{2} \left[ \frac{770}{720} \right] \left[ \frac{1.5}{2.3} \right]$$

$P = 2140 \text{ LBS}$

THE MOMENT CAUSED BY P IS:

$$M = (12)(2140) = 25700 \text{ IN LB.}$$

ASSUMING, CONSERVATIVELY, THAT THIS MOMENT IS TAKEN AS A COUPLE BY BEAMS ① & ② EACH CARRYING A LOAD P', WE HAVE:

$$P' = \frac{M}{6.5} = \frac{25700}{6.5}$$

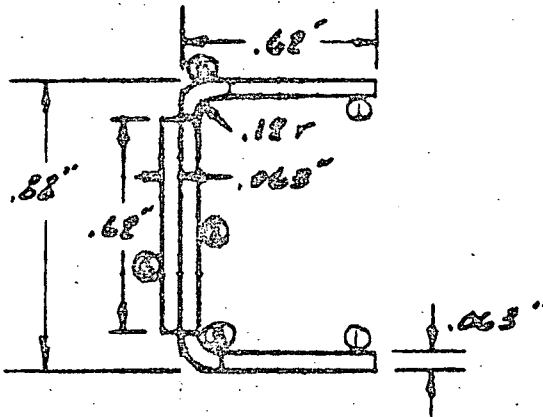
$$P' = 3920 \text{ LBS.}$$

OF THE TWO BEAMS (① & ②) WHICH WILL CARRY THIS LOAD, BEAM ① HAS THE SMALLEST SECTION PROPERTIES, WE SHALL, THEREFORE, CHECK BEAM ①.

FOR 2024-T4 ALUM ALLOY

$$E = 10^7 \text{ PSI} \quad F_{cy} = 38000 \text{ PSI}$$

BOTTOM SECTION (CONT.)



ITEM	b/t	* F <sub>cr</sub>	A	P
1	9.85	34500	.0551	1900
2	14	47000	.0324	1525
3	.12r	50000	.0300	1500
4	4.9	48500	.0390	1890
Σ			.1565	6815

THE CRIPPLING ALLOWABLE IS :

$$F_{cr} = \frac{6815}{.1565} = 43500 \text{ PSI}$$

HOWEVER, THE FATIGUE ALLOWABLE OF

$F_{fat} = 40,800 \text{ PSI}$  IS MORE CRITICAL THAN  $F_{cr}$ .

THE ACTUAL STRESS IS :

$$f = P/A = \frac{3920}{.1565} = 25000 \text{ PSI}$$

HENCE :

$$MS = \frac{40800}{25000(1.25)} - 1 = .31 \text{ (ULTIMATE)}$$

$$MS = \frac{38000}{25000(1.15)} - 1 = .32 \text{ (YIELD)}$$

\* FROM DESIGN CRIPPLING CURVES



Astro Electronics  
Division

Princeton, New Jersey

Prepared for: \_\_\_\_\_ Report No. \_\_\_\_\_

Approved: \_\_\_\_\_ Project: \_\_\_\_\_

Date: \_\_\_\_\_ Contract No. \_\_\_\_\_

Subject: ITOS DAE STRESS ANALYSIS Page No. A28 of \_\_\_\_\_

## Very High Resolution Radiometer (VHRR)

The bottom portion of the front panel is subjected to local loads from two VHRR's, each weighing 35 lbs. The structure is critical for the sinusoidal vibration input loads,  $g_i$ , of 1.5g in the lateral and 2.3g in the thrust directions. Design vibration amplification factors are determined from the Improved TOS Mechanical Test Model Test (Ref B) and are equal to

X-X direction (lateral & parallel to panel) = 10.0  
Y-Y direction (lateral & perpendicular to panel) = 7.5  
Z-Z direction (thrust) = 10.0

The load from each VHRR unit is equal to  $P = Wg_i Q$ . Then

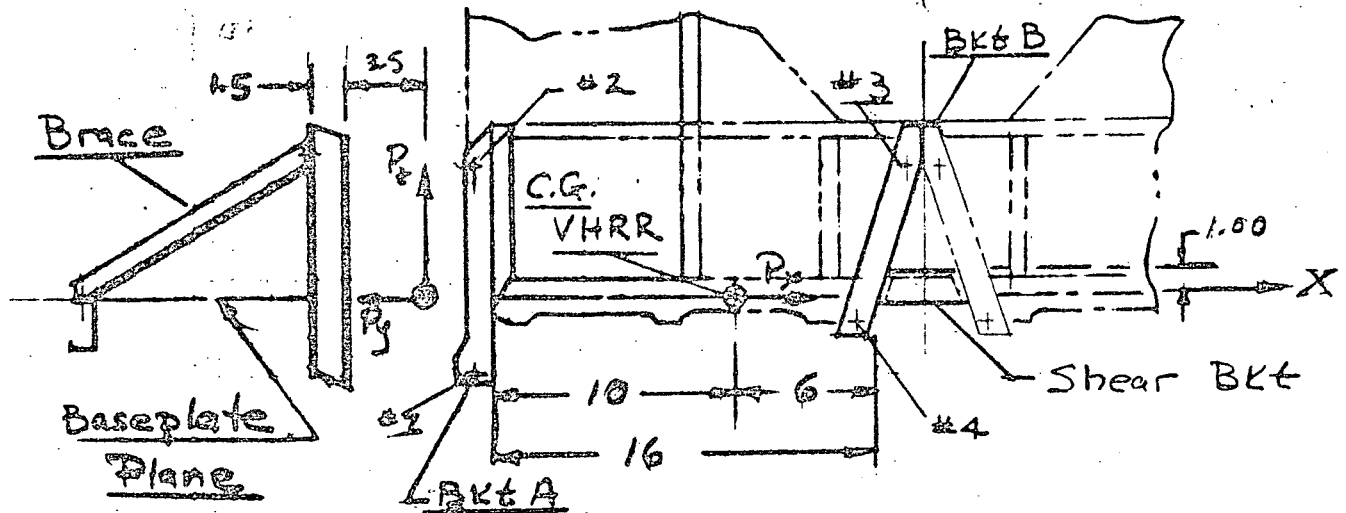
$$P_x = 35 \times 1.5 \times 10 = 525 \text{ lbs}$$

$$P_y = 35 \times 1.5 \times 7.5 = 394 \text{ lbs}$$

$$P_z = 35 \times 2.3 \times 10 = 805 \text{ lbs}$$

These loads act independently of each other.

The VHRR's are attached to the front panels by channel shaped brackets.



For Lateral Load  $P_x = 525$  lbs

Load Assumptions:

1. The VHRR acts as a rigid body.
2. All the lateral load  $P_x$  is reacted by the baseplate and is carried by the web of the shear bracket.
3. The C.G. of the VHRR falls within 1 inch of the web of the shear bracket (See figure).
4. The moment caused by the eccentricity between the load and web of the shear bracket is reacted by a couple load

between the 16 inch spaced brackets. This load is equal to  $P = \bar{P}_x / 16 = 33 \text{ lbs}$ , and acts along the length of the brackets, and is small enough to be ignored in the stress analysis.

5. The load  $P_x$  acts in the plane of the baseplate skin.

6. Each VHRR load are reacted by 4 bolts attached to the brackets (see sketch).

### Shear Bracket

The shear bracket reacts the load from both VHRR's. The total load on the bracket is then equal to

$$P = 2 \times P_x = 2 \times 525 = 1050 \text{ lbs.}$$

The shear bracket is attached to the two VHRR "B" brackets by four  $5/32$ " rivets.

$$P_{\text{rivet}} = P/4 = 1050/4 = 262.5 \text{ lbs.}$$

(in tension)

The ultimate static tensile strength for a 5/32 inch protruding head rivet in the 0.090 inch thick shear bracket is equal to  $P_{t0} = 758$  lbs. Ref D pg D.1.28 The shear bracket is captured between the two UHRR "B" brackets and the rivets will be subjected to alternating loads from 0 to maximum. The allowable tension allowable for the rivet will be assumed to equal 50% of the static value.

$$P_{All} = .50 \times 758 = 379 \text{ lbs}$$

$$M.S. = \frac{379}{262.5 \times 1.25} - 1 = .16$$

The shear bracket in turn is attached to the front panel by three 5/32" rivets.

$$\text{Shear Allowable} = P_S = 575 \text{ lb/rivet} \quad \text{Ref D pg D.1.24}$$

$$M.S. = \frac{3 \times 575}{1050 \times 1.25} - 1 = .31$$

Shear in Web

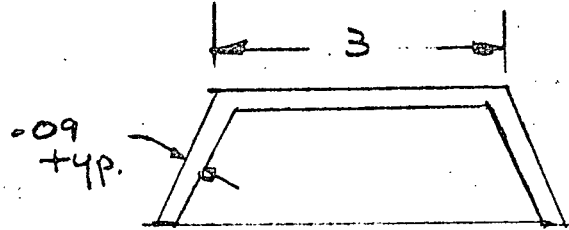
$$A_s = \text{shear area}$$

$$= 3 \times .09 = .27 \text{ inch}^2$$

$$P = 1050 \text{ lbs}$$

$$f_s = P/A_s = 1050/.27 = 3890 \text{ psi}$$

M.S. is large



Loads on VHR Brackets

Since the shear load  $P_x$  is reacted by the shear bracket, this load must come through bracket "B" via bolt location #3 and #4. The moment due to the 3.5 inch eccentricity of the C.G. above the VHR supports is reacted as a couple load between Bracket "A" and Bracket B.

On Bracket "B"

$$P_B = P_x = 525 \text{ lbs}$$

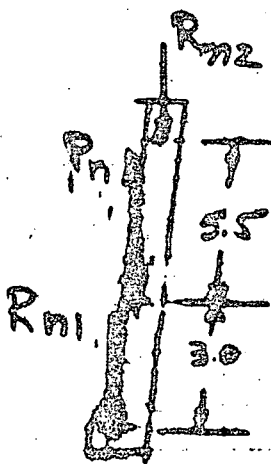
$$P_m = 3.5 P_x / 16 = 114.8 \text{ LBS}$$

On Bracket "A"

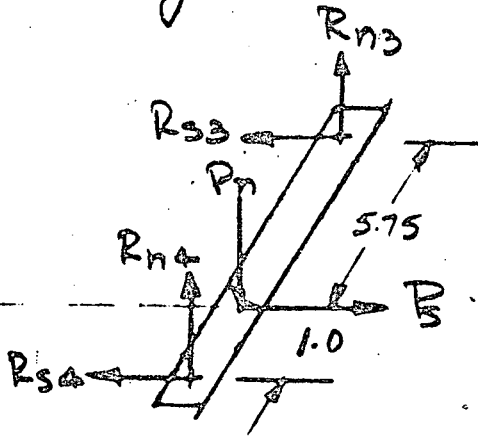
$$P_s = 0$$

$$P_n = 114.8 \text{ lbs}$$

Beaming over the above loads to the 4 bolt attachment points results in the following bolt loads.



Bracket A



Bracket B

$$P_n = 114.8 \text{ lb}$$

$$P_s = 525 \text{ lb}$$

$$R_{n1} = \frac{5.5}{8.5} P_n = 74.3 \text{ lb}$$

$$R_{n2} = \frac{3.0}{8.5} P_n = 40.5 \text{ lb}$$

$$R_{n3} = \frac{1}{6.75} P_n = 17.0 \text{ lb}$$

$$R_{s4} = \frac{1}{6.75} P_s = 77.8 \text{ lb}$$

$$R_{n4} = \frac{5.75}{6.75} \times 114.8 = 97.8 \text{ lbs}$$

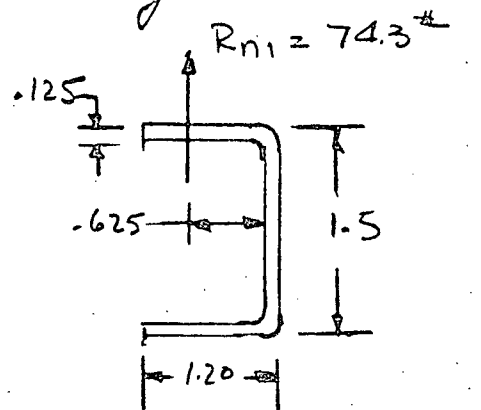
$$R_{s4} = \frac{5.75}{6.75} \times 525 = 447.2 \text{ lbs}$$

Bracket A

The local load at bolt location #1 loads the flange in bending

$$M = .625 \times 74.3 = 46.4 \text{ in lb}$$

For an effective flange width,  $b = 1.5$  inches the bending stress is equal to



Bkt 'A' @ Bolt #1

$$f_b = \frac{6M}{bt^2} = \frac{6 \times 46.4}{1.5 \times .125^2} = 11900 \text{ psi}$$

M.S. is large

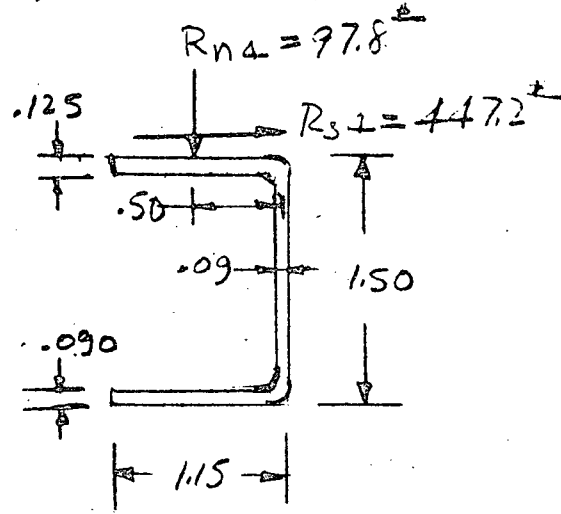
This loading is not as critical as the load from vibration in the thrust direction (Ret page A39).

## Bracket B

The maximum load normal to the flange occurs at Bolt #4.

$$R_{n4} = 97.8 \text{ lbs.}$$

Bracket "B" has an end plate which will react 1/2 of the local load. Therefore the flange bending moment is equal to



$$M = \frac{1}{2} (.50 \times R_{n4}) = \frac{1}{2} \times .50 \times 97.8 = 24.5 \text{ in lb}$$

which is not critical by comparison with  $M = 46.4$  in lb of Bracket "A" (Ref pg A34)

The loads from Bolt #4 will result in twisting and bending of the entire section. The torque on the section is equal to

$$T = \frac{1.5}{2} R_{sa} - .50 R_{na}$$



Astro Electronics  
Division  
Princeton, New Jersey

Prepared for: \_\_\_\_\_ Report No. \_\_\_\_\_  
Approved: \_\_\_\_\_, \_\_\_\_\_ Project: \_\_\_\_\_  
Date: \_\_\_\_\_ Contract No. \_\_\_\_\_  
Subject: ITCS D&E STRESS ANALYSIS Page No. A36 of \_\_\_\_\_

$$T = \frac{1.5}{2} \times 447.2 - 97.8 \times .5 = 286.5 \text{ in lb.}$$

The shear stress due to the torque is equal to

$$f_s = \frac{3T}{\sum bt^2} = \frac{3 \times 286.5}{(1.15 \times .125^2 + 1.5 \times .09^2 + 1.15 \times .09^2)}$$
$$= 21800 \text{ psi}$$

$$F_{su} = 37,000 \text{ psi}$$

$$M.S. = \frac{37000}{21800 \times 1.25} - 1 = .36$$

Bolt #4 is 1.5 inches away from the attachment point to the front panel. The maximum bending moment is then equal to

$$M = R_{s4} (1.5) = (447.2)(1.5) = 671 \text{ in lb.}$$

The bracket is approximately a 1.125 x 1.500 x .092 channel. From section A3.14 of Ref D the

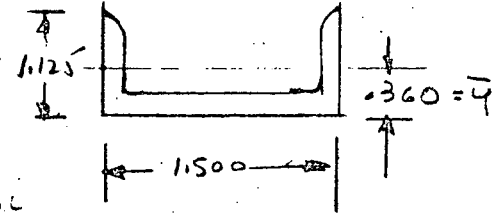
section properties of the section are

$$I = .0414 \text{ in.}^4$$

$$\bar{y} = .360 \text{ in.}$$

$$c = 1.125 - .360 = .765 \text{ in.}$$

$$f_b = \frac{Mc}{I} = \frac{671 \times .765}{.0414} = 12,400 \text{ psi}$$



$$F_{\text{fat}} = 40,800 \text{ psi}$$

M.S. is large

The bending stresses, therefore, have a small effect on the combined bending and torsion stresses and consequently are ignored.

REPRODUCIBILITY OF THE  
ORIGINAL PAGE IS POOR

For Thrust Load  $P_z = 805$  lbs.

The bending moment at the bolt plane is equal to

$$M = 3.5 P_z = 3.5 \times 805 = 2820 \text{ in lb.}$$

Proportioning this bending moment to Bracket "A" and Bracket "B" according to their distances from the VARR center of gravity

$$M_A = \frac{6}{16} M = 1058 \text{ in lb.}$$

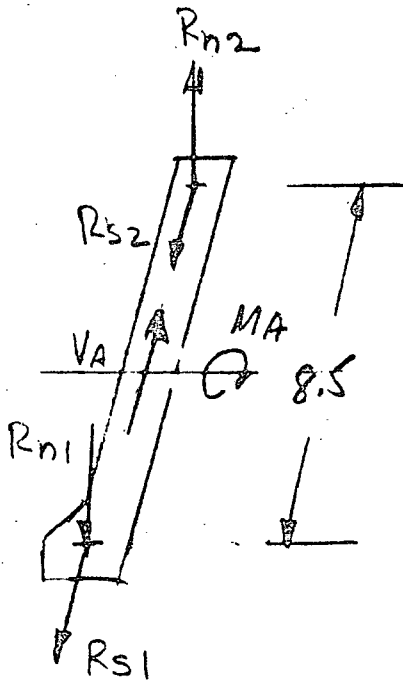
$$M_B = \frac{10}{16} M = 1762 \text{ in lb.}$$

Similarly for the shear loads

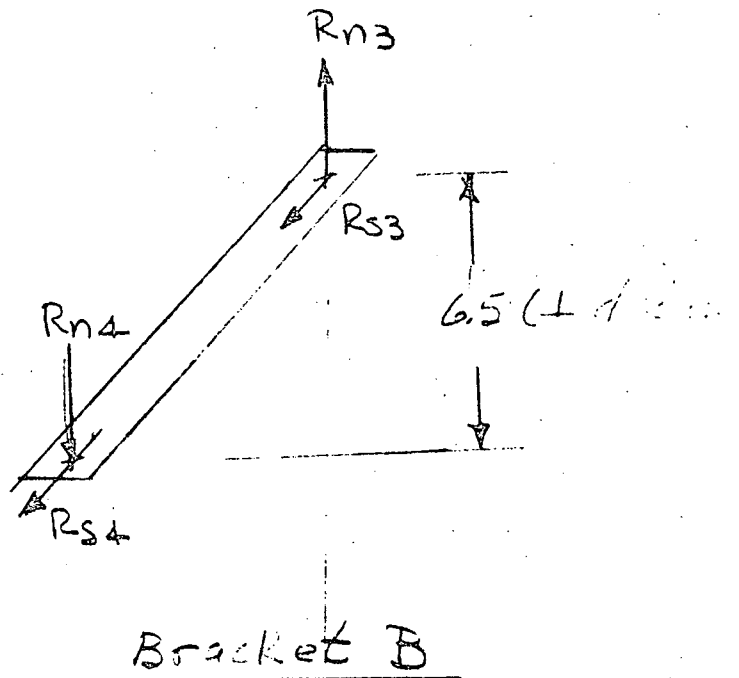
$$V_A = \frac{6}{16} P_z = \frac{6}{16} \times 805 = 302 \text{ lbs.}$$

$$V_B = \frac{10}{16} P_z = \frac{10}{16} \times 805 = 503 \text{ lbs.}$$

The shear loads will be equally reacted by two bolts at each bracket and the bending moments by normal couple loads.



Bracket A



Bracket B

$$R_{S1} = R_{S2} = V_A / 2 = 302 / 2 = 151 \text{ lbs}$$

$$R_{N1} = R_{N2} = M_A / 8.5 = 1058 / 8.5 = 124.5 \text{ lbs}$$

$$R_{S3} = R_{S4} = V_B / 2 = 503 / 2 = 251.5 \text{ lbs}$$

$$R_{N3} = R_{N4} = M_B / 6.5 = 1762 / 6.5 = 271 \text{ lbs}$$

The normal loads  $R_{N3}$  and  $R_{N4}$  locally load the flanges in bending (Ret page A3A) At Bolt #4

$$M = \frac{1}{2} (.50 \times R_{N4}) = \frac{1}{2} \times .50 \times 271 = 67.75 \text{ in-lb.}$$

$$f_b = \frac{6M}{bt^2} = \frac{(6)(67.75)}{(1.5)(.125)^2} = 17,344 \text{ psi}$$



Astro Electronics  
Division  
Princeton, New Jersey

Prepared for: \_\_\_\_\_ Report No. \_\_\_\_\_  
 Approved: \_\_\_\_\_, \_\_\_\_\_ Project: \_\_\_\_\_  
 Date: \_\_\_\_\_ Contract No. \_\_\_\_\_  
 Subject: ITOS D&E STRESS ANALYSIS Page No. A40 of \_\_\_\_\_

At Bolt #3 there is more flange width about the bolt hole, but no end plate. Then

$$M = .500 R_{n3} = (.500)(271) = 135.5 \text{ in lb}$$

Let the effective width  $b = 2.00$  inches, then

$$f_b = \frac{GM}{bt^2} = \frac{(6)(135.5)}{(2)(.125)^2} = 26000 \text{ psi}$$

In addition to the flange bending stress, there is an axial load from  $R_{s3}$  in the flange.

$$f_t = \frac{R_{s3}}{A_f} \quad \text{where } A_f = 1.15 \times .09 = .1035 \text{ in}^2$$

$$= 251.5 / .1035 = 2400 \text{ psi}$$

Ret SKETCH  
PG. A35

The maximum stress is equal to

$$f = f_b + f_t = 26000 + 2400 = 28400 \text{ psi}$$

$$F_{Fat} = 40,800 \text{ psi}$$

$$M.S. = \frac{40800}{28400 \times 1.27} - 1 = .15$$

V. OTHER ITEMSBRACE & BASEPLATE

The brace reacts loads from the VHR's that act normal to the plane of the front panel.

From thrust vibration,  $P_z = 805$  lbs/unit

The total bending moment from the two VHR's from thrust is equal to

$$M = 2 \times 5 P_z \quad \text{Ref Sketch p. A29}$$

$$= 2 \times 5 \times 805 = 8050 \text{ in lb.}$$

Proportioning the moment between the VHR brackets, the bending moment reacted at the brace plane is equal to

$$M_{\text{brace}} = \frac{10}{16} M = 5030 \text{ in lb.}$$

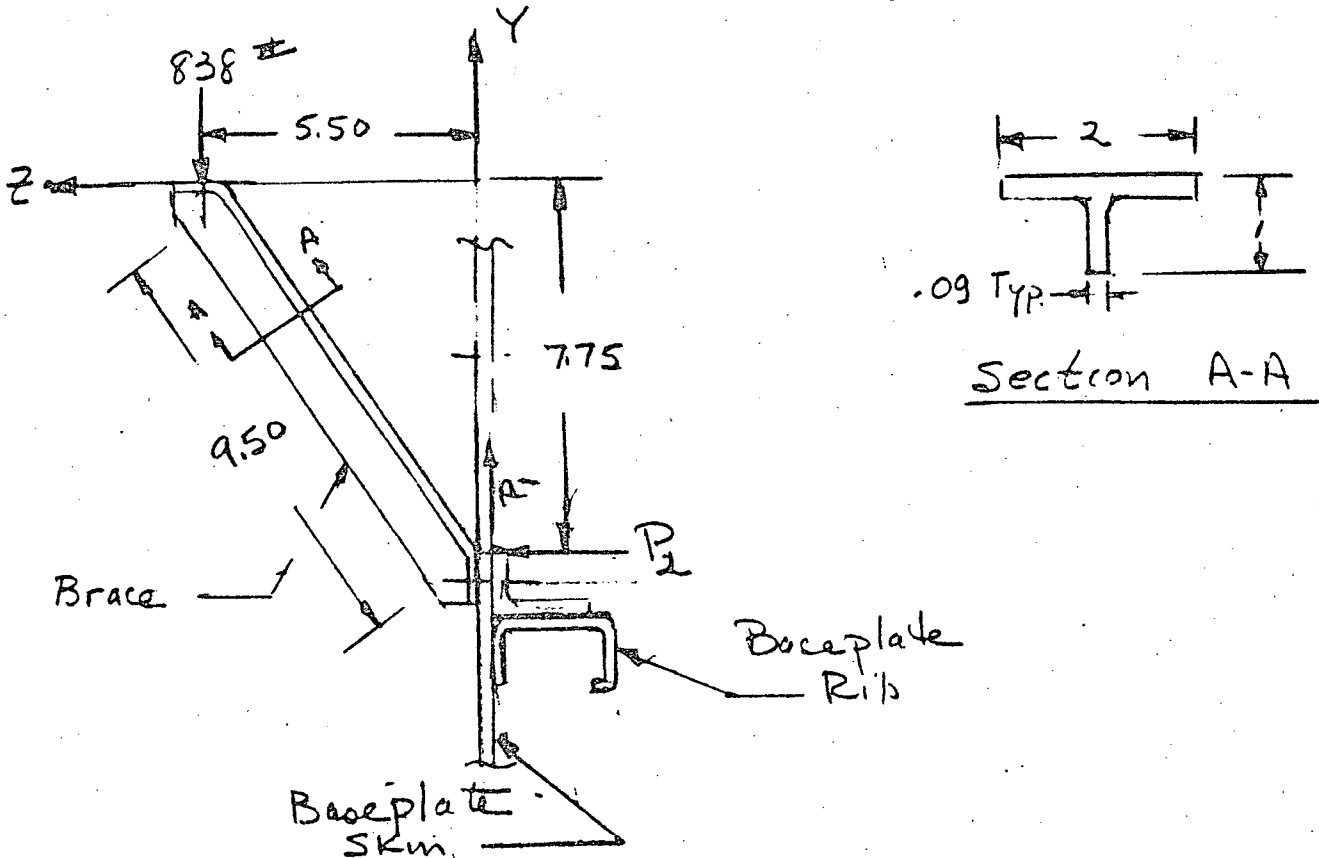
This moment is reacted as a couple load between the brace attachment point and the baseplate, 6 inches apart

$$P_c = \frac{M_{brace}}{G} = 838 \text{ lbs.}$$

The load from the Y-Y lateral vibration input is less critical than the thrust load since the total load from the VHRR's is only

$$P = 2 P_y = 2 \times 394 = 788 \text{ lbs.}$$

The loads on the brace and baseplate are determined from the geometry as follows:





Astro Electronics  
Division  
Princeton, New Jersey

Prepared for: \_\_\_\_\_ Report No. \_\_\_\_\_  
Approved: \_\_\_\_\_ Project: \_\_\_\_\_  
Date: \_\_\_\_\_ Contract No. \_\_\_\_\_  
Subject: ITOS D&E STRESS ANALYSIS Page No. A43

The axial load in the brace is equal to

$$P_{br} = \frac{9.50}{7.75} P_c = \frac{9.50 \times 838}{7.75} = 1027 \text{ lbs}$$

The stress in the brace is equal to

$$f = P_{br}/A = 1027 / (2 \times .09 + .91 \times .09) = 3920 \text{ psi}$$

M.S. is Large

The load from the brace is reacted at the baseplate by two components. Ref. A42

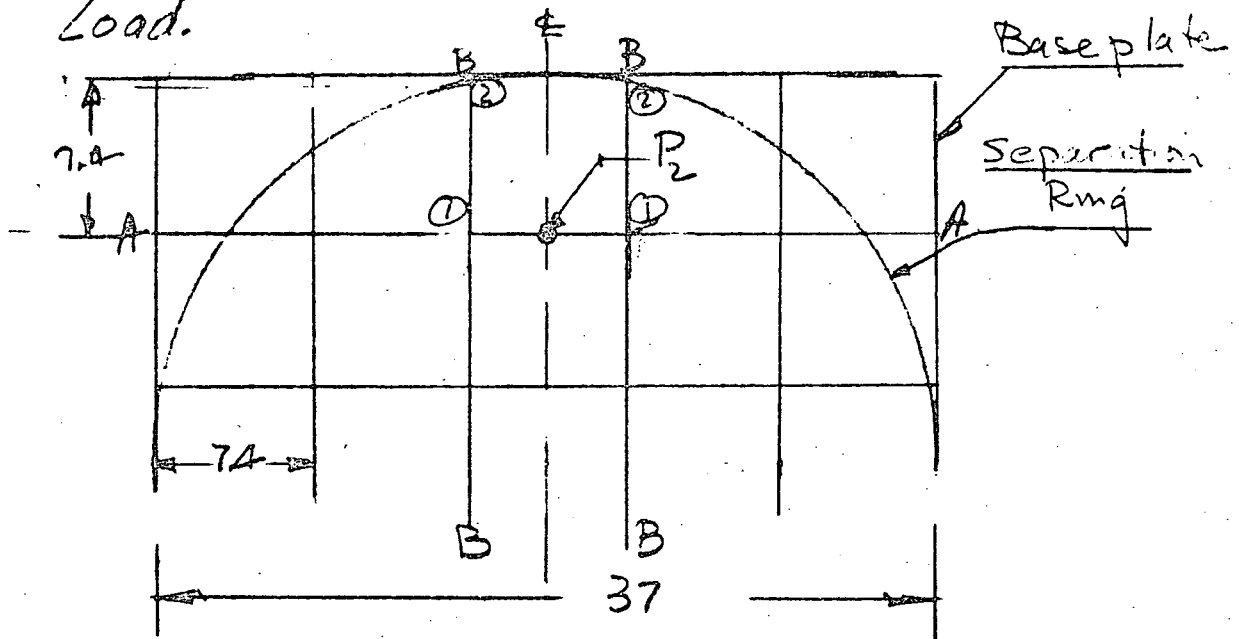
$$P_1 = 1027 \times \frac{7.75}{9.50} = 838 \text{ lbs}$$

$$\text{and } P_2 = 1027 \times \frac{5.50}{9.50} = 595 \text{ lbs}$$

The  $P_1$  load can be reacted by tension in the baseplate skin and is obviously not critical.

The  $P_2$  load acts normal to the baseplate plane and is reacted by the ribs. A simplified and conservative

stress analysis is given below for the local stress effect of the  $P_2$  load.



The  $P_2$  load is beamed over to point 1 on Beam A. The shear at point 1 is then equal to

$$V_1 = P_2/2 = 595/2 = 297.5 \text{ lbs}$$

The maximum bending moment on Beam A is then equal to

$$M_A = \frac{7.4}{2} V_1 = 1101 \text{ in lb. at the Z.}$$

On Beam B the maximum moment occurs at point 1.



Astro Electronics  
Division

Princeton, New Jersey

Prepared for: \_\_\_\_\_ Report No. \_\_\_\_\_

Approved: \_\_\_\_\_ Project: \_\_\_\_\_

Date: \_\_\_\_\_ Contract No. \_\_\_\_\_

Subject: ITCS D&E STRESS ANALYSIS A45

The shear load at the support point  
is equal to

$$V_2 = \frac{V_1 (37 - 7.4)}{37} = 238 \text{ lbs and}$$

$$M_1 = 7.4 V_2 = 1761 \text{ in lb. (Critical value)}$$

Both beams have the same section  
properties. From page 6.1.4 of Ref A.

$$I/c = .206 \text{ in}^3 \text{ at SKM surface (upper)}$$

$$I/c = .139 \text{ in}^3 \text{ at lower surface}$$

$$F_{cr} = 25080 \text{ psi (upper) Ref A pg 6.1.6}$$

$$F_{cr} = 46,040 \text{ psi (lower) "}$$

$$F_{fat} = 40,800 \text{ psi}$$

$$\text{Then } f = M/I/c.$$

At upper surface of baseplate rib

$$f = 1761 / .206 = 8550 \text{ psi}$$

$$M.S. = \frac{25080}{8550 \times 1.25} - 1 = 1.34$$



Astro Electronics  
Division

Princeton, New Jersey

Prepared for: \_\_\_\_\_ Report No. \_\_\_\_\_

Approved: \_\_\_\_\_, \_\_\_\_\_ Project: \_\_\_\_\_

Date: \_\_\_\_\_ Contract No. \_\_\_\_\_

Subject: ITOS D&E STRESS ANALYSIS Page No. A46 01

At lower surface of baseplate rib

$$f = 1761 / .139 = 12670 \text{ psi}$$

$$M.S. = \frac{40800}{12670 \times 1.25} - 1 = 1.58$$



Astro Electronics  
Division  
Princeton, New Jersey

Prepared for: \_\_\_\_\_ Report No. \_\_\_\_\_  
Approved: \_\_\_\_\_, \_\_\_\_\_ Project: \_\_\_\_\_  
Date: \_\_\_\_\_ Contract No. \_\_\_\_\_  
Subject: YTOS D&E STRESS ANALYSIS Page No. A47

## VII CONSTANT ACCELERATION

The maximum allowable constant acceleration level,  $N$ , that the spacecraft can safely withstand is calculated in this section for loading in the thrust direction. The spacecraft is accelerated in the forward direction.

### Front Panel

This area is critical for the local loads from the VHRR. The worst stress condition occurs in the flange of the channel  $f = 28400$  psi (Ref. p A40) for the response load  $P_z = 805$  lbs (Ref. p A35) in vibration in the thrust direction from the 35 pound VHRR. The critical stress in the flange due to constant



Astro Electronics  
Division

Princeton, New Jersey

Prepared for: \_\_\_\_\_ Report No. \_\_\_\_\_

Approved: \_\_\_\_\_ Project: \_\_\_\_\_

Date: \_\_\_\_\_ Contract No. \_\_\_\_\_

Subject: ITOS D&E STRESS ANALYSIS Page No. A48 of \_\_\_\_\_

acceleration is due to yield. The allowable yield stress is equal to  $F_{cy} = 40,000$  psi for 2024-T4 Al. Al. The constant acceleration stress is equal to

$$f = \frac{28400 \times 35 N}{805} = 1235 N$$

Equating this stress to the allowable with a yield safety factor  $FS = 1.15$

$$1235 N = \frac{40,000}{1.15}$$

$$\underline{N = 28.2 \text{ g's.}}$$

### Base plate (Ref. A. Section 6.1)

The stress levels in the base plate for a constant acceleration load can be determined from the formulas for the bending moment per unit width for a uniformly loaded square plate simply

supported along its edges.

$$f_b = \frac{.2208 w l^2 (m+1)}{m t^2}$$

Ref E. Formula 30  
p. 224

where  $l$  is the length of the side of the plate. For a plate

$$f_b = \frac{6 M'}{t^2}$$

The bending moment per unit width is then found by equating  $f_b$

$$M' = \frac{.2208 w l^2 (m+1)}{6 m}$$

For the baseplate (Ref. A p. 6.1.7)

$$l = 37.0'' , m = 3.0 \text{ for Al. Al.}$$

The baseplate weight is equal to  $W = 225 \text{ lbs}$

Then  $w = 225 \text{ N/l}^2$ . Substituting these values into the equation for  $M'$ .

$$M' = \frac{(.2208)(225 \text{ N}) l^2 (3+1)}{(6) l^2 (3)} = 11.00 \text{ N}$$

The rib spacing is equal to  $b = 7.5$  in (Ref. A p. 6.1.7)

The bending moment on the rib is

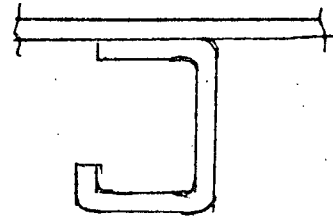
$$M = bM' = (7.5)(11 \text{ N}) = 82.5 \text{ N}$$

For a typical section

$$I/c_{\text{upper}} = .206 \text{ in}^3; \quad I/c_{\text{lower}} = .139 \text{ in}^3$$

$$F_{cr \text{ upper}} = 25,080 \text{ psi}, \quad F_{cr \text{ lower}} = 46,040 \text{ psi}$$

$$F_{cy} = 40,000 \text{ psi} \quad \text{For 2024 T4 ALAL}$$



(Ref. A p. 6.1.4, 6.1.6)

$$f_b = M / (I/c)$$

$$f_{b \text{ upper}} = (82.5 \text{ N}) / .206 = 402 \text{ N}$$

$$f_{b \text{ lower}} = (82.5 \text{ N}) / .139 = 594 \text{ N}$$

Using a safety factor of S.F. = 1.25 for ultimate loads and S.F. = 1.15 for yield loads

$$F_{\text{upper}} = 25080 / 1.25 = 20100 = 402 \text{ N}$$

$$\underline{N = 50}$$

$$F_{\text{lower}} = 46040 / 1.25 = 36,800 \text{ psi} \quad (\text{Not critical})$$

$$\text{or } F_{\text{lower}} = 40,000 / 1.15 = 34,800 \text{ psi} \quad (\text{Critical})$$

$$34,800 = 594 \text{ N} \quad \text{and} \quad \underline{N = 58.5}$$



Astro Electronics  
Division  
Princeton, New Jersey

Prepared for: \_\_\_\_\_ Report No. \_\_\_\_\_  
Approved: \_\_\_\_\_ Project: \_\_\_\_\_  
Date: \_\_\_\_\_ Contract No. \_\_\_\_\_  
Subject: ITOS D&E STRESS ANALYSIS Page No. A-51

The baseplate intercostals are spliced. The critical load occurs at the splice at joint 3 of beam BDB (Ref. A. p. 6.1.20, 6.1.21). The bending moment at the splice is approximately 90% of the maximum bending moment on the baseplate.

$$M_{\text{splice}} = .90 M = .90 \times 82.5 N = 74.4 N.$$

The intercostal splices are attached to the rib flanges which are 2.085 in. apart.

$$P = \frac{M_{\text{splice}}}{2.085} = \frac{74.4 N}{2.085} = 35.7 N$$

where the splice load,  $P$ , is taken by three rivets critical for yield in bearing.  $P_{\text{brg}} = 631 \text{ lb/rivet}$ . Using a S.F. = 1.15.

$$35.7 N = \frac{3 \times 631}{1.15}$$

$$\underline{N = 46.1}$$



Astro Electronics  
Division  
Princeton, New Jersey

Prepared for: \_\_\_\_\_ Report No. \_\_\_\_\_  
 Approved: \_\_\_\_\_ Project: \_\_\_\_\_  
 Date: \_\_\_\_\_ Contract No. \_\_\_\_\_  
 Subject: ITOS D&E STRESS ANALYSIS Page No. A-52 of \_\_\_\_\_

Cross Brace (Ref. A Section 6.7)

The cross brace was analyzed for a 60g sinusoidal input load, with a maximum bending moment  $M_{sine} = 2400$  in.lb. Loading a beam uniformly instead of sinusoidally increases the maximum bending moment.

$$M_{uniform} = \frac{\pi^2}{8} M_{sine}$$

The bending moment due to constant acceleration is then equal to

$$M = \left(\frac{\pi^2}{8}\right) \left(\frac{2400}{60}\right) N = 49.4 N$$

$$I/c = .0904 \text{ in}^3$$

Ref. A p. 6.7.7, 6.7.8

$$F_{cy} = 40,000 \text{ psi}$$

$$F_{cy}/S.F. = 40,000 / 1.15 = 34800 \text{ psi}$$

$$F_{cr} = 45500 \text{ psi}$$

$$F_{cr}/S.F. = 45,500 / 1.25 = 36400 \text{ psi}$$

$$f = M/(I/c) = 49.4 N / .0904 = 34800$$

$$\underline{N = 63.5}$$



Astro Electronics  
Division

Princeton, New Jersey

Prepared for: \_\_\_\_\_ Report No. \_\_\_\_\_

Approved: \_\_\_\_\_ Project: \_\_\_\_\_

Date: \_\_\_\_\_ Contract No. \_\_\_\_\_

Subject: ITOS D&E STRESS ANALYSIS Page No. A53 of \_\_\_\_\_

The cross brace channels flanges are spliced at the intersection of the braces. The splice attachments are critical for the rivets in bearing. The flanges are 2 in. apart. The load is taken by three rivets with a bearing yield allowable

$P = 498$  lbs (Ref. A p. 6.7.9). Then using a  
S.F. = 1.15 for yield.

$$\frac{3 \times 498}{1.15} = \frac{M}{2} = \frac{494 N}{2}$$

$$\underline{M = 52.6}$$

Separation Ring (Ref A. Section 6.6)

The ring buckling allowable is

$$F_{cr} = 9450 \text{ psi (conservative) Ref 6.6.14}$$

$$f = P / 2\pi R t ; R = 18.5 \text{ in.}, t = .060 \text{ in.}, \text{S.F.} = 1.25$$

The S/C weight is  $W = 770$  lbs. Then  $P = 770 N$

$$\frac{9450}{1.25} = \frac{770 N}{2\pi (18.5)(.060)}$$

$$\underline{N = 68.5}$$



Astro Electronics  
Division  
Princeton, New Jersey

Prepared for: \_\_\_\_\_ Report No. \_\_\_\_\_  
Approved: \_\_\_\_\_ Project: \_\_\_\_\_  
Date: \_\_\_\_\_ Contract No. \_\_\_\_\_  
Subject: ITOS D&E STRESS ANALYSIS Page No. A54

## Attachment Box Structure to Baseplate

The attachment of the equipment panels, the front panel and the back panel to the baseplate channels were critical at the cross M spacecraft lateral vibration resonant frequencies. The maximum load at the attachment was  $P = 6165 \text{ lbs}$  with a M.S. = .06.

At constant acceleration the total load is equal to  $P = W_e N$  where  $W_e$  is the spacecraft weight less the baseplate and separation ring weights.

$$W_e = 770 - 225 - 12 = 533 \text{ lbs.}$$

Most of the total load will be carried by the equipment panel attachments because of the more heavily loaded equipment panels. Allow the front and back



Astro Electronics  
Division  
Princeton, New Jersey

Prepared for: \_\_\_\_\_ Report No. \_\_\_\_\_  
Approved: \_\_\_\_\_ Project: \_\_\_\_\_  
Date: \_\_\_\_\_ Contract No. \_\_\_\_\_  
Subject: XTOS D&E STRESS ANALYSIS A55  
Page No. \_\_\_\_\_

---

panels to each be 25% as effective  
in reacting the total load as an  
equipment panel

$$P = P_{EP} + P_{EP} + .25 P_{EP} + .25 P_{EP}$$

Then  $P_{EP} = .4P$  or each equipment  
panel reacts 40% of the total load.

Then  $6165 \times 1.06 = (.40)(533 N)$  on the  
on the equipment panel attachment

$$\underline{N = 30.7}$$



Astro Electronics  
Division

Princeton, New Jersey

Prepared for: \_\_\_\_\_ Report No. \_\_\_\_\_

Approved: \_\_\_\_\_, \_\_\_\_\_ Project: \_\_\_\_\_

Date: \_\_\_\_\_ Contract No. \_\_\_\_\_

Subject: ITOS D&E STRESS ANALYSIS Page No A56

## VI. REFERENCES

- A. TIRDS M STRESS REPORT , JULY 17, 1967
- B. IMPROVED TDS (ITOS) TEST ANALYSIS REPORT  
FEB. 1, 1968
- C. ITOS SPACECRAFT VIBRATION TEST PROCEEDURE  
TP-V-1975000 REV. B NOV. 4, 1969
- D. ANALYSIS & DESIGN OF FLIGHT VEHICLE  
STRUCTURES , BRUNN , TRI-STATE OFFSET CO
- E. FORMULAS FOR STRESS AND STRAIN - ROARK  
IV EDITION MCGRAW-HILL BOOK CO

## APPENDIX B

### MECHANICAL DESIGN PARAMETERS

This appendix is a summary of design parameters assumed in the mechanical configuration of the ITOS D and E spacecraft design.

<u>ITEM</u>	<u>ASSUMPTIONS</u>
<p>1. <u>Launch Compatibility Envelope</u></p>	<p>a) A 3/4" (min) annular clearance envelope between the spacecraft and I. D. of fairing at STA 687.696, increasing linearly to a 1-3/8" annulus at the top of the spacecraft (STA 633.47). For definition, see Launch Compatibility Drawing (Fig. II-4).</p> <p>b) Move fairing annular reinforcing ring at STA 672.98 to STA 670.10 and ring at STA 638.98 to STA 642.48.</p> <p>c) Required radial clearance envelope in the area of the Marmon clamp is a 2.75" annulus added to the 37.75" O.D. of the MDAC attach fitting, i.e., clamp will be retained within a 43.25" diameter when bolts are cut and Marmon clamp halves open up.</p>

<u>ITEM</u>	<u>ASSUMPTIONS</u>
<p>2. <u>Spacecraft Imbalance*</u> (in launch configuration)</p> <p>RCA Ref. Letter #1963 dtd. 1/28/70</p>	<p>a) Eccentricity effects on the launch vehicle, due to imbalance, are within acceptable levels; i.e., during booster, turn-around, and spin-up phases.</p>

---

\*These numbers do not reflect a reduction in VHRR weight, which reduces the total spacecraft weight from 775 lbs to 735 lbs.

• Static - 1,705 in-lbs

• Dynamic

$$I_{12} \text{ (Yaw-Roll Plane)} = \\ +6.6 \text{ in-lb-sec}^2$$

$$I_{13} \text{ (Yaw-Pitch Plane)} = \\ -10.7 \text{ in-lb-sec}^2$$

$$I_{23} \text{ (Roll-Pitch Plane)} = \\ -6.0 \text{ in-lb-sec}^2$$

b) Separation springs will be force-matched to minimize coning effects during spacecraft separation from launch vehicle.

### 3. Spacecraft Spin-Up\*

a) Impart momentum of  $213 \pm 20$  in-lb-sec during second stage/spacecraft spin-up which for the ITOS D and E inertia is approximately  $2.7 \pm 0.3$  rpm.

NOTE: Higher ITOS D and E spacecraft inertia requires lower spin-up, to achieve equivalent stored momentum.

### 4. Sensors

a. Solar Proton Monitor (SPM)

1) Same Sensor Assembly as used on TIROS M; i.e., field-of-view, mounting and configuration remain status quo.

2) Electronics - one added connector, otherwise, same as used on TIROS M.

---

\*These numbers do not reflect a reduction in VHRR weight, which reduces the total spacecraft weight from 775 lbs to 735 lbs.

ITEM

ASSUMPTIONS

4. Sensors (Continued)

b. Scanning Radiometer (SR)

- 1) Same Sensor Assembly as used on TIROS M; i.e., field-of-view, mounting and configuration remain status quo.
- 2) Sun shield will be modified to incorporate a visible fused silica calibration target. Exact configuration is not defined as yet.
- 3) Electronics outline will remain the same as used on TIROS M.

c. Vertical Temperature Profile Radiometer (VTPR)

- 1) Configuration per "Barnes" Outline Drawing #204701-1031.
- 2) 62° - 54' total earth scan, 31° - 27' each side of sub-satellite point, normal to orbital plane.
- 3) VTPR inclined 17° - 27' with respect to roll/pitch plane when mounted to structure.
- 4) Approximately once in every 20 minutes of operation the VTPR mirror rotates 60° from its zero scan position to view cold space, and an additional 70° to view a self-contained calibration patch.
- 5) Alignment mirrors are provided on the instrument (total 3).
- 6) Three mounting bosses on each of two sides provide same hand configuration to be fastened to each of two spacecraft equipment panels.
- 7) Uncompensated momentum  $\leq 1$  in-oz-sec.

ITEM

ASSUMPTIONS

4. Sensors (Continued)

c. Vertical Temperature  
Profile Radiometer (VTPR)  
(Continued)

- 8) Weight of instrument 20 lbs. max.
- 9) Since sensor is mounted internal to equipment module, spacecraft thermal control will limit VTPR housing between zero to 30°C.

d. Very High Resolution  
Radiometer (VHRR)

- 1) Sensor configuration, including electronics per outline drawing SK 1976879
- 2) Configuration of motor and sensor electronics not fully identified.
- 3) Weight of sensor and electronics  $\approx$ 20 pounds.
- 4) Uncompensated momentum  $\leq$ 1 in-oz-sec.
- 5) Field of view - see Figure II-3.
- 6) Sensor is essentially thermally decoupled from the spacecraft. Normal screw fastening to the structure (without RTV interface) is adequate.
- 7) All non-sensory elements and the I. D. of the cooler will be covered by thermal blankets.

## APPENDIX C

### COMMUNICATION LINK ANALYSES

#### 1. ORBITAL CONSTRAINTS

##### a. Link Geometry and Path Losses

The ITOS D and E satellites will orbit the earth at an altitude of 790 nautical miles. Given orbit altitude, the slant range, R, may be calculated from the following formula:

$$R = -r \sin \psi + [r^2 (\sin^2 \psi - 1) + (r + H)^2]^{1/2} \text{ nautical miles}$$

where

r is radius of earth = 3440 nautical miles,

$\psi$  is ground antenna elevation angle, and

H is altitude of the satellite = 790 nautical miles.

The corresponding free space path loss, L, at a given frequency of transmission, is\*

$$L_{\text{(dB)}} = 92.45 + 20 \log f + 20 \log d$$

where

f is the frequency of transmission in GHz

d is slant range in kilometers = range in nautical miles x 1.852.

Slant ranges as a function of ground antenna elevation angle for a satellite orbit of 790 nautical miles are given in Table C-1.

##### b. View Angle Subtended by Earth

In the determination of the required spacecraft antenna coverage in the earth locked operational mode, an important parameter is the half angle of the

---

\*Reference Data for Radio Engineers, Fifth Edition. Howard W. Sams Co., 1968, pg. 34-3.

TABLE C-1. SLANT RANGES FOR CIRCULAR ORBIT

Elevation Angle (Deg.)	Slant Range*		
	(Naut. Mi.)	(KM)	(Statute Mi.)
0	2460.8	4557.5	2831.9
5	2179.4	4036.2	2508.0
10	1935.3	3584.1	2227.1
15	1727.0	3198.4	1987.4
20	1551.5	2873.4	1785.5
25	1404.9	2601.8	1616.7
30	1282.8	2375.8	1476.3
35	1181.6	2188.3	1359.7
40	1097.6	2032.8	1263.2
45	1028.2	1904.2	1183.2
50	970.8	1798.0	1117.2
55	923.7	1710.7	1063.0
60	885.4	1639.7	1018.9
65	854.6	1582.7	983.5
70	830.5	1538.1	955.8
75	812.5	1504.7	935.0
80	799.9	1481.4	920.5
85	792.5	1467.6	912.0
90	790.0	1463.1	909.1

\*These slant ranges are used to compute path loss in the Link Analyses.

cone subtended by the earth. The half-cone angle,  $\alpha$ , may be calculated from the following formula:

$$\alpha = \arcsin\left(\frac{R}{R + H}\right)$$

where:

R is the radius of earth = 3440 nautical miles

H is the altitude of the satellite.

For the ITOS D and E mission,  $H = 790$  nautical miles and therefore the half-cone angle  $\alpha = 54.4$  degrees. The corresponding solid angle is given by the expression

$$\psi = 2\pi (1 - \cos \alpha) \text{ steradians}$$

which for the ITOS D and E mission is  $\psi = 2\pi (0.4183)$  steradians. This expression is used to compute command link received noise.

## 2. COMMAND LINK ANALYSIS

### a. Path Loss

Using the formulas previously described in paragraph 1, the approximate path losses as a function of ground antenna elevation angle for a satellite orbit of 790 nautical miles are listed in Table C-2.

### b. RF Power Margin Calculation

Sufficient signal level must be provided at the input of the dual command receiver to reliably operate the command decoder decoding circuits. The dual decoder is designed to respond to input levels equal to or greater than its threshold value of 0.70 volt rms. The command receiver output is 0.77 volt rms when the input level is -107 dBm, which is the receiver agc threshold. The summary of link calculations is given in Table C-3. These figures are identical to those of TIROS M.

The link calculations show that the worst-case input rf level to the receiver is 3.0 dB above the -107 dBm agc threshold in the unstabilized mode and 10.0 dB above the agc threshold in the normal operation stabilized mode, using 1 kW of command transmitter power. In the stabilized mode, 200 watts of command transmitter power are sufficient to provide a 3 dB margin above the agc threshold. The link calculations have been performed

under the assumption that the Avien, Inc. ground antenna is used mounted on the 85-foot dish. This antenna has a gain of 12 dB and a 3-dB line loss. The performance margin may be improved above the values shown in the table by increasing the transmitter output power and/or using a higher efficiency command antenna. The net improvements in signal margin, achievable by several available command transmitter/antenna combinations, are shown in Table C-4.

TABLE C-2. PATH LOSS FOR COMMAND LINK AS A FUNCTION OF ELEVATION ANGLE

[ORBITAL ALTITUDE (NAUTICAL MILES) = 790  
 FREQUENCY (MHz) = 148.56]

Elevation Angle $\psi$ (Degrees)	Path Loss, L (dB)
0	149.1
5	148.0
10	147.0
15	146.0
20	145.0
25	144.2
30	143.4
35	142.7
40	142.0
45	141.5
50	141.0
55	140.5
60	140.2
65	139.9
70	139.6
75	139.4
80	139.3
85	139.2
90	139.2

TABLE C-3. WORST-CASE RF COMMAND LINK CALCULATION

Parameter	Unstabilized		Stabilized	Remarks
	Panels Stowed	Panels Deployed	Panels Deployed	
Transmitter Power	60.0 dBm	60.0 dBm	60.0 dBm	1 kW normal operating level
Ground Antenna Gain	12.0 dB	12.0 dB	12.0 dB	Avien antenna
Line Losses Transmitter-to-Antenna	- 3.0 dB	- 3.0 dB	- 3.0 dB	
Path Loss	-148.0 dB	-148.0 dB	-148.0 dB	5 degree elevation
Polarization Loss	- 3.0 dB	- 3.0 dB	- 3.0 dB	Circular-to-linear
Spacecraft Antenna Gain	- 14.0 dB	- 14.0 dB*	- 7.0 dB	Min. Spec. Limit
Passive Circuit Losses:				
Bandpass Filter Loss (148 MHz)	- 2.5 dB	- 2.5 dB	- 2.5 dB	Max. Spec. Limit
Notch Filter (2) Losses	- 1.0 dB	- 1.0 dB	- 1.0 dB	Max. Spec. Limit
Spacecraft Cable Losses	- 0.3 dB	- 0.3 dB	- 0.3 dB	Max. Spec. Limit
Stub and Reflection Losses	- 0.7 dB	- 0.7 dB	- 0.7 dB	Max. Spec. Limit
Hybrid Insertion Loss	- 0.5 dB	- 0.5 dB	- 0.5 dB	Max. Spec. Limit
Hybrid Power Splitter	- 3.0 dB	- 3.0 dB	- 3.0 dB	Power split between two receivers

\*Except Region IV of Antenna Pattern.

TABLE C-3. WORST-CASE RF COMMAND LINK CALCULATION  
(Continued)

Parameter	Unstabilized		Stabilized	Remarks
	Panels Stowed	Panels Deployed	Panels Deployed	
Receiver rf Power (each receiver)	-104.0 dBm	-104.0 dBm	- 97.0 dBm	
Command Receiver agc Threshold	-107.0 dBm	-107.0 dBm	-107.0 dBm	0.77 volt at decoder
rf Margin Above agc Threshold	+ 3.0 dB	+ 3.0 dB	+ 10.0 dB	

c. Receiver Bandwidth Requirements

The minimum if, bandwidth of the receiver should be able to handle the modulation bandwidth, the maximum doppler shift, and the maximum frequency offsets due to frequency instability in the transmitter and in the receiver local oscillator.

(1) DOPPLER SHIFT

The doppler shift is indicated by the following expression and is a maximum at the minimum elevation angle:

$$\Delta F = \frac{FV}{C} \cos B,$$

where V is the spacecraft velocity, C is the velocity of light, and B is the angle between the ground station and the direction of the spacecraft velocity vector. At the command link frequency of 148 MHz, the maximum doppler shift is  $\pm 2.9$  kHz, or a total of 5.8 kHz.

(2) FREQUENCY STABILITY

The receiver local oscillator stability is specified at  $\pm 0.005$  percent maximum, yielding a maximum frequency instability of  $\pm 6.4$  kHz or a total of 12.8 kHz over a temperature range from  $-15$  to  $+60^\circ\text{C}$ . The if filter center frequency stability is specified at  $\pm 3$  kHz or a total of 6 kHz.

TABLE C-4. IMPROVEMENT IN COMMAND RF SIGNAL MARGINS WITH  
 VARIOUS ALTERNATE COMMAND TRANSMITTER/  
 ANTENNA COMBINATIONS

Command System	Transmitter Power (kW)	Antenna Gain* (dB)	Ground Line Loss (dB)	Improvement in rf Signal Margin (dB)
ITA-120H Transmitter and Avien Disc-on-Rod Rod Antenna	1.0	12.0	-3.0	+0.0 (reference)
	2.5			+4.0
ITA-120H Transmitter and RSI Disc-on-Rod Rod Antenna	1.0	13.6	-3.4	+1.2
	2.5			+5.2
Hughes HC-300 Transmitter and RSI 9 Disc-on-Rod Rod Array/SATAN Pedestal Antenna	2.5	23.7	-1.7	+17.0
GE-4BT91A1 or ITA-2500H Transmitter and RSI 9 Disc-on-Rod Array/SATAN Pedestal Antenna	5.0	23.7	-1.7	+20.0
*Handbook of NASA/GSFC Tracking, Data Acquisition and Communications Antennas, Oct. 1964; N 65-18255				

(3) MODULATION BANDWIDTH

The modulation bandwidth is a maximum of  $\pm 11.3$  kHz or a total of 22.6 kHz. This is the bandwidth required when the highest frequency FSK tone is being transmitted.

(4) WORST-CASE IF BANDWIDTH

The required if. bandwidth is obtained by adding all the individual frequency instabilities and uncertainties, as shown in Table C-5.

The worst-case bandwidth of 47.6 kHz corresponds to a 6 dB signal loss in the highest FSK sideband of the IF signal. This loss corresponds to an effective modulation index loss from  $m$  to  $3/4 m$ , or a 2.5 dB loss in the receiver output signal level.

Table C-5 also includes the expected if. bandwidth requirement based on measured receiver oscillator drift over the predicted spacecraft baseplate temperature range of  $+10$  to  $+30^{\circ}\text{C}$ . This data was obtained from environmental tests of eight TOS dual command receivers. The results shows that, even though the worst-case calculation indicates a 6 dB signal loss in the highest FSK sideband of the if. signal, the actual operating environment will not produce this worst-case condition.

The expected signal loss due to IF filter and local oscillator drift characteristics is less than 1 dB compared to a 6 dB signal loss for the worst-case conditions.

d. Interference Signals

The presence of interference signals is unavoidable due to the physical proximity of the beacon, real-time, and S-band transmitters. Interfering signals might produce a desensitization of the receiver, reducing the effective threshold margin. Intensive tests on the TIROS M receivers have shown that for the interfering signals at frequencies around 136 MHz (12 MHz away from command frequency) negligible desensitization occurs if the interfering level is maintained below  $-30$  dBm. Interfering signals lying in the receiver passband have to be maintained below  $-113$  dBm. The interference levels from the transmitters and the required isolation between the transmitters and the command receiver port are given in Table C-6.

The total interference level in the receiver if. passband is the sum of the interference powers of the first six entries in Table C-6. The resultant interference level is  $-117.2$  dBm, which is low enough to prevent receiver desensitization.

TABLE C-5. REQUIRED WORST-CASE COMMAND RECEIVER  
IF BANDWIDTH

	Receiver Temperature Range	
	-15°C to +60°C	+10°C to +30°C
Transmitter Instability*	0.4 kHz	0.4 kHz
Receiver Local Oscillator Instability (Spec.)	12.8 kHz	5.2 kHz**
Receiver if. Filter Instability (Spec.)	<u>6.0 kHz</u>	<u>6.0 kHz</u>
Total Receiver Frequency Uncertainty	19.2 kHz	11.6 kHz
Doppler Shift	5.8 kHz	5.8 kHz
Maximum Modulation Bandwidth	<u><u>22.6 kHz</u></u>	<u><u>22.6 kHz</u></u>
Worst-Case if. Bandwidth Required	47.6 kHz	40.0 kHz
Command Receiver if. Bandwidth Spec. ±1 dB	40.0 kHz Min.	-
-6 dB	48.0 kHz Min.	-
*Telegram 13/2238Z Oct. GMOR **Predicted values based on measurements of 8 command receivers.		

TABLE C-6. INTERFERENCE LEVELS AT THE  
COMMAND RECEIVER PORT

Source of Interference	Frequency (MHz)	Transmitter Level at Command Port (dBm)	Allowable Interference Level at Command Receiver Port (dBm)	Minimum Isolation Required (dB)
Beacon Transmitter	148	-100	-125	25
	108	- 50	-125**	25*
VHF Real-Time Transmitter	148	- 80	-125	45
	108	- 50	-125**	25*
S-Band Transmitter	148	- 90	-125	35
	108	- 70	-125**	5*
Beacon Transmitter (250 mW)	136.7	+ 24	- 40	64
VHF Real-Time Transmitter (5 W)	137.5	+ 37	- 30	67
<p>*50-dB image rejection is provided by the receiver internal circuitry.</p> <p>**Effective interference level in the if. passband.</p>				

e. Random Noise Temperature

The overall link noise temperature consists of the receiver noise temperature, the noise temperature due to prereceiver circuit losses, the cosmic noise temperature, and the earth noise temperature. The receiver noise temperature is the most important contributor to the overall link noise temperature.

(1) RECEIVER NOISE TEMPERATURE

The noise figure, F, of the receiver is specified at 10 dB max. This corresponds to a receiver temperature of

$$T_R = 290^\circ (F-1) = 2610^\circ\text{K}.$$

(2) PRERECEIVER CIRCUIT NOISE TEMPERATURE

The prereceiver circuit includes all cables and filters between the antenna and the receiver input. The losses in the prereceiver circuit contribute noise power proportional to the actual thermodynamic (thermal) temperature of the loss elements,  $T_t$ , and is given by

$$T = \left(1 - \frac{1}{L}\right) T_t$$

where L is the circuit loss expressed as a power ratio.

Consider  $T_t$  to be approximately equal to  $333^\circ\text{K}$ , and the circuit loss to be equal to 5 dB. This corresponds to the 8 dB maximum spec loss between antenna and receiver, less the 3 dB power-splitting loss of the hybrid coupler which does not contribute noise power. Then:

$$T = \left(1 - \frac{1}{3.16}\right) 333^\circ\text{K} = 227^\circ\text{K}.$$

The noise power is split equally between the two receiver channels, which yields an effective circuit noise temperature, at the input of the receiver, of

$$T_c = \frac{227^\circ}{2} = 113.5^\circ\text{K}.$$

(3) COSMIC NOISE TEMPERATURE

For a broad beam antenna, such as the spacecraft command antenna, the value of the cosmic temperature,  $T_s$ , may be assumed to correspond to the average sky temperature which is  $1200^\circ\text{K}$  at 148 MHz.\*

---

\*L. V. Blake, Antenna and Receiving-System Noise Temperature Calculation, U.S. Naval Research Laboratory Report 5668 (AD-265-414) Sept. 19, 1961.

However, since the earth covers a significant portion of the sky (108.8-degree subtended angle), a correction,  $\Delta T$ , proportional to the fraction of solid angle intercepted by the earth should be applied. The correction,  $\Delta T$  is given by

$$\begin{aligned}\Delta T &= (T_s) \times \frac{(\text{solid angle subtended by earth})}{4\pi \text{ steradians}} \text{ } ^\circ\text{K} \\ &= 1200 \text{ } ^\circ\text{K} \times \frac{2\pi(1-\cos 54.4^\circ)}{4\pi} = 251^\circ\text{K}\end{aligned}$$

The effective sky temperature is:

$$T_{se} = T_s - \Delta T = 1200 - 251 = 949^\circ\text{K}$$

The worst-case effective temperature at the receiver port,  $T_{se}$ , is obtained by taking the lowest (measured) 6.7 dB loss from antenna to receiver into account.

$$T_{se} = \frac{949^\circ\text{K}}{4.7} = 202^\circ\text{K}.$$

#### (4) EARTH NOISE TEMPERATURE

The radio black-body temperature of the earth is  $254^\circ\text{K}$ .\* The contribution of the earth noise temperature at the command antenna is given by

$$\begin{aligned}T_E &= \frac{(\text{solid angle subtended by earth})}{4\pi \text{ steradians}} \times (T_{\text{Earth}}) \\ &= \frac{2\pi(1-\cos 54.4)}{4\pi} \times 254^\circ\text{K} = 53.2^\circ\text{K}.\end{aligned}$$

There is a 6.7-dB (4.7 power ratio) loss between receiving antenna and receiver port which yields the effective earth noise temperature at the receiver port of

$$T_{Ee} = \frac{53.2^\circ\text{K}}{4.7} = 11.3^\circ\text{K}.$$

---

\*Reference Data for Radio Engineers, 5th Ed. Howard W. Sams Co. 1968., pp 34-5.

(5) TOTAL IF NOISE POWER

The overall system noise temperature is then given by the summation below:

Receiver	2610.0°K
Prereceiver Circuit	113.5°K
Cosmic	202.0°K
Earth	11.3°K
<hr/>	<hr/>
System	2936.8°K

The system noise temperature at the receiver input port is then  $T_{\text{sys}} = 2936.8^\circ\text{K}$ .

The noise power in the if. is  $N$ , and  $N = kT_{\text{sys}} B_{\text{if}}$ .

where

$k$  = Boltzman's constant =  $1.38 \times 10^{-23}$  Joules/°K and

$B_{\text{if}}$  = Receiver if. noise bandwidth = 48 kHz.

The total if. noise power is

$$N = 1.38 \times 10^{-23} \times 2.9368 \times 10^3 \times 48 \times 10^3 = 1.94 \times 10^{-15} \text{ watts or}$$

$$N = -117.1 \text{ dBm for an if. bandwidth of 48 kHz.}$$

f. Carrier-To-Noise Ratio

For an if. bandwidth of 48 kHz and a receiver rf power input of -107 dBm, corresponding to the receiver agc threshold, the if. carrier-to-random-noise ratio is

$$C_{\text{if}} / N_{\text{if}} = -107 \text{ dBm} + 117.1 \text{ dBm} = 10.1 \text{ dB.}$$

The if. carrier-to-interference ratio at rf power threshold is

$$-107 \text{ dBm} + 117.2 \text{ dBm} = 10.2 \text{ dB.}$$

The total average power of combined random noise and interference is

$$P_n \text{ total} = -114.2 \text{ dBm.}$$

The overall carrier-to-noise ratio (including interference power) at the receiver agc threshold is

$$\frac{C}{N_t} = +7.2 \text{ dB for an if. bandwidth of 48 kHz.}$$

Note that the actual worst-case expected value is above this value by the calculated rf margins shown in Tables C-3 and C-4.

**g. Subcarrier Signal-to-Noise Ratio**

The command system performance is not limited by the 7.2-dB carrier-to-noise ratio in the if. The parameter of importance is the subcarrier-to-noise ratio in the subcarrier bandwidth,  $B_{sc}$ , which is given by the expression:

$$(S/N)_{sc} = m^2 \frac{B_{if}}{B_{sc}} \cdot \frac{C}{N}$$

where  $m$  is the carrier modulation index.

The subcarrier-to-noise ratios for random noise only and for total noise and interference are given in Table C-7 where the signal-to-noise ratios of both FSK subcarriers have been corrected for the calculated 2.5 dB possible modulation loss due to the worst-case possible upper sideband attenuation.

TABLE C-7. SUBCARRIER-TO-NOISE RATIOS AT RECEIVER AGC THRESHOLD

Subcarrier	Bandwidth (Hz)	Random Noise Only $S_c/N_c$ (rms/rms)	Random Noise and Interference (rms/rms)
FSK 2	1575	21.6 dB	18.7 dB
FSK 1	1103	23.1 dB	20.2 dB
TONE 2	810	27.0 dB	24.1 dB
TONE 1	585	28.4 dB	25.5 dB

The frequencies  $f_c + \Delta f$  and  $f_c - \Delta f$  are extracted by two bandpass filters having a  $\pm 2$  percent bandwidth. These tones are subsequently envelope-detected and trigger a threshold device. Next, they are integrated and digitally processed. The detected-pulse signal-to-noise ratio is improved by 5.4 dB above the subcarrier signal-to-noise ratio by the tone filters. This yields a demodulated signal-to-noise ratio in excess of 24.1 dB rms/rms (27.1 dB peak/rms). This

corresponds to a bit-error probability of less than 1 part in  $10^6$ , which quite adequately meets system requirements.

### 3. BEACON LINK ANALYSIS

#### a. Receiver IF Bandwidth Requirements

##### (1) RECEIVER IF INFORMATION BANDWIDTH

A signal-to-noise ratio of 38.4 dB rms/rms is obtained at the 3.9-kHz channel demodulator threshold of 12 dB. A margin of 5.3 dB above the 12-dB fm threshold of the subcarrier demodulator is obtained in the operational mode with the phase index of the highest subcarrier frequency (3.9 kHz) set at 0.50 radian. With this phase index, a negligible amount of power lies outside the first pair of 3.9-kHz sidebands of the carrier frequency. Since the bandwidth of the 3.9 kHz subcarrier is 703 Hz, the rf information bandwidth is then:

$$\text{Information bandwidth} - 2 (3,900) + 703 = 8,503 \text{ Hz.}$$

##### (2) DOPPLER SHIFT

At a ground antenna elevation of 5 degrees, the maximum doppler shift at 136.77 MHz is  $\pm 2.65$  kHz or a total of 5.3 kHz.

##### (3) TRANSMITTER FREQUENCY UNCERTAINTY

The transmitter frequency instability is  $\pm 0.005$  percent or  $\pm 6.8$  kHz, which yields a total of 13.7 kHz.

The total rf bandwidth is:

Information	8.5 kHz
Doppler Shift	5.3 kHz
Instability	13.7 kHz
Total rf bandwidth	<hr/> 27.5 kHz

The ground station phase-lock loop receiver tracks the frequency shifts due to doppler and transmitter frequency uncertainty. Therefore, the if. bandwidth of the receiver need only be wide enough to pass the 8.5-kHz information bandwidth. It has an if. bandwidth of 30 kHz which is adequate to handle the total rf bandwidth.

**b. Subcarrier Phase Deviations**

The rf input into the phase lock loop receiver can be expressed as  $g(t) \approx A_c \cos(\omega_c t + \phi(t))$ , where  $\phi(t)$  is the phase modulation due to the two subcarriers of frequencies ( $f_A$ ) and ( $f_B$ ). The  $\phi(t)$  is given by

$$\phi(t) = b_A \sin \omega_A t + b_B \sin \omega_B t.$$

The output of the phase lock detector is proportional to  $\sin \phi(t)$ . It can be shown\* that the demodulated subcarriers are

$2J_1(b_A) J_0(b_B) A_c \sin \omega_A t$  (for subcarrier  $f_A$ )  
and,  
 $2J_1(b_B) J_0(b_A) A_c \sin \omega_B t$  (for subcarrier  $f_B$ )

The individual subcarrier signal-to-noise power ratio is given by:

$$S_c / N_c = 2J_1^2(b_A) J_0^2(b_B) \left( \frac{P_c}{\eta B_{scA}} \right) \quad (\text{for subcarrier A})$$

where

$P_c = A_c^2 / 2$  is average carrier power,

$\eta$  is if. noise density (watts in 1 Hz), and

$B_{sc}$  is subcarrier bandwidth.

$J_0(b_A)$ ,  $J_1(b_A)$  are Bessel Functions of the first kind.

For small phase indices, the subcarrier signal-to-noise power ratio expression

becomes approximately equal to  $\frac{b^2}{2\eta B_{sc}}$ .

It is desirable to design the system such that both subcarriers have approximately equal margin above the fm threshold. The phase deviation  $b_B$  of the 2.3-kHz subcarrier was selected to satisfy the following equation:

$$\frac{b_A}{\sqrt{B_{scA}}} \approx \frac{b_B}{\sqrt{B_{scB}}}$$

\*B. D. Martin, The Pioneer IV Lunar Probe: A Minimum Power FM/PM System Design, JPL TR-32-215, 1962.

The subcarrier bandwidths are given below:

Channel A (3.9-kHz subcarrier IRIG channel No. 9)

Center Frequency	3.9 kHz
Deviation ( $\Delta f$ )	$\pm 7.5$ percent of center frequency
Baseband ( $f_m$ )	59 Hz
Subcarrier Bandwidth	703 Hz
Rf Carrier Phase Index	0.50 radian

Channel B (2.3 kHz)

Center Frequency	2.3 kHz
Deviation	$\pm 20$ percent
Baseband	160 Hz
Subcarrier Bandwidth	1240 Hz
Rf Carrier Phase Index	0.70 radian

As in TIROS M, the 3-dB attitude data bandwidth is 160 Hz. In order to obtain a reasonable demodulated baseband signal-to-noise, a nonstandard deviation has to be selected. With this deviation, the composite subcarrier spectrum extends from 1.68 to 4.25 kHz. A voice channel of the long lines can handle a spectrum extending from 1.60 to 4.4 kHz. An increase of subcarrier deviation beyond  $\pm 20$  percent would extend the composite subcarrier spectrum beyond the capacity of a voice channel of the long lines. The composite spectrum is shown in Figure C-1.

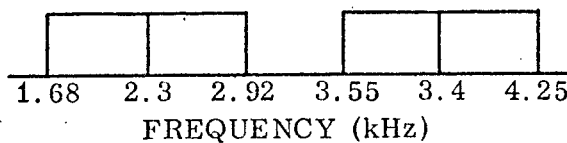


Figure C-1. Composite Subcarrier Spectrum of Demodulated Beacon and Telemetry Baseband

c. **Distortion Products**

The distortion signals from the phase detector can be shown to be as follows:

<u>Frequency</u>	<u>Power Level</u>
$f_A \pm 2f_B$	$2J_1^2(b_A) J_2^2(b_B) P_c$
$f_B \pm 2f_A$	$2J_1^2(b_B) J_2^2(b_A) P_c$
$3f_A$	$2J_0^2(b_B) J_3^2(b_A) P_c$
$3f_B$	$2J_0^2(b_A) J_3^2(b_B) P_c$

The calculated principal distortion products, and their relative amplitudes with respect to the 3.9 kHz subcarrier are shown in Table C-8. It can be observed that all the distortion terms fall outside the subcarrier spectrum. In addition, the subcarrier filters will provide at least 20-dB attenuation of the intermodulation products.

TABLE C-8. PRINCIPAL DISTORTION PRODUCTS AND RELATIVE AMPLITUDE

Term	Frequency (kHz)	Relative Amplitude (dB)
$f_A - 2f_B$	0.7	-22.8
$f_B$	2.3	+ 3.2*
$f_A$	3.9	0.0 (Ref)*
$f_B - 2f_A$	5.5	-25.7
$3f_B$	6.9	-29.4
$2f_B + f_A$	8.5	-22.8
$f_B + 2f_A$	10.1	-25.7
$3f_A$	11.7	-38.2
*Desired output terms shown for reference.		

d. RF Link Calculation

The circularly polarized beacon signal is intercepted by the 85-foot parabolic dish antenna system, using polarization diversity reception. The ground station parameters are summarized in Table C-9.

TABLE C-9. CDA GROUND STATION PARAMETERS  
(BEACON RECEPTION)

Antenna Gain*	27.6 dB at 136.77 MHz
Polarization	Polarization diversity reception (-1.0 dB)
Receiver Noise Figure	4.5 dB
IF Bandwidth	30 kHz
*Handbook of NASA/GSFC Tracking, Data-Acquisition, and Communications Antennas N65-18255 Oct. 1964.	

(1) SYSTEM NOISE TEMPERATURE

The receiver noise temperature,  $T_R$ , corresponding to a noise figure,  $F$ , of 4.5 dB is

$$T_R = 290 (F-1) = 522^\circ\text{K}.$$

The sky noise temperature at 136 MHz for 95 percent of the sky is taken to be  $T_s = 1400^\circ\text{K}$ .\*

The total effective system temperature is

$$T_{\text{sys}} = 522 + 1400 = 1922^\circ\text{K}.$$

The noise power density at if. is then

$$\eta = K T_{\text{sys}} = -165.8 \text{ dBm in 1 Hz.}$$

Using the above value for  $\eta$ , the noise power for each subcarrier has been derived as shown in Table C-10.

\*NRL Report 5668 (AD-265-414)

TABLE C-10. SUBCARRIER NOISE POWER COMPUTATIONS

Subcarrier Channel	3.9 kHz	2.3 kHz	PLL*
Subcarrier Bandwidth	703 Hz	1240 Hz	200 Hz
Subcarrier Bandwidth in dB-Hz	28.4 dB-Hz	30.9 dB-Hz	23 dB-Hz
Noise Power Density in 1 Hz	-165.7 dBm	-165.7 dBm	-165.7 dBm
Subcarrier Noise Power *Phase-Locked Loop	-137.3 dBm	-134.8 dBm	-142.7 dBm

(2) LINK LOSSES

The space loss is -147.3 dB at 5 degrees elevation, 790 nautical miles altitude, at 136.77 MHz.

(3) SUBCARRIER MODULATION LOSSES

The demodulated subcarrier power is given by  $2J_1^2(b_A) J_0^2(b_B) P_c$

where  $P_c$  is the total carrier power,  $b_A$  is the peak phase deviation produced by the subcarrier of interest, and  $b_B$  is the peak phase deviation of the second subcarrier. The factor  $2J_1^2(b_A) J_0^2(b_B)$  is the fraction of the carrier power recovered in the subcarrier. It is the modulation loss. The loss in the carrier frequency term is  $J_0^2(b_A) J_0^2(b_B)$ .

The beacon transmitter deviation sensitivity can vary ±12.5 percent from the nominal value. The resulting modulation losses are shown in Table C-11.

TABLE C-11. MODULATION LOSS OF BEACON SUBCARRIERS

Signal	Modulation Loss		
	Unfavorable Tolerances	Nominal	Favorable Tolerances
Carrier	-2.10 dB	-1.65 dB	-1.25 dB
3.9 kHz Subcarrier	-11.80 dB	-10.40 dB	-9.18 dB
2.3 kHz Subcarrier	-8.38 dB	-7.20 dB	-6.19 dB

#### (4) WORST-CASE RF LINK CALCULATIONS

The worst-case link calculations are tabulated in Tables C-12, C-13, and C-14.

##### e. Estimated S/N Degradation in Long Lines

The signal-to-noise ratios given previously cover only the link and receiving equipment noise. The multiplexed subcarriers at the CDA receiver output are transmitted via long lines to NESC/Suitland. These lines introduce additional noise.

Published measurements on the long lines\* have shown the subcarrier-to-noise ratio to be 33.0 dB rms/rms for the beacon and telemetry channel over a bandwidth of approximately 3000 Hz from Gilmore to NESC/Suitland. The long lines from Wallops to NESC/Suitland have a better ratio (-44.5 dB). The design goal for both lines is 23 dB rms/rms.

With this subcarrier-to-noise ratio, the demodulated baseband  $S_o/N_{LL}$  contributed by the lines alone (i.e., assuming a noiseless subcarrier into the line) is given in Table C-15. The signal-to-noise ratio due to the link  $S_o/N_o$  is combined with the long line S/N to yield the overall S/N at Suitland. The ratios are combined according to the following equation:

$$\frac{N_T}{S_o} = \frac{N_{J.L}}{S_o} + \frac{N_o}{S_o}.$$

---

\*TOS Communications Test Results, Report TER-111, Telcom, Inc., prepared for ESSA-NESC, March 30, 1966.

TABLE C-12. WORST-CASE RF BEACON LINK CALCULATION

Parameter	Unstabilized		Stabilized	Re- marks
	Panels Stowed	Panels Deployed	Panels Deployed	
Transmitter Power	24.0 dBm	24.0 dBm	24.0 dBm	spec value
Transmitting Circuit Loss	- 2.0 dB	- 2.0 dB	- 2.0 dB	spec value
Spacecraft Antenna Gain	- 9.5 dBi	- 14.5 dBi**	- 9.5 dBi	over linear isotropic
Space Path Loss	-147.3 dB	-147.3 dB	-147.3 dB	5 degree elevation
Diversity Reception Loss*	- 1.0 dB	- 1.0 dB	- 1.0 dB	
Receiving Antenna Gain	27.6 dB	27.6 dB	27.6 dB	85 foot dish
Total Received Power	-108.2 dBm	-113.2 dBm	-108.2 dBm	
Received Noise Spectral Density	-165.8 dBm/Hz	-165.8 dBm/Hz	-165.8 dBm/Hz	$T_{sys} = 1922^{\circ}K$
Carrier Modulation Loss	- 2.1 dB	- 2.1 dB	- 2.1 dB	
Received Carrier Power	-110.3 dBm	-115.3 dBm	-110.3 dBm	
PLL Noise Power	-142.7 dBm	-142.7 dBm	-142.7 dBm	PLL bandwidth = 200 Hz
PLL Signal-to-Noise Ratio	32.4 dB	27.4 dB	32.4 dB	

\*If one of the diversity channels falls below threshold, a 3 dB loss is incurred.  
 \*\*Except Regions III and IV of Antenna Pattern.

TABLE C-12. WORST-CASE RF BEACON LINK CALCULATION  
(Continued)

Parameter	Unstabilized		Stabilized	Re- marks
	Panels Stowed	Panels Deployed	Panels Deployed	
PLL Threshold	6.0 dB	6.0 dB	6.0 dB	as- sumed***
PLL Margin above Threshold	26.4 dB	21.4 dB	26.4 dB	
***F. Gardner - Theory of Phase Lock Techniques, Wiley, 1964.				

TABLE C-13. WORST-CASE LINK CALCULATION FOR 3.9 kHz CHANNEL

Parameter	Unstabilized		Stabilized	Remarks
	Panels Stowed	Panels Deployed	Panels Deployed	
Total Received Power	-108.2 dBm	-113.2 dBm	-108.2 dBm	from Table C-12
Subcarrier Modulation Loss	- 11.8 dB	- 11.8 dB	- 11.8 dB	from Table C-11
Received Subcarrier Power	-120.0 dBm	-125.0 dBm	-120.0 dBm	
Subcarrier Noise Power	-137.3 dBm	-137.3 dBm	-137.3 dBm	from Table C-10
Subcarrier-to- Noise Ratio	17.3 dB	12.3 dB	17.3 dB	rms/rms
FM Detector Threshold	12.0 dB	12.0 dB	12.0 dB	assumed
Subcarrier Margin	5.3 dB	0.3 dB	5.3 dB	5° elevation
Baseband S/N at Subcarrier Threshold	38.4 dB	38.4 dB	38.4 dB	

TABLE C-13. WORST-CASE LINK CALCULATION FOR 3.9 kHz CHANNEL  
(Continued)

Parameter	Unstabilized		Stabilized	Remarks
	Panels Stowed	Panels Deployed	Panels Deployed	
Worst-Case Baseband S/N	43.7 dB	38.7 dB	43.7 dB	rms/rms in 59 Hz bandwidth
	52.7 dB	47.7 dB	52.7 dB	p-p/rms in 59 Hz bandwidth

TABLE C-14. WORST-CASE LINK CALCULATION FOR 2.3 kHz CHANNEL

Parameter	Unstabilized		Stabilized	Remarks
	Panels Stowed	Panels Deployed	Panels Deployed	
Total Received Power	-108.2 dBm	-113.2 dBm	-108.2 dBm	from Table C-12
Subcarrier Modulation Loss	- 8.4 dB	- 8.4 dB	- 8.4 dB	from Table C-11
Received Subcarrier Power	-116.6 dBm	-121.6 dBm	-116.6 dBm	
Subcarrier Noise Power	-134.8 dBm	-134.8 dBm	-134.8 dBm	from Table C-10
Subcarrier-to-Noise Ratio	18.2 dB	13.2 dB	18.2 dB	
FM Detector Threshold	12.0 dB	12.0 dB	12.0 dB	assumed
Subcarrier Margin	6.2 dB	1.2 dB	6.2 dB	5° elevation
Baseband S/N at Subcarrier Threshold	31.9 dB	31.9 dB	31.9 dB	
Worst-Case Baseband S/N	38.1 dB	33.1 dB	38.1 dB	rms/rms in 160 Hz bw.
	47.1 dB	42.1 dB	47.1 dB	p-p/rms in 160 Hz bw.

TABLE C-15. S/N CONTRIBUTION BY THE LONG LINES

Subcarrier	Baseband Link S/N at Threshold	Baseband Long Lines S/N	Net S/N	Bandwidth
2.3 kHz ( $\pm 20$ percent dev.)	31.9 dB rms/rms	46.7 dB rms/rms	31.8 dB rms/rms	160 Hz
3.9 kHz ( $\pm 7.5$ percent dev.)	38.4 dB rms/rms	55.7 dB rms/rms	38.4 dB rms/rms	59 Hz

The long lines are not expected to produce any appreciable degradation of the demodulated baseband signal-to-noise ratio.

#### 4. VHF REAL-TIME LINK ANALYSIS

##### a. Receiver Bandwidth Requirements

The significant information bandwidth is:  $bw = 2 (f_d + f_H)$  where  $f_d$  is peak deviation and  $f_H$  is maximum modulating frequency.

The visible channel of the radiometer has baseband components up to 1.2 kHz. For the visible channel,  $f_H = 2.4 + 1.2 = 3.6$  kHz. The maximum  $f_d = 10$  kHz; thus, an information bandwidth of 27.2 kHz is required to include all the significant sidebands.

The doppler shift of the signal is 5.3 kHz, while the allowance for transmitter instability is 13.8 kHz ( $2 \times 0.005$  percent of 137.5 MHz). The total bandwidth required is therefore 43.6 kHz. The 50-kHz if. bandwidth of the present APT field station receivers is therefore adequate.

##### b. RF Link Calculation

The results of the link analysis are summarized in Table C-16.

The receiver is assumed to have a noise figure of 4.5 dB maximum, the corresponding receiver noise temperature is 522°K. A sky noise temperature of 1400°K is taken for the carrier frequency of 137.62 MHz.\*

Assuming a received circuit loss of 1.0 dB, the effective sky noise temperature at the received input is 1110°K. The equivalent noise temperature of the

\*NRL Report 5668 (AD 265414)

TABLE C-16. REAL-TIME LINK PARAMETERS (FIELD STATIONS)

Parameter	Worst-Case Value	Remarks
Transmitter Power	+37.0 dBm	5 watts min.
Transmitting Circuit Losses	- 1.8 dB	spec value
Transmitter Antenna Gain	- 3.5 dB	spec value over circular isotropic
Polarization Loss	- 3.0 dB	Linear to circular
Path Loss (5 degree elevation angle)	-147.4 dB	137.62 MHz
Receiver Antenna Gain	+12.5 dB	
Receiver Circuit Losses	- 1.0 dB	assumed value
Received Power	-107.2 dBm	
Effective Noise Temperature	1692°K	
Predetector Noise Bandwidth	50 kHz	
Equivalent Noise Input	-119.3 dBm	
C/N ratio	+12.1 dB	50 kHz bandwidth
Threshold	+12.0 dB	
Rf Carrier Margin	+ 0.1 dB	
Am Subcarrier S/N	+29.7 dB	4 kHz bandwidth
Video peak-to-peak rms noise:		
1.2 kHz video bandwidth	+35.0 dB	
900 Hz video bandwidth	+36.4 dB	
450 Hz video bandwidth	+39.5 dB	

received circuit losses is 60°K. The effective system noise temperature at the received input is then  $522 + 1110 + 60 = 1692^{\circ}\text{K}$ .

In the 50 kHz if. bandwidth, the resulting noise power is then -119.3 dBm. The corresponding carrier-to-noise ratio is therefore +12.1 dB.

c. **RF Link Contribution to Signal-to-Noise Ratio**

The signal-to-noise ratio at the output of the receiver can be determined by first calculating the signal-to-noise ratio at the discriminator output (sub-carrier) and then determining the signal-to-noise ratio after the am detector (baseband). The subcarrier signal-to-noise ratio is:

$$(S/N)_{sc} = \frac{3\Delta f^2 B_{IF}}{2 \left[ 3f_{sc}^2 + \frac{B_{sc}^2}{4} \right] B_{sc}} \frac{C}{N} = 29.7 \text{ dB rms/rms,}$$

where  $C/N = 12.1 \text{ dB (worst-case)}$

$$\Delta f = 8 \text{ kHz (worst-case),}$$

$$f_{sc} = 2.4 \text{ kHz}$$

$$B_{sc} = 4.0 \text{ kHz, and}$$

$$B_{IF} = 50 \text{ kHz.}$$

The baseband S/N can be calculated from the subcarrier-to-noise ratio. The peak subcarrier voltage into the transmitter is  $A_p = 2.8$  volts p-p. The minimum voltage is  $A_m = 0.11$  volt p-p. This yields the AM modulation index,  $m$ , with respect to the unmodulated subcarrier:

$$m = \frac{A_p - A_m}{A_p + A_m} = 92.5 \text{ percent.}$$

The peak fm deviation,  $\Delta f$ , corresponds to the peak subcarrier level  $A_p$  and not to the unmodulated subcarrier level,  $A_o$ . The peak subcarrier level and unmodulated subcarrier levels are related by the expression:

$$A_o = \frac{A_p}{1+m}$$

Assuming an output filter bandwidth equal to the maximum modulation frequency  $f_m$ , and a subcarrier filter bandwidth  $B_{sc} = 2 f_m$ , the output power signal-to-noise ratio becomes:

$$\frac{S_o}{N_o} = \left( \frac{m}{1+m} \right)^2 \left( \frac{S}{N} \right)_{sc} \text{ rms/rms.}$$

Alternatively, the  $S_o/N_o$  can also be obtained directly by the following equation.\*

$$\frac{S_o}{N_o} = \left( \frac{2m}{1+m} \right)^2 \frac{\Delta f_c^2 B_{IF}^2}{16 \left[ \frac{f_m^3}{3} + f_{sc}^2 f_m \right]} \cdot \frac{C}{N} \text{ rms/rms}$$

where  $m = 0.925$ ,  $\Delta f_c = 8 \text{ kHz}$ ,

$B_{IF} = 50 \text{ kHz}$ ,  $f_{sc} = 2.4 \text{ kHz}$ , and

$(C/N)_{IF} = 12.0 \text{ dB}$  at threshold,

For a video bandwidth  $f_m = 1.2 \text{ kHz}$ :

$$S_o/N_o = 12.0 + 13.9 = 25.9 \text{ dB rms/rms at threshold.}$$

At 5 degrees elevation:

$$S_o/N_o = 25.9 + 0.1 = 26 \text{ dB rms/rms (worst-case).}$$

To obtain the peak-to-peak signal/rms noise ratio, +9 dB is added to the rms/rms S/N, yielding:  $S_o/N_o$  at carrier threshold = 34.9 dB p-p/rms, and worst-case  $S_o/N_o$  at 5 degrees elevation = 35 dB p-p/rms.

Table C-16 lists the resulting worst-case  $S_o/N_o$  ratios for various output (video) filter bandwidths.

#### d. CDA Station Margins

Rf margins available at CDA stations which monitor VHF real-time transmissions are higher than those computed for the field station data link. Minimum CDA ground-antenna gain is 27.0 dB versus a field station gain of 12.5 dB; therefore, the link margins and all signal-to-noise ratios increase by a minimum value of 14.5 dB.

---

\*Final Report for HRIR Real-Time Transmission Study (AED R-2534), Contract NAS5-3776, October 15, 1964 (with  $m = (1 - \alpha)/(1 + \alpha)$ ).

e. Overall Baseband Signal-to-Noise Ratio

The signal-to-noise ratios given in Table C-16 are the link contributions only. The scanning radiometer sensor S/N ratios are approximately:

$$(S/N)_{IR} = 45 \text{ dB p-p/rms Infrared channel (450 kHz bandwidth)}$$

$$(S/N)_{VIS} = 44 \text{ dB p-p/rms Visible channel (900 kHz bandwidth).}$$

The signal-to-noise ratio of the SR recorder used to obtain the time multiplexed output is approximately:

$$(S/N)_{SRR} = 38 \text{ dB p-p/rms}$$

The resulting overall system S/N ratio (worst case) at the field stations is shown in Table C-17.

TABLE C-17. WORST-CASE BASEBAND S/N RATIOS OF VHF REAL-TIME SYSTEM AT THE FIELD STATIONS

Contributing Parameter	IR Channel (450 Hz Bandwidth) p-p/rms	Visible Channel (900 Hz Bandwidth) p-p/rms
Sensor	45 dB	44 dB
SR Recorder	38 dB	38 dB
RF Link	39.5 dB	36.4 dB
Overall System	35.2 dB	33.7 dB

## 5. S-BAND REAL-TIME LINK ANALYSIS

### a. Receiver Bandwidth Requirements

The significant information bandwidth, by Carson's Rule is:  $bw = 2(f_d + f_h)$ , where  $f_d$  is the peak carrier deviation and  $f_h$  is the maximum modulating frequency. The maximum modulating frequency is determined by the upper frequency subchannel in the two-subcarrier backup mode, which has a center frequency of 230 kHz, a baseband frequency of 35 kHz and a deviation index of unity. The maximum modulating frequency is therefore  $230 + 2 \times 35 = 300$  kHz. The peak carrier deviation is the sum of the subcarrier deviations, or  $50 + 150 = 200$  kHz. Thus the total information bandwidth is:  $bw = 2(200 + 300) = 1.0$  MHz. This is the receiver bandwidth required when using a receiver\* with an afc system compatible with fm modulation of the carrier. If such a receiver is not used, bandwidth allowance for the long-term transmitter stability and for the maximum doppler shift must also be included. In this case the minimum bandwidth of the ground receiver is 1.24 MHz, as tabulated below:

Information	$2(200 + 300)$	$= 1,000.0$ kHz
Doppler Shift at 1697.5 MHz	$2 \times 32.8$	$= 65.6$ kHz
Total transmitter instability at 1697.5 MHz	$\pm 0.005\%$	$= 169.8$ kHz
		<hr/>
		1,235.4 kHz

Utilizing a receiver bandwidth of 1.25 MHz will degrade the rf margin by approximately 1.0 dB from the figure obtained for the 1.0 MHz receiver.

### b. RF Link Calculations

#### (1) SYSTEM NOISE-TEMPERATURE

The overall system noise-temperature comprises contributions from cosmic noise within the main beam of the antenna and earth noise as seen by the antenna side lobes, line losses, preamplifier noise, and receiver noise. Preamplifier noise-temperature is the major contributor to the overall system noise-temperature.

\*For example, receivers that automatically center the peak modulation spectrum in the passband, such as DEI models TMR-70 or TR-711, Scientific Atlanta model 410A and others.

The contribution of the cosmic sky noise and earth noise as seen by the antenna sidelobes, is approximately  $70^{\circ}\text{K}^*$  for a typical parabolic antenna at 5 degrees elevation angle at 1700 MHz. A 1.0 dB antenna feed and preselector circuit loss will reduce this figure to  $56^{\circ}\text{K}$ . The noise-temperature contribution of the pre-selector circuit loss will be  $(1 - 0.794) 290^{\circ}\text{K} = 60^{\circ}\text{K}$ . A conservative noise figure for the receiver is 10 dB. A preamplifier with a gain of 17 dB\*\* will reduce this receiver noise contribution to  $(10 - 1) 290^{\circ}\text{K}/50 = 52^{\circ}\text{K}$ .

The preamplifier noise-temperature is the major contributor to the overall system noise-temperature. With the selected spacecraft transmitter power of 5 watts and the requirement to utilize a 10-foot diameter antenna on the ground, an uncooled parametric preamplifier front-end is mandatory. An off-the-shelf paramp\*\* will provide an equivalent noise-temperature of  $101^{\circ}\text{K}$ . The overall system noise temperature is then as follows:

Antenna temperature (sky + earth noise, 5 deg. elevation, 1 dB circuit loss)	=	$56^{\circ}\text{K}$
Preselector circuit losses (1 dB)	=	$60^{\circ}\text{K}$
Preamplifier (uncooled paramp, 1.3 dB NF)	=	$101^{\circ}\text{K}$
Receiver (10 dB NF, 17 dB preamp gain)	=	$52^{\circ}\text{K}$
		<hr/>
Overall system noise temperature	=	$269^{\circ}\text{K}$

## (2) PATH LOSSES

The propagation losses have been computed, as described in Section IX of this report, for various elevation angles. The results are listed in Table C-18.

## (3) S-BAND ANTENNA PERFORMANCE

The performance of the S-band antennas, with the new spacecraft mounting configuration and the new sensor outlines is described in detail in Appendix D of this report. The maximum and minimum measured gain figures are summarized in Table C-18.

## (4) RF MARGIN CALCULATION

The worst-case link calculation assuming 5 degrees elevation, a 1.0-MHz receiver IF bandwidth, a 10-foot diameter parabola receiving antenna, and

\*L. V. Blake, Antenna and Receiving-System Noise-Temperature Calculation,  
US Naval Research Laboratory Report 5668 (AD 265 414) Sept. 19, 1961.

\*\*Micromega model L1100G

TABLE C-18. VARIATION OF RF MARGIN WITH ELEVATION AND NADIR ANGLES

Elevation (degrees)	Nadir (degrees)	Slant Range (km)	Measured Antenna Gain		Propagation Loss (dB)	Combined Min. Antenna Gain & Propagation Loss (dB)	Worst Case C/N Margin over FM Threshold (dB)
			Maximum (dB)	Minimum (dB)			
0	54.4	4557.5	+5.8	+1.9	-170.2	-168.3	0.2
5	54.1	4036.2	+5.8	+1.9	-169.2	-167.3	1.25
10	53.2	3584.1	+5.8	+2.0	-168.1	-166.1	2.4
15	51.8	3198.4	+5.8	+2.0	-167.1	-165.1	3.4
20	49.8	2873.4	+5.7	+2.1	-166.2	-164.1	4.4
30	44.8	2375.8	+5.8	+1.1	-164.6	-163.5	5.0
40	38.5	2032.8	+5.9	+1.5	-163.2	-161.7	6.8
50	31.5	1798.0	+5.0	-0.4	-162.1	-161.7	6.8
60	24.0	1639.7	+4.5	-2.3	-161.3	-159.0	9.5
90	0.0	1463.1	+0.0	-1.3	-160.3	-158.8	9.7

a 1.3-dB noise figure parametric amplifier front-end is given in Table C-19. A margin of 1.25 dB above a conservative 12 dB  $f_m$  threshold is obtained with the 5-watt spacecraft transmitter. The variation in rf margin with changing ground antenna elevation and spacecraft antenna nadir angle is given in Table C-18.

(5) SUBCARRIER SIGNAL-TO-NOISE RATIO CALCULATION

The subcarrier signal-to-noise ratio is given by the expression:

$$\left(\frac{S}{N}\right)_{sc} = \frac{3 \Delta f_c^2 B_{IF}}{2 \left[ 3f_{sc}^2 + \frac{B_{sc}^2}{4} \right] B_{sc}} \cdot \frac{C}{N} \text{ (rms/rms)}$$

where

- C/N = 13.25 dB (worst case)
- $\Delta f_c$  = 300 kHz for the normal mode of operation (1 subcarrier, 80 kHz)
- = 50 kHz for the backup mode subcarrier No. 1 (80 kHz)
- = 150 kHz for the backup mode subcarrier No. 2 (230 kHz)
- $B_{if}$  = 1.0 MHz
- $f_{sc}$  = 80 kHz for the normal mode subcarrier or for backup mode subcarrier No. 1.
- = 230 kHz for backup mode subcarrier No. 2
- $B_{sc}$  = 140 kHz

The resultant subcarrier S/N ratios are listed in Table C-20.

(6) RF LINK CONTRIBUTION TO BASEBAND SIGNAL-TO-NOISE RATIO

The baseband signal-to-noise ratio is given by the expression:

$$\left(\frac{S}{N}\right)_{bb} = \frac{\Delta f_{sc}^2 \Delta f_c^2 B_{if}}{4 \left[ \frac{f_h^5}{5} + \frac{f_{sc}^2 f_h^3}{3} - \frac{f_L^5}{5} - \frac{f_{sc}^2 f_L^3}{3} \right]} \cdot \frac{C}{N} \text{ (rms/rms)}$$

where

- $\Delta f_{sc} = 35$  kHz
- $f_h = 35$  kHz
- $f_L = 0$

and  $\Delta f_c$ ,  $f_{sc}$ ,  $B_{if}$  and C/N are the same as previously defined.

TABLE C-19. WORST-CASE S-BAND REAL-TIME LINK CALCULATION

No.	Parameter	Value	Remarks
1	Total Transmitter Power	36.99 dBm	5 watts
2	Transmitting Circuit Loss	- .70 dB	estimated
3	Transmitting Antenna Gain	1.90 dB	Ant #1, 5 deg elev.
4	Transmitting Pointing Loss	0.00 dB	
5	Path Loss Range = 2.180+03 nmi Frequency = 1697.50 MHz Elevation = 5.00 degrees	-169.18 dB	
6	Polarization Loss	- .57 dB	
7	Receiving Circuit Loss	- 1.00 dB	assumed
8	Receiving Antenna Gain	32.00 dB	10-foot parabola*
9	Receiving Pointing Loss	- .50 dB	
10	Net Circuit Loss	-138.05 dB	
11	Total Received Power	-101.06 dBm	
12	Received Noise Spectral Density System Temp = 269.0 Deg. K	-174.30 dB/Hz	
13	Received Power/Noise Spec. Density	73.25 dB/Hz	
14	Received Noise Power IF Bandwidth = 1000.00 kHz	-114.30 dBm	
15	Carrier to Noise Ratio	13.25 dB	
16	Threshold CNR	12.00 dB	
17	Performance Margin	1.25 dB	

\*Assumes 0.54 illumination factor.

TABLE C-20. VHRR REAL-TIME SUBCARRIER S/N RATIOS

Mode	Subcarrier No.	S/N Ratio (rms/rms)	Margin Above 12 dB fm Threshold
Primary	1	29.27 dB	17.27 dB
Backup	1	13.71 dB	1.71 dB
	2	14.93 dB	2.93 dB

The resultant baseband S/N ratios are listed in Table C-21, where a value of 8 dB has been used to convert between rms video level to p-p video level, (9 dB theoretical loss 1.0 dB allotted to sync pulse and dc restore).

TABLE C-21. VHRR REAL-TIME LINK BASEBAND S/N RATIOS

Mode	Subcarrier No.	Baseband Link S/N Ratio	
		(rms/rms)	(p-p signal/rms noise)
Primary	1	37.57 dB	45.57 dB
Backup	1	22.00 dB	30.00 dB
	2	22.78 dB	30.78 dB

c. VHRR Real-Time Ground Station RF Parameters

A summary of the required minimum rf parameters for local real-time VHRR ground stations is shown in Table C-22.

TABLE C-22. SUMMARY OF VHRR REAL-TIME GROUND STATION RF PARAMETERS

Parameter	Value
Antenna:	
Type	Parabola on tracking pedestal
Size	10-foot minimum
Polarization	Right-hand circular
Preselector Loss	1.0 dB max
Preamplifier:	
Type	Uncooled paramp
Noise Figure	1.3 dB max (101°K)
Gain	17 dB min
Receiver:	
Type	FM
AFC	Mean-of-peaks type
IF Bandwidth	1.0 MHz
Noise Figure	10 dB max
Demodulator:	
Type	2 FM Subcarrier
Bandwidth	140 kHz (each subcarrier)
Baseband Output Bandwidth	35 kHz

d. Overall Baseband Signal-to-Noise Ratios

The VHRR sensor signal-to-noise ratio is specified as 45.2 dB (p-p/rms) for the IR channel and 43.7 dB (p-p/rms) for the visible channel. The overall baseband S/N ratio at the baseband demodulators will include contributions for the individual S/N terms tabulated below:

VHRR Sensor		S/N (p-p/rms)	
	IR Channel	45.2 dB	
	Vis Channel	43.7 dB	
VHRR Processor		49 dB	(estimated)
Link		see Table C-21	
Demodulator		49 dB	(estimated)

The overall baseband output signal-to-noise ratio at the ground station demodulators will therefore be as listed in Table C-23.

TABLE C-23. OVERALL S/N RATIOS VHRR REAL-TIME DATA

Mode	Subcarrier No.	S/N Ratio (p-p signal/rms noise)	
		IR Data	Visible Data
Primary	1	40.8 dB	40.2 dB
Backup	1	29.8 dB	29.7 dB
	2	30.5 dB	30.4 dB

## 6. S-BAND PLAYBACK LINK ANALYSIS

### a. Receiver Bandwidth Requirements

The significant information bandwidth, by Carsons Rule is:  $bw = 2(f_d + f_h)$ , where  $f_d$  is the peak carrier deviation and  $f_h$  is the maximum modulating frequency which is determined by the highest frequency subchannel, which is the VHRR flutter-and-wow subchannel at 500 kHz. The spectrum of this subchannel can extend up to 501 kHz. The peak carrier deviation is the sum of the deviations of all the subcarriers, or  $25 + 25 + 160 + 160 + 80 + 25 + 285 + 35 + 80 + 50 = 925$  kHz. Thus, the total information bandwidth is  $bw = 2(501 + 925) = 2.852$  MHz. Since the CDA station receiver has an afc system compatible with fm modulation, this is the minimum receiver bandwidth required. Thus, the present if. bandwidth of 3.0 MHz is satisfactory.

### b. RF Link Calculations

#### (1) CDA STATION RF PARAMETERS

The rf link calculations for the S-band playback link have been calculated using the CDA station parameters shown in Table C-24.

TABLE C-24. CDA STATION RF PARAMETERS

Parameter	Value
Antenna Gain (measured*)	47.75 dB
Antenna Noise Temperature (sky + earth noise, measured)	170°K
Receiver Noise Figure	2.2 dB
Receiver Predetection Bandwidth	3.0 MHz

#### (2) SYSTEM NOISE-TEMPERATURE

The system noise-temperature,  $T_{sys}$ , is equal to the receiver noise-temperature plus the antenna noise-temperature. The receiver noise-temperature is given by:

$$T_R = (\text{Noise Figure} - 1) 290^\circ\text{K}$$

$$\text{Noise Figure} = 2.2 \text{ dB} = \text{power ratio of } 1.66\text{-to-}1;$$

\*P. Lantz, Handbook of NASA/GSFC Tracking, Data Acquisition, and Communications Antennas, X-525-64-222(N65-18255), October 1964.

hence

$$T_R = (1.66-1) 290^\circ\text{K} = 191^\circ\text{K}$$

The measured antenna noise temperature is

$$T_{ANT} = 170^\circ\text{K}$$

$$T_{sys} = T_R + T_{ANT} = 191 + 170^\circ\text{K} = 361^\circ\text{K}.$$

The receiver noise density is given by

$$P = kT_{sys} = -173 \text{ dBm in 1 Hz}$$

where k is Boltzman's constant.

### (3) PATH LOSSES

The propagation losses are identical to those previously calculated for the S-band real-time link, and are listed in Table C-18.

### (4) S-BAND ANTENNA PERFORMANCE

The spacecraft S-band antenna performance is described in detail in Appendix D of this report. The maximum and minimum gain figures in the ITOS D and E configuration are summarized in Table C-18.

### (5) RF MARGIN CALCULATIONS

The worst-case link calculation, assuming the CDA station rf parameters of Table C-24 at 5 degrees elevation above the horizon is given in Table C-25. A margin of 11.95 dB above a conservative fm threshold of 12 dB is obtained with the 5-watt spacecraft transmitter. This is an improvement of 6.2 dB over the TIROS M/ITOS-1 figure. The difference is due to:

- a) Use of a 5-watt transmitter instead of 2 watts,
- b) Reduction in transmitting circuit losses from -4.2 dB to -0.7 dB by removal of the hybrid splitter and use of two separate S-band antennas,
- c) Spacecraft antenna gain degradation from 3.2 dB to 1.9 dB due to the new mounting and sensor configurations.

TABLE C-25. WORST-CASE S-BAND PLAYBACK LINK CALCULATION

No.	Parameter	Value	Remarks
1	Total Transmitter Power	36.99 dBm	5 watts estimated
2	Transmitting Circuit Loss	-.70 dBm	
3	Transmitting Antenna Gain	1.90 dBm	Ant #1, 5 deg. elev.
4	Transmitting Pointing Loss	0.00 dBm	
5	Path Loss Range = 2, 180 nmi Frequency = 1697.50 MHz Elevation = 5.00 Degrees	-169.18 dBm	
6	Polarization Loss	-.57 dBm	
7	Receiving Circuit Loss	0.00 dBm	
8	Receiving Antenna Gain	47.75 dBm	measured
9	Receiving Pointing Loss	-.50 dBm	
10	Net Circuit Loss	-121.30 dBm	
11	Total Received Power	-84.31 dBm	
12	Receiver Noise Spectral Density System Temp = 361.0 Deg. K	-173.03 dBm/Hz	
13	Received Power/Noise Spec. Den.	88.72 dBm/Hz	
14	Received Noise Power IF Bandwidth = 3000.00 kHz	-108.25 dBm	
15	Carrier-To-Noise Ratio	23.95 dBm	
16	Threshold CNR	12.00 dBm	
17	Performance Margin	11.95 dBm	

(6) RF DEVIATION ALLOTMENTS

The allotment of rf carrier deviation among the various data sub-carriers was optimized with the assistance of a link analysis program available on a time-shared computer. The following criteria were used, as a basis for optimization:

- a) Total peak deviation should be compatible with the CDA station receiver IF bandwidth of 3.0 MHz.
- b) All video channels should have approximately the same baseband S/N ratio, better than 40 dB p-p/rms.

- c) All fm subcarriers should have at least 3-dB margin above the demodulator threshold, assumed to be 12 dB.
- d) Ratio of highest-to-lowest deviation subcarrier should be no greater than 15-1 in deviation.
- e) Digital data channels should have a minimum baseband S/N of 20 dB (p-p signal/rms noise).
- f) Flutter and wow channels should have a minimum baseband S/N of 32 dB ( $2\sigma$  p-p signal/rms noise).
- g) Pilot tone subcarriers should have a minimum of 3-dB margin above PLL acquisition threshold, assumed to be 10 dB rms/rms.

The resultant carrier deviations are shown in Table C-26.

TABLE C-26. WORST-CASE SUBCARRIER SIGNAL-TO-NOISE RATIOS, S-BAND PLAYBACK LINK.

Channel	Peak Carrier Deviation $\Delta f_c$ (kHz)	Subcarrier Frequency (kHz) $f_{sc}$	Subcarrier Bandwidth (kHz) $B_{sc}$	Rf Link Subcarrier S/N Ratio (rms/rms)
SRR-A F & W	25	12.5	1.5	59.96
SRR-B F & W	25	25.0	2.0	52.70
VHRR Video	160	88.0	99.0	40.51
SRR-A Video	160	212.0	64.0	35.17
Digital-A	80	300.0	32.0	29.17
Pilot Tone No. 1	25	300.0	0.1	44.13
SRR-B Video	285	388.0	64.0	34.96
Pilot Tone No. 2	35	450.0	0.1	43.53
Digital-B	80	460.7	14.0	29.04
VHRR F & W	50	500.0	4.0	29.69

(7) SUBCARRIER SIGNAL-TO-NOISE CALCULATIONS

The subcarrier signal-to-noise ratios are given by the expression\*;

$$\left(\frac{S}{N}\right)_{sc} = \frac{3 \Delta f_c^2 B_{IF}}{2 \left[ 3 f_{sc}^2 + \frac{B_{sc}^2}{4} \right] B_{sc}} \cdot \frac{C}{N} \text{ (rms/rms)}$$

where

$$C/N = 23.95 \text{ dB (worst case)}$$

$$B_{if} = 3.0 \text{ MHz}$$

and  $\Delta f_c$ ,  $f_{sc}$  and  $B_{sc}$  are as given in Table C-26.

The resultant subcarrier S/N ratios are listed in Table C-26.

It can be seen from Table 3-26 that sufficient margin is maintained above the 12 dB fm demodulator threshold value in all the fm subcarriers.

(8) RF LINK CONTRIBUTION TO BASEBAND S/N RATIO

In the case of fm subcarriers, the baseband signal-to-noise ratio is given by the expression:

$$\left(\frac{S}{N}\right)_{FM}^{bb} = \frac{\Delta f_{sc}^2 \Delta f_c^2 B_{IF}}{4 \left[ \frac{f_H^5}{5} + \frac{f_{sc}^2 f_H}{3} - \frac{f_L^5}{5} - \frac{f_{sc}^2 f_L^3}{3} \right]} \frac{C}{N} \text{ (rms/rms)}$$

where

$\Delta f_{sc}$ ,  $f_H$  are as shown in Table C-27.

$$f_L = 0$$

and  $\Delta f_c$ ,  $f_{sc}$ ,  $B_{if}$  and  $C/N$  are the same as previously defined.

\*J. Fargot & P. Magne, Frequency Modulation Theory, Permagon Press, 1961, P 117.

The resultant baseband signal-to-noise ratios are listed in Table C-27, where the following values have been used to convert from rms signal levels to p-p signal levels:

VHRR Video:	8 dB (9dB theoretical, less 1 dB allotted to sync pulse and dc restore amplitudes)
SR Video:	7.8 dB (9 dB theoretical, less 1.2 dB allotted to sync pulse and dc restore amplitudes)
VHRR and SR F&W:	12 dB (2 $\sigma$ value)
Pilot Tone:	9 dB (cw signal)

In the case of am subcarriers, the baseband signal-to-noise ratio is given by the expression\*:

$$\left(\frac{S}{N}\right)_{\text{bb AM}} = \frac{\left(\frac{2m_{\text{sc}}}{1+m_{\text{sc}}}\right)^2 \Delta f_c^2 B_{\text{if}}}{16 \left[ \frac{f_H^3}{3} + f_{\text{sc}}^2 f_H - \frac{f_L^3}{3} - f_{\text{sc}}^2 f_L \right]} \frac{C}{N}$$

The baseband signal-to-noise ratio of the digital data channels may be obtained by first computing the baseband signal-to-noise ratio of an equivalent am subcarrier having the same peak carrier deviation and a subcarrier modulation index  $m_{\text{sc}} = 1$ . Noting that the waveshape of the band-limited digital data is very nearly sinusoidal, it can be shown\*\* that a double sideband suppressed carrier signal, such as the Digital-A channel, under equal peak envelope amplitude conditions delivers four times, or 6 dB greater, output signal-to-noise ratio than the equivalent am signal. Similarly, it can also be shown\*\* that a single sideband suppressed carrier signal of the same peak amplitude, such as the Digital-B channel, delivers 9 dB greater output signal-to-noise

\*C. Devieux, Final Report for the HRIR Real-Time Transmission Study, AED R-2534, Appendix II, Oct. 1964, with  $m_{\text{sc}} = \frac{1-\alpha}{1+\alpha}$ .

\*\*Downing, Modulation Systems and Noise. Prentice-Hall, Inc., 1964, Sect 4.4.

ratio than the equivalent am signal. The resultant baseband signal-to-noise ratio ratios based on these assumptions are shown in Table C-27, where a figure of 9 dB has been used to convert between rms signal levels and p-p signal levels for the digital channels. The tabulated signal-to-noise ratios are the rf link contributions only.

TABLE C-27. BASEBAND S/N RATIOS OF S-BAND PLAYBACK LINK

Channel	Peak Subcarrier Deviation (kHz) $\Delta f_{sc}$	Baseband Bandwidth (kHz) $f_h$	Baseband S/N Ratio	
			(rms/rms)	(p-p/rms)
SRR-A F & W	0.075*	0.5	50.02	62.02
SRR-B F & W	0.15*	0.5	50.02	62.02
VHRR Video	14.5	35.0	39.17	47.17
SRR-A Video				
Visible	13.25	18.75	39.26	47.06
IR	13.25	9.38	48.30	56.10
Digital-A	n/a	16.0	29.15	38.15
Pilot Tone No. 1	n/a	0.1	44.13	53.13
SRR-B Video				
Visible	13.25	18.75	39.04	46.84
IR	13.25	9.38	48.07	55.87
Pilot Tone No. 2	n/a	0.1	43.53	52.53
Digital-B	n/a	16.0	28.43	37.43
VHRR F&W	0.30*	0.5	36.04	48.04
*2 $\sigma$ value				

c. Baseband Signal-to-Noise Ratio of Video Channels

The overall baseband signal-to-noise ratio of each channel includes contributions from the sensors, the spacecraft signal processors, the spacecraft tape recorders, the multiplexer, the rf link, the demultiplexer, the

ground station tape recorders and the long lines. The individual noise sources are independent. Consequently, the total noise power at the Data Processing and Analysis Facility at Suitland, Md. is the sum of the individual noise powers properly referenced to the same signal level and measured in the same baseband bandwidth.

(1) SR VIDEO OVERALL SIGNAL-TO-NOISE RATIO

The SR video signals are processed in the spacecraft SR processor and then recorded as an FM subcarrier in the SR tape recorder. The SR tape recorder is later played back at 20.833 times the record speed over the multiplexer and S-band link. The 20.833:1 speedup increases the baseband, deviation and subcarrier bandwidth by a factor of 20.833, resulting in no net change in S/N due to the processing. The multiplexer shifts the signal frequencies by linear translation for simultaneous transmission by the S-band link. At the output of the ground receiver, the SR subcarriers are separated from the composite signal and linearly translated back to the original frequencies by the demultiplexer. The signals are then recorded and later played back at 1/4 the record speed over the long lines. The 4:1 slowdown reduces the baseband, deviation and subcarrier bandwidth by a factor of 4, resulting again in no net change in S/N due to the processing. The long lines wideband channel A has a measured S/N of 30 dB rms/rms over a measured bandwidth of 19 kHz\*. At the long lines interface, the baseband of the SR signal is 4.7 kHz for the visible channel and 2.35 kHz for the IR channel, and the subcarrier deviation is  $\pm 3.3$  kHz.

The effective S/N contribution of the long lines referred to the baseband output of the fm demodulator is therefore\*\*:

$$\left(\frac{S}{N}\right)_{LLo} = 3D^2 \left(\frac{B_{sc}}{2B_m}\right) \left(\frac{S}{N}\right)_{LL}$$

where

$D = \frac{3.3 \text{ kHz}}{4.7 \text{ kHz}} = 0.702$  for the visible channel and  $\frac{3.3 \text{ kHz}}{2.35 \text{ kHz}} = 1.4$  for the IR channel.

---

\*ESSA Memorandum S24 dated June 26, 1969

\*\*Downing, Modulation Systems and Noise, Prentice-Hall, Inc. 1964. Sec 5.2.

$$B_{sc} = 19 \text{ kHz}$$

$$B_m = 4.7 \text{ kHz for the visible channel and } 2.35 \text{ kHz for the IR channel.}$$

and  $\left(\frac{S}{N}\right)_{LL} = 1000 \text{ (30 dB)}$

The resultant noise contribution of the long lines is 34.8 dB rms/rms (43.8 dB p-p/rms) for the visible channel and 43.7 dB rms/rms (52.7 dB p-p/rms) for the IR channel.

The overall S/N ratio at the end of the long lines can now be determined by combining the contributions of the individual S/N ratios given in Table C-28.

TABLE C-28. WORST-CASE OVERALL SR BASEBAND S/N RATIOS AT DAPAF END OF LONG LINES

Contributing Parameter	IR Channel (2.35 kHz Bandwidth) p-p/rms	Visible Channel (4.7 kHz Bandwidth) p-p/rms
SR Sensor	45 dB	44 dB
SR Processor	49 dB	49 dB
SR Recorder	39 dB	39 dB
Multiplexer	49 dB	49 dB
RF Link	56 dB	47 dB
Demultiplexer	49 dB	49 dB
Ground Recorder*	52 dB	52 dB
Long Lines	53 dB	44 dB
Overall System	37 dB	36 dB
*Calculated from Mincom G-100 Tape recorder W&F spec at 15 ips playback speed.		

(2) VHRR VIDEO OVERALL SIGNAL-TO-NOISE RATIO

The VHRR video signals are processed in the spacecraft VHRR processor and then recorded as an fm subcarrier in the VHRR tape recorder. The VHRR tape recorder is later played back at the same speed over the multiplexer and S-band link. The multiplexer merely passes the VHRR subcarrier signal, without translation. At the output of the ground receiver, the VHRR subcarrier is separated from the composite signal and doubled in frequency by the demultiplexer.

The doubled subcarrier signal is then recorded and later played back at 1/8 the record speed over the long lines. The 8:1 slowdown reduces the baseband, deviation, and subcarrier bandwidth by a factor of 8, resulting in no net change in S/N due to the processing. At the long lines interface, the baseband of the VHRR signal is 4.38 kHz and the subcarrier deviation is  $\pm 3.62$  kHz. The effective S/N contribution of the long lines referred to the baseband output of the FM demodulator can be calculated in the same manner as for the SR case and is 36.5 dB rms/rms or 45.5 dB p-p/rms.

The overall S/N ratio at the end of the long lines can now be determined by combining the contributions of the individual S/N ratios given in Table C-29.

TABLE C-29. WORST-CASE OVERALL VHRR S/N RATIO AT DAPAF  
END OF LONG LINES

Contributing Parameter	IR Channel (4.38 kHz Bandwidth) p-p/rms	Visible Channel (4.38 kHz Bandwidth) p-p/rms
VHRR Sensor	45 dB	44 dB
VHRR Processor	49 dB	49 dB
VHRR Recorder	39 dB	39 dB
Multiplexer	49 dB	49 dB
RF Link	47 dB	47 dB
Demultiplexer	49 dB	49 dB
Ground Recorder*	47 dB	47 dB
Long Lines	45 dB	45 dB
Overall System	36 dB	36 dB
*Calculated from Mincom G-100 Tape Recorder W&F spec at 7.5 ips playback speed.		

# APPENDIX D

## PERFORMANCE TESTS OF ITOS D AND E S-BAND ANTENNAS

### 1. SUMMARY

Tests have been made of the proposed ITOS D and E S-band antenna arrangement. These tests included measurement of the patterns of both S-band antennas, of the VSWR of both antennas, and of the isolation between the two antennas. Test results\*\* show the proposed antenna configuration to be acceptable and capable of meeting required mission performance. As compared with the TIROS M antenna, there is some attenuation of antenna gain in certain regions due to the projection of the spacecraft sensors into the fringes of the antenna field. This attenuation, however, is offset by the increase in transmitter power and the use of two antennas, which eliminates the hybrid coupler and its attendant loss.

### 2. DESCRIPTION OF TESTS

A full-scale mock-up was built of the proposed configuration of the ITOS D and E earth-facing panel, including approximations of the sensor contours (see Figure D-1). In this configuration, the S-band antennas were located by ray-tracing to avoid interference with the required coverage regions of the spacecraft sensors and to minimize antenna coverage obstruction by the sensors. The mock-up was built to fit the AED antenna pedestal, having a mounting that could accommodate either of the two antennas on the axis of rotation. The coordinates used to describe the antenna performance and the antenna arrangement is shown in Figure D-2; the antenna numbering is completely arbitrary. Antenna 1 was a flight unit, Serial 04; Antenna 2 was the ETM\* dipole mounted on the serial 01P base.

For the antenna pattern tests, the mock-up was attached to the antenna pedestal. A right-hand circularly polarized (1 dB axial ratio) S-band source (1697 MHz) was located about 40 feet away to illuminate the test region. The ground between the source and the pedestal was covered with rf absorbers to reduce the ground reflections to an acceptable level. The source antenna was connected to an amplitude-modulated S-band generator and TWT amplifier. The test antenna was connected to a crystal detector and the detected 1000-Hz modulation was fed through amplifiers to a pattern recorder.

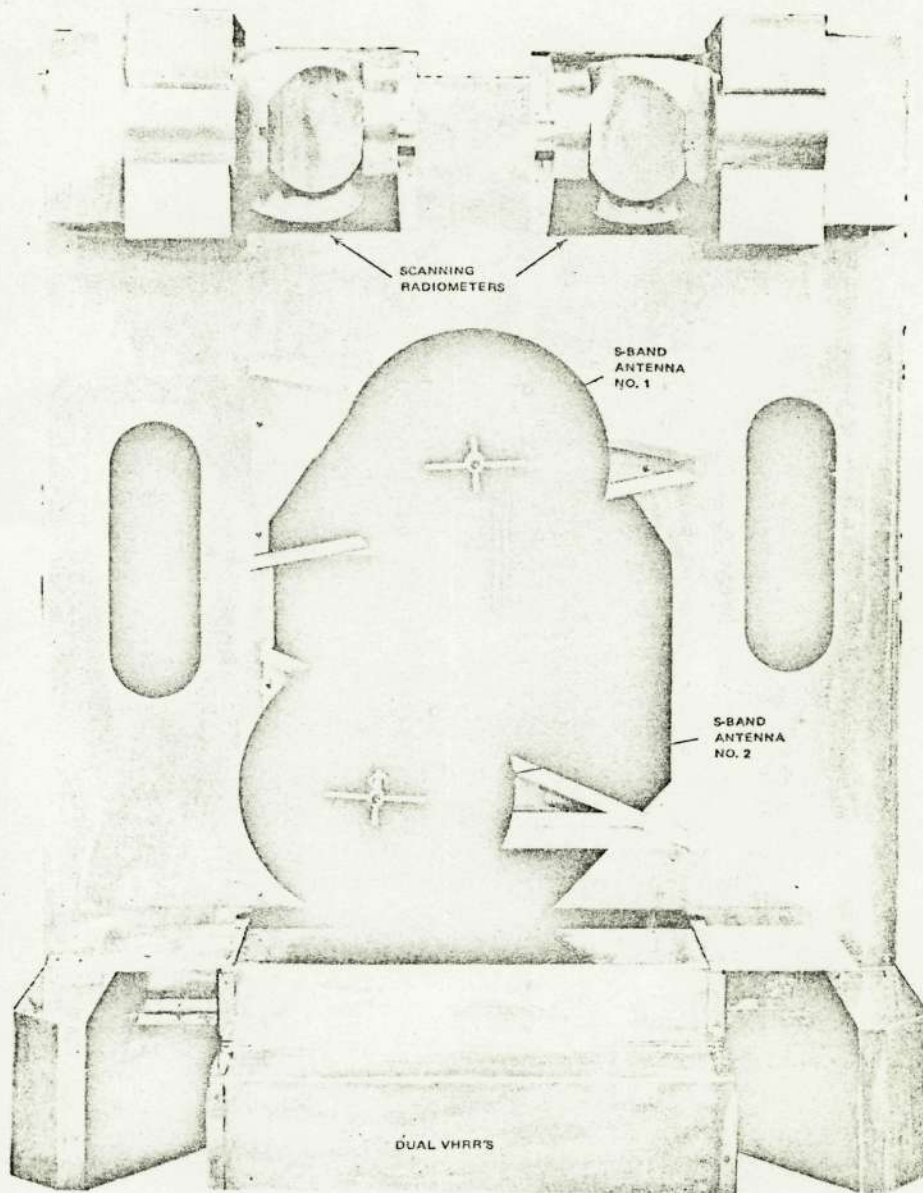
The VSWR and isolation tests were made outdoors with the mock-up supported off the ground and the antennas pointed up and away from any reflecting structure. The VSWR was measured through a 4-foot section of RG-9 cable with a

---

\*Engineering Test Model

\*\*These tests were performed with larger VHRR's.

Reproduced from  
best available copy. 



REPRODUCIBILITY OF THE  
ORIGINAL PAGE IS POOR

Figure D-1. S-Band Antenna Test Model

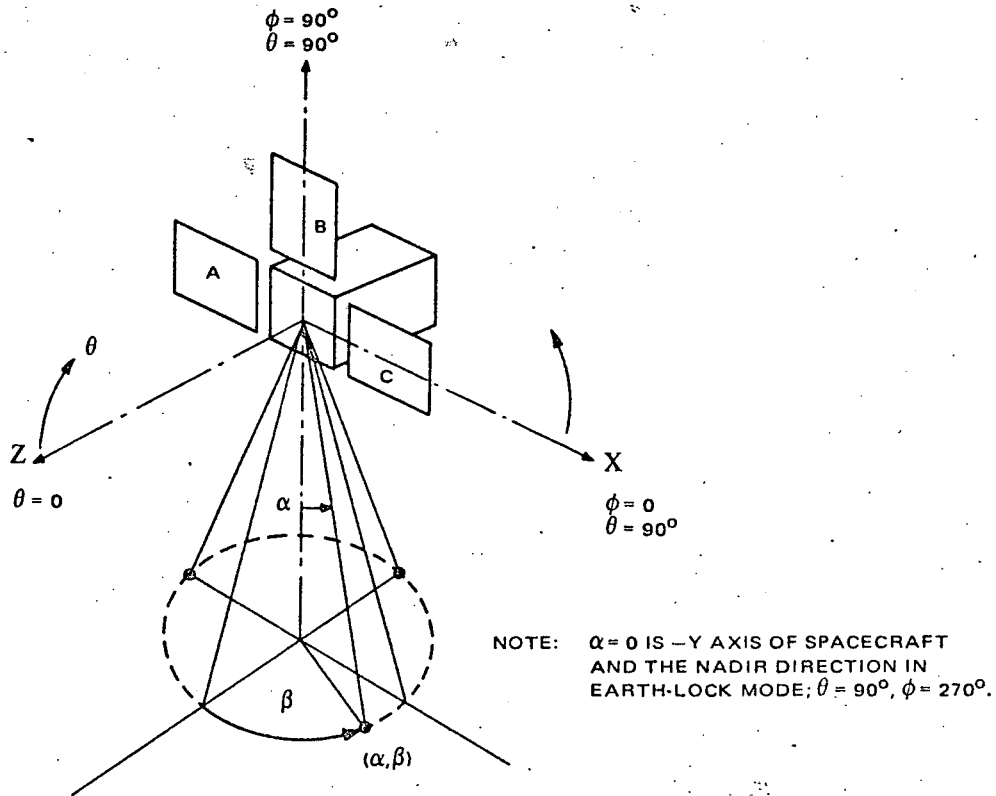


Figure D-2. Antenna Coordinates

PRD 219. The isolation was measured by the substitution method, using the calibrated attenuator of the signal generator as the standard.

### 3. RESULTS OF TESTS

The results of the antenna pattern measurements, traced from the original pen recordings, are summarized in Figures D-3 through D-6. The performance of each antenna (see Figure D-1 for identification) is shown together with the present TIROS M specification requirement. Also shown is the relative path loss versus nadir angle and the ground station elevation angle for a spacecraft in a 790 - nautical mile orbit.

Figures D-3 and D-4 show the performance of Antenna 1. Figure D-3 shows the pattern taken in the  $\beta = 0^\circ, 180^\circ$  plane. This is the plane through the momentum wheel axis and the nadir, and through the SR and VHRR protrusions. The frequency of the ripple in the central part of the pattern ( $0 < \alpha < 30^\circ$ ) is consistent with the reflections and diffraction off a large reflecting surface located where the VHRR is located. Figure D-4 is the envelope of seven patterns between  $\beta = 22-1/2^\circ$  and  $\beta = 167-1/2^\circ$ . In both of the above cases, the patterns satisfy the specification requirements although the performance is marginal at  $\alpha = 55^\circ$  (left side of Figure D-4).

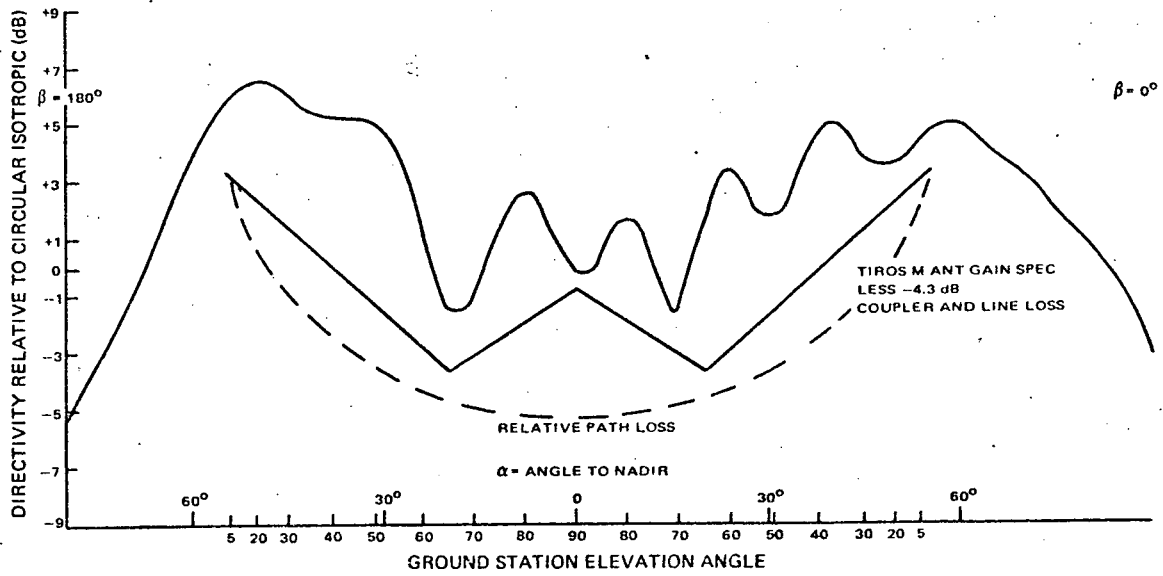


Figure D-3. Antenna No. 1 Pattern for  $\beta = 0^\circ, 180^\circ$  Plane

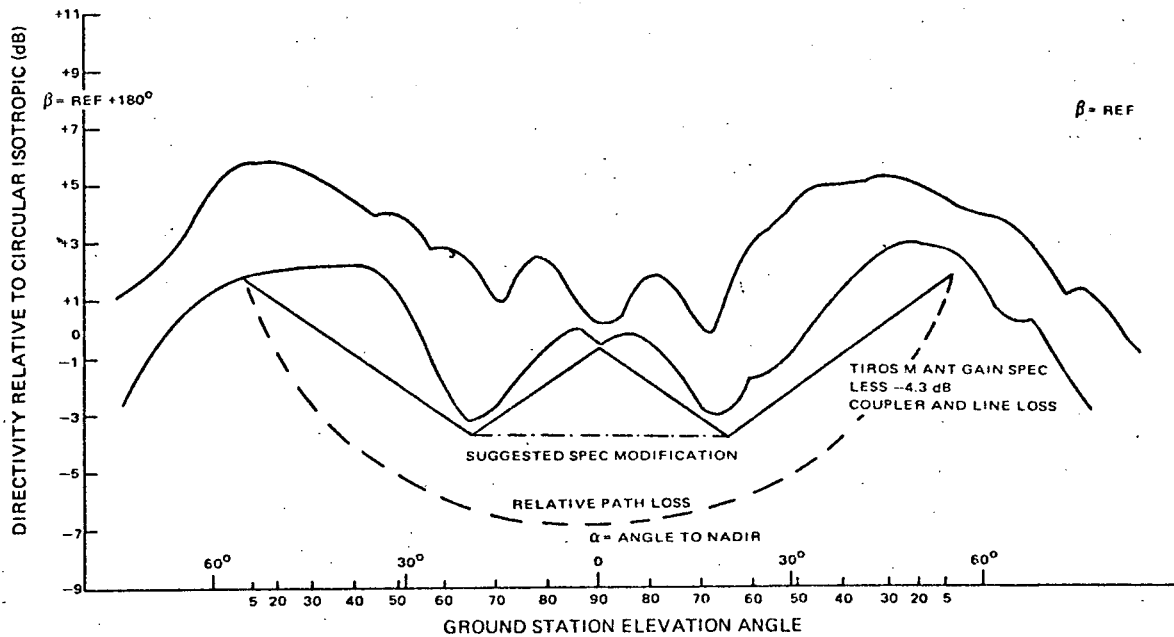


Figure D-4. Antenna No. 1 Envelope of Patterns for  $\beta = 22\frac{1}{2}^\circ$  to  $167\frac{1}{2}^\circ$  Planes

Figures D-5 and D-6 show the performance of Antenna 2. Figure D-5 shows the  $\beta = 0, 180^\circ$  plane; the frequency of the ripple is reduced in the central region because the antenna is closer to the VHRR envelope. However, the ripple now causes the pattern to fall below the specification requirement. The same thing happens in the envelope of the other patterns shown in Figure D-6.

The important factor of the coverage required for system operation can be appreciated by comparing the region of non-conformance against the relative path loss. This curve can be interpreted as the gain level which would provide a constant signal/noise from horizon to horizon. The minimum nonconforming point in any of the measured patterns is 3-1/2 dB greater than this level. The central contour of the TIROS M specification was determined originally by the patterns produced by the antenna, not by the gain required by the system. The intent was to produce a simple contour which described the minimum gain versus angle of a typical antenna mounted on TIROS M. In the present situation, however, the operational requirements should be reconsidered and the specifications should be changed accordingly. A suggested change is shown in Figure D-6.

The isolation between the two antennas was measured at 1690, 1700, and 1710 MHz and found to be a constant 32 dB. The VSWR of both antennas was measured and found to easily meet the specification requirement of 1.5/1. Further analysis of the data is needed to pin-point the exact values.

#### 4. DIRECTIVITY CONTOURS

The preceding data of Figures D-3 through D-6 is presented in a different manner in Figures D-7 and D-8. In these figures, the data has been plotted as contours of constant directivity on rectangular representation of the  $\phi, \theta$  coordinates of the spacecraft. This representation is useful to determine the actual directivity levels attained during a spacecraft-to-ground contact. For comparison, the data of TIROS M is shown in Figure D-9 and an approximation of the basic antenna, plotted from limited data, is shown in Figure D-10. Comparing this figure with the other plots illustrates the distortion introduced by the spacecraft body and sensors.

#### 5. CONCLUSIONS

The proposed ITOS D and E S-band antenna configuration is completely acceptable. The gain contours delineated in the TIROS M S-band antenna specification, as updated for ITOS D and E, should be modified to accept the performance described by the reported measurements.

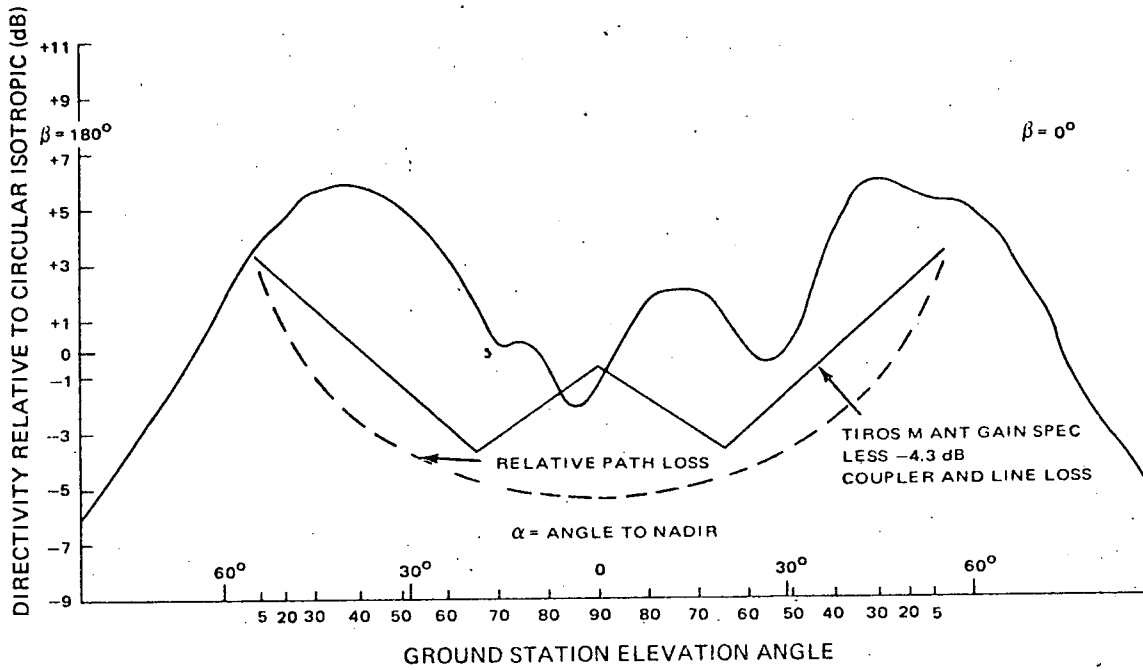


Figure D-5. Antenna No. 2 Pattern for  $\beta = 0^\circ, 180^\circ$  Plane

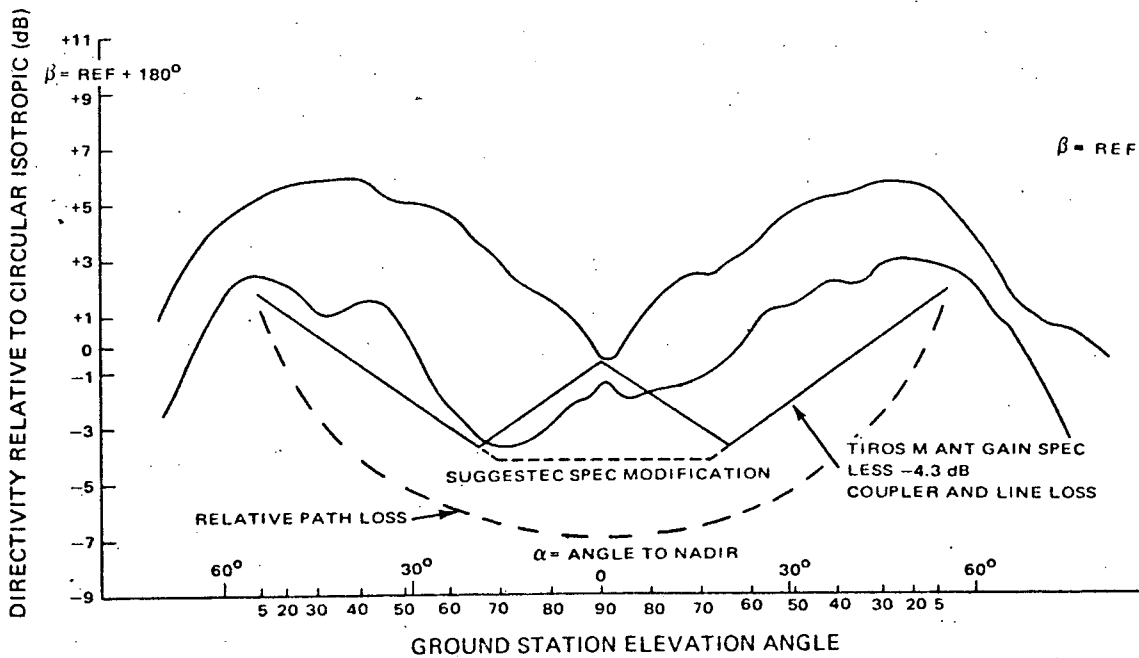


Figure D-6. Antenna No. 2 Envelope of Patterns for  $\beta = 22\frac{1}{2}^\circ$  to  $167\frac{1}{2}^\circ$  Planes

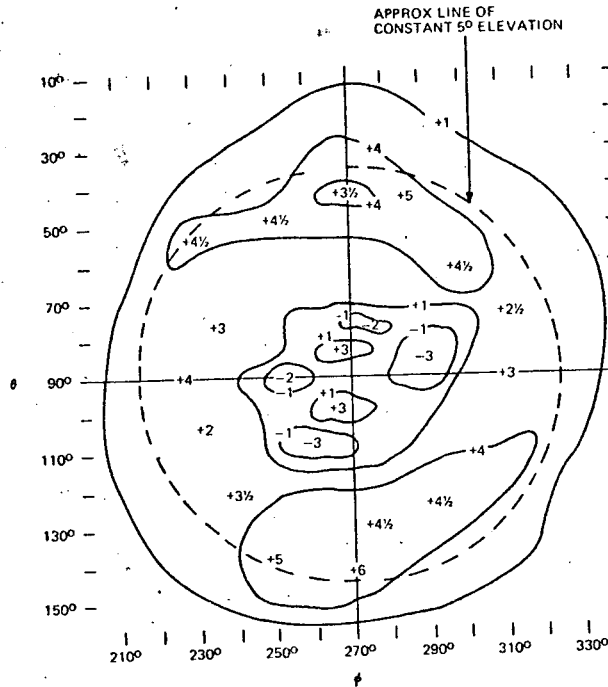


Figure D-7. ITOS D and E, Antenna No. 1, Directivity Contours Relative to RHC Isotropic

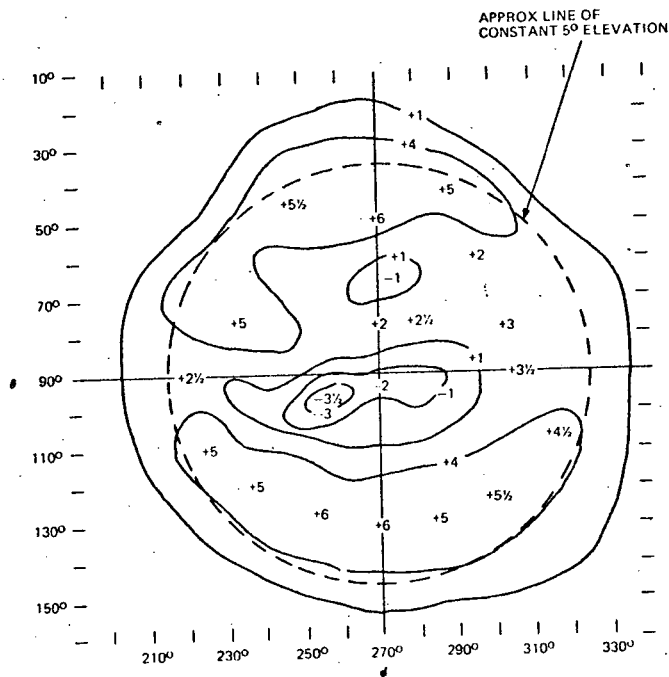


Figure D-8. ITOS D and E Antenna No. 2, Directivity Contours Relative to RHC Isotropic

